UNIVERSITY OF SOUTHAMPTON

FACULTY OF ENGINEERING, SCIENCE AND MATHEMATICS

School of Chemistry

POLY(ANILINE) MICROELECTRODES FOR ASCORBATE MEASUREMENTS

By

Alejandro Martinez-Bonastre

A Thesis Submitted for the degree of

DOCTOR OF PHILOSOPHY

August 2007

UNIVERSITY OF SOUTHAMPTON

FACULTY OF ENGINEERING, SCIENCE AND MATHEMATICS

SCHOOL OF CHEMISTRY

Doctor of Philosophy

POLY(ANILINE) MICROELECTRODES FOR ASCORBATE MEASUREMENTS

By Alejandro Martinez-Bonastre

ABSTRACT

The aim of this research was the production of a needle type microelectrode to monitor rapid changes of ascorbic acid, AA, in physiological fluids. Poly(aniline), PANi, composites have been shown to be excellent electrocatalytic surfaces for the oxidation of NADH and AA. Electrodeposition of PANi films on small platinum disc and elliptical microelectrodes was carried out under potentiodynamic and potentiostatic control. The effect of the electrolyte and counter ion were studied in order to produce reproducible, stable and conducting PANi films. Special attention was given to the final morphology of the resulting polymer film. Following previous work at Southampton University the incorporation of two poly(anions) was studied on a small scale: poly(vinylsulfonate), PVS, and poly(styrenesulfonate), PSS. In addition alkylated and crosslinked PANi microelectrodes were investigated as an alternative to PANi composites to retain PANi conductivity at neutral pH. The kinetic model proposed by Bartlett and Wallace on the RDE was compared with the data obtained at composite PANi microelectrodes. It was found that the counter ion plays an important role during ascorbate oxidation. The observed current responses to AA are half of the theoretical value for PANi-PSS microelectrodes. A different reaction mechanism is proposed for PANi-PVS and PANi-PSS where an ascorbate radical anion intermediate might be present for the later composite. The excellent electroanalytical properties shown by the modified PANi films were applied to real systems. PANi-PSS microelectrodes were used as amperometric sensors for AA in low volume of human plasma. PANi-PVS elliptical needle type microelectrodes were successfully applied for the detection of ascorbate in the substomatal cavities of Barley leaves.

Table of contents

Acknowledgements

First, I would like to thank my supervisor Professor Phil N. Bartlett for his patience and enthusiasm along these years. During my time in his group, I have seen him teaching undergraduates and professors, presenting key talks in conferences and discussing data in the lab in such a way that makes a difficult subject as physical chemistry easy and enjoyable. I cannot describe in these lines how lucky I feel for being part of his group.

I also would like to thank Dr. Stefan Hanstein for proposing this research and his family for making my stays in Germany enjoyable. I would like to thank the German B.M.B.F. nanobiotechnology program for funding, grant No. 0312006A.

My advisor, Dr. Guy Denuault for his opinions and discussions through the course of this work. I would like to thank previous members in Phil's group who dedicated their time and effort to the electrodeposition of poly(aniline) films. I would like to thank Dr. Janis Shute, Dr. Paul Kilmartin, Dr. Peter Roach and Mrs. F. Martin for their help during our experiments in *in vivo* systems. I would like to thank Dr. A. Russell and my present colleagues at work in Johnson Matthey for their welcome to the research group.

I would like to thank Melanie, member of the Southampton glass blowers group for her outstanding work on the electrochemical cells and microelectrodes used in this work. Alistair Clark for his advice when using the SEM. Also, many thanks to Jill Queen, Sally Dady and Beverly Price for all their help with the initial paperwork and for being so helpful with the admin.

I believe that to make a good thesis having the right people by your side is as important as having a good supervisor and advisors. I have been extremely lucky with the people I have met in Southampton and this is why I thank the following friends:

I would like to thank to Dr. Sergio Martinez-Montequin and Dr. Maciej Sosna for all the useful help with the IT, day trouble shooting in the lab and endless discussions of our

electrochemical data even when being in a pub with a couple of pints. I really miss the laughs and remember "*do not panic, unplug the network*!".

Dr Stuart Evans for all his help during the very first stage of my stay in the group. Dr Mamdouh Abdelsalam for all his senior advice. Dr. David Cook, Dr. Rob Wood and Dr. Tim Dumford for being my British influence and teaching me so much about the UK. Dr. Toru Imokawa for his nice friendship. Ken, Veronica, Sumeet, Clelia and of course all the people in the physical chemistry department for the laughs during the coffee breaks.

Special thanks to Diego Astuy and Emilio Mayoral for their friendship and support from the distance and to all my close friends back home in Alicante, Spain.

Last but not least, I would like to thank my family. Thanks mum and dad for being there everyday with all your support and love. A big hug to my sister Maria Eugenia for all her telephone calls. You were there every day. My brother Antonio for his support from the distance. Special thanks to my girlfriend Laura broken pocket for all her patience during my long writing up stage but most importantly for loving me. Finally yet importantly, I would like to specially thank you my brother Oscar for encouraging me to enjoy this opportunity from the first day I left home.

A mis padres

Rosa y Antonio

List of Symbols

Symbol	Description	Usual unit
K_a	acidic constant	-
a_i	activity of species *i*	mol cm^{-3}
k_{cat}	catalytic reaction rate	s^{-1}
Q	charge density	mC cm^{-2}
μ_i°	chemical potential of species *i* in the standard state	J mol^{-1}
C	concentration	mol cm^{-3}
Γ_{sites}	concentration of polymer active sites per surface area	mol cm^{-2}
c_i	concentration of species *i*	mol cm^{-3}
i	current	A
j	current density	A cm^{-2}
DP	Degree of polymerization	-
D	diffusion coefficient	cm^2 s^{-1}
δ	diffusion layer thickness	cm
K_S	dissociative constant for the enzyme substrate complex	mol cm^{-3}
Φ_{Donnan}	Donnan chemical potential	J mol^{-1}
k'_{ME}	effective electrochemical rate constant	cm s^{-1}
$\tilde{\mu}_i$	Electrochemical potential of species *i*	J mol^{-1}

Symbol	Description	Usual unit
E	electrode potential *vs.* a reference electrode	V
F	Faraday constant	C mol^{-1}
R	gas constant	J K^{-1} mol^{-1}
A	geometric area of the electrode	cm^2
V	initial rate of the reaction	s^{-1}
ν	kinematic viscosity	cm^2 s^{-1}
i_{lim}	limiting current	A
pH	$-\log_{10}[H^+]$	-
pK_a	$-\log_{10} K_a$	-
b	major ellipse radius	µm
$k_D^{'}$	mass transport rate constant	cm s^{-1}
K_M	Michaelis-Menten constant	mol cm^{-3}
a	microelectrode disc radius	µm
MW	molecular weight	g mol^{-1}
n	number of electrons involved in overall reaction	-
λ	number of points	-
i_t	overall current	A
$\Phi_{polymer}$	polymer film chemical potential	J mol^{-1}
ℓ	polymer thickness	µm

Symbol	Description	Usual unit
k	rate constant for a chemical reaction	s^{-1}
$k_E^{'}$	rate of polymer electro-regeneration	s^{-1}
ξ	ratio between the electrode radius and the polymer thickness	-
W	rotation rate	Hz
R_f	roughness factor	-
v	scan rate	$mV\ s^{-1}$
$\Phi_{solution}$	solution (electrolyte) chemical potential	$J\ mol^{-1}$
T	temperature	K
t	time	s

Common abbreviations

Symbol	Description
AA *or* H_2A	Ascorbic acid
BQ	Benzoquinone
BSA	Bovine serum albumin
BMBF	Bundesministerium für Bildung und Forschung (Federal ministry of Education and Research)
CME	Chemically modified electrode
CA	Chronoamperometry
[E]	Concentration of enzyme
[ES]	Concentration of enzyme/substrate complex
[P]	Concentration of product
[S]	Concentration of substrate
CV	Cyclic Voltammetry
DHA	Dehydroascorbic acid
DBS	Dodecylbenzylsulfonate
ESR	Electron Paramagnetic Resonance
EPR	Electron Spin Resonance
EDTA	Ethylenediaminetetraacetic acid
FSCV	Fast scan cyclic voltammetry
FT-IR	Fourier transform infrared
GSH	Glutathione
HPLC	High pressure liquid chromatography

Symbol	Description
HQ	Hydroquinone
MPA	Metaphosphoric acid
HA^-	Monodeprotonated ascorbate anion
NADH	Nicotinamide adenine dinucleotide
OCV	Open circuit potential
NAD^+	Oxidized form of NADH
PANi	Poly(aniline)
PPy	Poly(pyrrole)
PSS	Poly(styresulfonate)
PVS	Poly(vinylsulfonate)
r.d.s.	Rate determining step
RDE	Rotating disc electrode
SCE	Saturated calomel electrode
SMSE	Saturated mercury sulphate electrode
SECM	Scanning electrochemical microscopy
TFA	Trifluoroacetic acid
UA	Uric acid

Chapter 1

Introduction

1.1 Microelectrodes

The geometric dimensions of electrodes have become progressively smaller with advances in technology. A conventional disc electrode becomes a microelectrode when the electrode diameter is smaller than 50 μm[1]. The geometry of microelectrodes is very diverse and the most common is the microdisc electrode. The electroactive area can protrude the insulating body presenting conical, hemispherical or cylindrical shapes[2]. Although, it can be recessed below the insulation material[3]. As the diffusion of the analyte to the electrode will depend on the electrode geometry, the choice of geometry will depend upon the application and properties desired. For instance, microdisc electrodes are normally used for *in vitro* analysis whereas elliptical microelectrodes are frequently used for *in vivo* measurements[4]. When considering the electroactive material, there are almost no limits as Pt, Au, C fibres, Cu or Ni microelectrodes, among others, are usually found.

The electrochemical properties of microelectrodes have been extensively investigated by different groups[2, 3, 5-11]. These authors have published the most reliable articles and reviews in text books of fundamentals in the area. Their work covers the range from theoretical studies and simulations, to applications in real systems.

Microelectrodes offer several advantages compared to conventional electrodes. First, due to their small dimensions, they can be used to take measurements in reduced spaces or in small volumes, even in single biological cells[12]. They are also really useful to monitor chemical events with very high spatial resolution as evidenced by several techniques like scanning electrochemical microscopy, SECM, and atomic force microscopy in electrochemical investigations[1, 10, 13-16].

However, microelectrodes are not just interesting due to their small dimensions. Analyte diffusion to a disc electrode of macroscopic dimensions is planar. However, as the radius of the electrode decreases, planar diffusion transforms to hemispherical diffusion also known as radial diffusion. The mass transport rate constant, $k_D^{'}$, is inversely dependent on the electrode radius, $k_D^{'} = \frac{4D}{\pi a}$. Where D is the diffusion coefficient and a is the microelectrode radius. Therefore, the mass transport rate constant can be very large for extremely small electrodes of micrometer dimensions. Radial diffusion allows fast transfer of analyte to the microelectrode surface. This means that the electrode is able to reach steady state response in short times. Since the measured current is proportional to the electrode area, the currents measured at microelectrodes will be very small, often in the range of nanoamps, picoamps or femtoamps. The overall mass transport limiting current, i_{lim}, for any electrode is given by equation 1[17].

$$i_{\text{lim}} = nFk_D^{'}AC \quad \textbf{(1.1)}$$

Where n is the number of electrons transferred, F is the Faraday constant, $k_D^{'}$ is the mass transport rate constant, A the area of the electrode and C the analyte concentration. Considering the mass transport rate constant $k_D^{'} = \frac{4D}{\pi a}$, and considering a disc shape, we obtain equation 1.2[17].

$$i_{\text{lim}} = 4nFDCa \quad \textbf{(1.2)}$$

This equation represents the steady state limiting current for a microdisc electrode. For a purely diffusion controlled process, where the electrode kinetics are not limiting, a plot of the steady state limiting current versus the microelectrode radius will give a linear plot crossing the origin. The gradient of this plot can be used to obtain the diffusion coefficient of the corresponding analyte. Equation (1.2) can also be used to calculate the microelectrode geometrical radius if solutions of different concentrations are used and the diffusion coefficient is known.

Steady state response at macroelectrodes can be also achieved with the Rotating Disc Electrode, RDE[17], where the electrode is rotated about its axis to facilitate mass transport

to the electrode surface by forced convection. Equation 1.3, gives the steady state limiting current density for a RDE, commonly known as the Levich equation[17].

$$j_{\lim} = 1.554nFD^{2/3}\nu^{-1/6}c^{\infty}W^{1/2} \quad \textbf{(1.3)}$$

Where, ν is the kinematic viscosity, W is the rotation rate in Hz, and the other values are as previously defined. Combining equations 1.2 and 1.3, the mass transport rate constant for a RDE can be derived as,

$$k_D^{'} = 1.554D^{2/3}\nu^{-1/6}W^{1/2} \qquad \textbf{(1.4)}$$

Hence, in theory, it would be possible to compare the steady state responses at microdisc and RDE electrodes, if the diffusion layer thickness is of the same magnitude for both.

Microelectrodes also present the benefit of having low capacitances. The double layer capacitance is reduced because it is proportional to the electrode area[18]. Low capacitance means that voltammetric experiments may be performed at very fast sweep rates without significant distortion in the voltammetric response. As the measured current when using microelectrodes is really low, the corresponding *iR* drop will be considerably reduced compared to conventional electrodes[19]. Nevertheless, the main advantage of having low *iR* drop, is that microelectrodes are an excellent choice to make measurements in poorly conductive electrolytes.

For small microelectrodes under high sweep rates, radial diffusion is negligible compared to planar diffusion. Sweep rates as large as $10^5 - 10^6$ V s^{-1} have been achieved by Andrieux *et al*[20]. This property is useful in kinetic studies as fast sweep rates can be used to detect reaction intermediate species with short lives. In this way, a precise reaction mechanism can be proposed and tested.

On the contrary, microelectrodes present several disadvantages. As the currents registered are low, electrical noise is an issue in the design of the electrochemical experiments. Earthed high impedance BNC connectors and a Faraday cage must be used. Although current filters might help as well when this is not possible, i.e. for *in vivo* measurements. Usually, microelectrodes are difficult to make and serious problems can arise if the sealing between the metal and the insulator is not properly done. This is probably the

main priority when making a microelectrode. A small imperfection in the seal could markedly increase the solution/electrode interface and result in high residual currents[21,22]. Errors due to edge effects can be tremendous and must be avoided. Due to their small size, microelectrodes are very fragile and they snap easily. Last, cleaning the microelectrode surface is a major problem, especially below $a < 5$ μm microdisc electrodes. Mechanical polishing with alumina, 1.0, 0.3 and 0.05 μm, and wet polishing cloths are normally used. Ultrasonic cleaning has to be applied with care, if needed, as it can snap fragile connections. Controlled electrochemical cleaning in acidic solutions, between hydrogen and oxygen evolution, can also complement mechanical polishing in order to obtain a clean electrode surface.

1.2 Microelectrodes applied to *in vivo* electrochemistry

In vivo chemical microsensors are miniaturized analytical devices for making chemical measurements in biological systems[12]. The application of electrochemistry to *in vivo* systems was introduced by Adams and nowadays is led by Wightman and Ewing [4, 12, 23-30]. Progress in the fabrication of new materials and the availability of producing microelectrodes with a tip dimension below 2 μm, including the insulating body, makes them useful tools in modern science.

The fabrication technique for *in vivo* microelectrodes differs from that used to fabricate conventional microelectrodes. Such small dimensions are normally achieved by a fast pulling method. A Wollaston wire (metal core surrounded by the insulating body) is heated and then pulled quite rapidly. The tip dimension is controlled by the time and force of the pulling step. These electrodes are polished to obtain the desired geometry. Another method to produce such small dimensions is by electrochemical etching[10]. Controlling the time of the experiment and the depth to which the metal is introduced into the solution, the desired dimensions can be obtained.

In the area of biological sensors, the choice of electrode material and geometry is limited by the system under study. Carbon fibre is normally the preferred electrode material because it is less prone to fouling by adsorption of proteins than gold or platinum[1].

However, the advances of chemically modified electrodes in the area of biosensors have expanded enormously the range of materials available. Related to the microelectrode geometry it is probably preferred to have an elliptical shape in order to avoid tissue damage. Elliptical microelectrodes provide a higher electrochemical area compared to a disc electrode. Nevertheless, the use of cylindrical and cone tips have been reported[10]. Figure 1.1 shows different microelectrode geometries used for *in vivo* experiments.

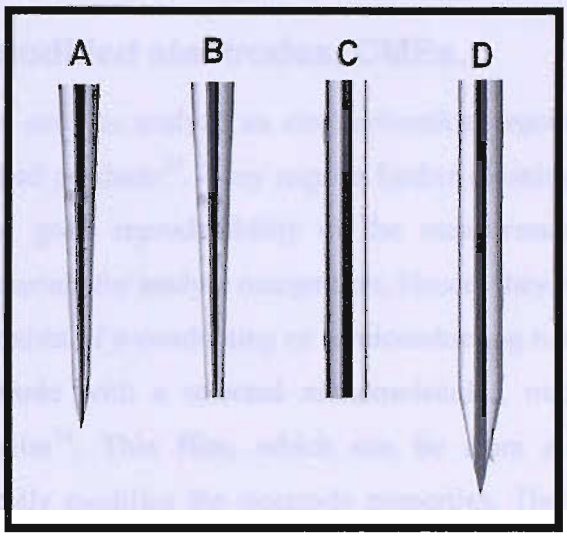

Figure 1.1 *Different microelectrode geometries used for in vivo analysis. Picture taken from Thomas Recording, GmbH.*

The equipment used for such difficult experiments is of key importance. For instance, when using these fragile microelectrodes, vibration free equipment is crucial. Positioning of the microelectrodes is done by the help of automatic micropositioners and optical microscopes. Even so, an experienced operator may need hours to position the microelectrodes before the experiment can be done.

The two electrochemical techniques most widely used for *in vivo* measurements are amperometry and fast scan cyclic voltammetry, FSCV. Amperometry allows measurement of the most rapid concentration changes whereas FSCV is particularly useful because the voltammogram provides information to identify the detected substance and possible reaction intermediates. In physiological fluids, it is common to collect a

background baseline of the supporting physiological electrolyte that is subtracted from the measurements afterwards.

Interesting examples are the *in situ* study of ascorbic acid in brain tissue[31] and also the detection of dopamine by a poly(pyrrole) coated carbon fibre elliptical microelectrode on the surface of single cells[32].

1.3 Chemically modified electrodes, CMEs.

Bare electrodes can be used to analyze an electrochemical reaction but suffer from the disadvantage of adsorbed products[33]. They require further cleaning, either mechanical or electrochemical, for a good reproducibility of the measurements. In addition, bare electrodes are poor materials for analyte recognition. Hence, they require modification. A modified electrode consists of a conducting or semiconducting material that is coated on top of the bare electrode with a selected monomolecular, multimolecular, ionic, or polymeric chemical film[34]. This film, which can be from a monolayer to a few micrometers thick, totally modifies the electrode properties. The sensing properties are now due to the coating material and the bare metal just acts as a support for transmitting the electrical signal.

Chemically modified electrodes, CMEs, find utility in a wide spectrum of basic electrochemical investigations; including heterogeneous electron transfer and chemical reactivity to electrode surface chemistry, electrostatic phenomena at electrode surfaces, and electron and ionic transport mechanisms in polymers[35]. They play an important role in the design of electrochemical devices and systems for applications in chemical sensing, energy conversion and storage, molecular electronics, electrochromic displays, corrosion protection, and electro-organic syntheses.

Although their applications are numerous, we will focus on their electroanalytical properties. CMEs can be used as electrocatalytic surfaces for analyte determination. In electrocatalysis, CMEs are used to amplify the electrode signal and to increase its specificity, reproducibility and lifetime. Figure 1.2, shows a scheme for a CME.

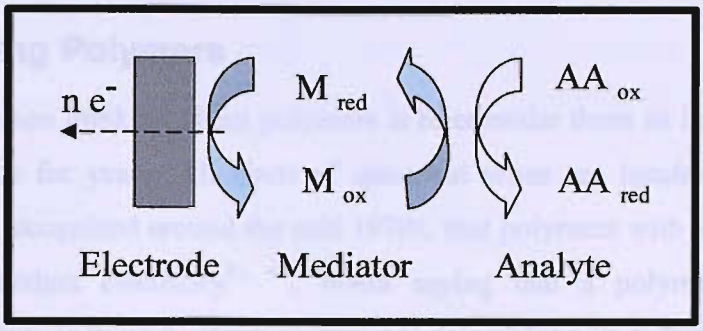

Figure 1.2 *Chemically Modified electrode, CME. The active sites of the mediator can act as recognition sites for a substrate in the presence of different interferences. When electron transfer occurs, the electrons percolate through the conducting film to the support electrode giving a rise on the electrical signal measured.*

The electroactive materials used in CMEs are diverse. Electrodes are chemically modified by one of these three approaches:

1) Chemisorption-adsorption: the chemical film is strongly and, ideally, irreversibly adsorbed onto the electrode surface. This approach usually yields monolayer coverage. A typical example is the adsorption of alkenes or isocyanides on platinum electrodes[36, 37].

2) Covalent bonding: linking agents, such as, organosilanes or organic thiols, are used to covalently attach one to several monolayers of the chemical modifier to the electrode surface. i.e. thiols molecules covalently attached to gold electrodes for further enzyme immobilization[38].

3) Polymer film coating: electron conductive and non conductive polymer films are held on the electrode surface by some combination of chemisorption, covalent bonding or by physical anchoring in the contacting solution. The polymer film can be organic, organometallic or inorganic and may contain up to many thousands of equivalent monomolecular layers of the chemical modifier. As discussed later in this thesis, poly(aniline)[39] or poly(pyrrole)[40] films can be electrodeposited on different electrode geometries by electrochemical polymerization of their monomers. Due to the scope of this thesis, we will focus on polymer film modified electrodes.

1.4 Conducting Polymers

The first reflex when thinking about polymers is to consider them as insulators, and this has been the case for years. All kinds of electrical wires are insulated with plastics. However, it was recognized around the mid 1970s, that polymers with a certain structure were able to conduct electricity[41, 42]. When saying that a polymer is electrically conducting, we have to think it allows electrons to move along its polymeric chains. This is possible when a conjugated polymeric chain is present. The simplest conducting polymer chain is a poly(acetylene) chain, figure 1.3.

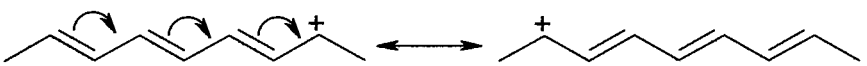

Figure 1.3. *Resonance of a poly(acetylene) chain[43]. The arrows show charge and electron motion.*

The delocalized π electrons of the conjugated bonds are able to move along the chains due to the overlap of π orbital and are able to move between energy band gaps. This provides electron mobility through the polymer chains making them conducting materials. The mechanism of electron movement is similar to that in metals, and can be explained by band theory[44]. It might be said that conducting polymers display quasi-metallic conductivity.

Although poly(acetylene) conductivity was discovered around the mid 1970s[42], it was not until the year 2000 that conducting polymers started to really make a difference in polymer science[43]. It was this year when the Nobel prize in chemistry was shared by Heeger[45], MacDiarmid[46] and Shirakawa[47] due to their developments in the area of conducting polymers. The breakthrough in the area came due to the discovery by these three scientists who stated that doping poly(acetylene) with iodine vapour increases its electrical conductivity a billion times compared to the undoped material. This was a massive step forward in the area, as doped conducting polymers could reach electrical conductivities similar to metals ~ 10^6 Ω^{-1} cm^{-1}. This is the reason why conducting

polymers are known these days as plastic metals. For further guide in this thesis, some values of typical electrical conductivities for different materials are given in figure 1.4.

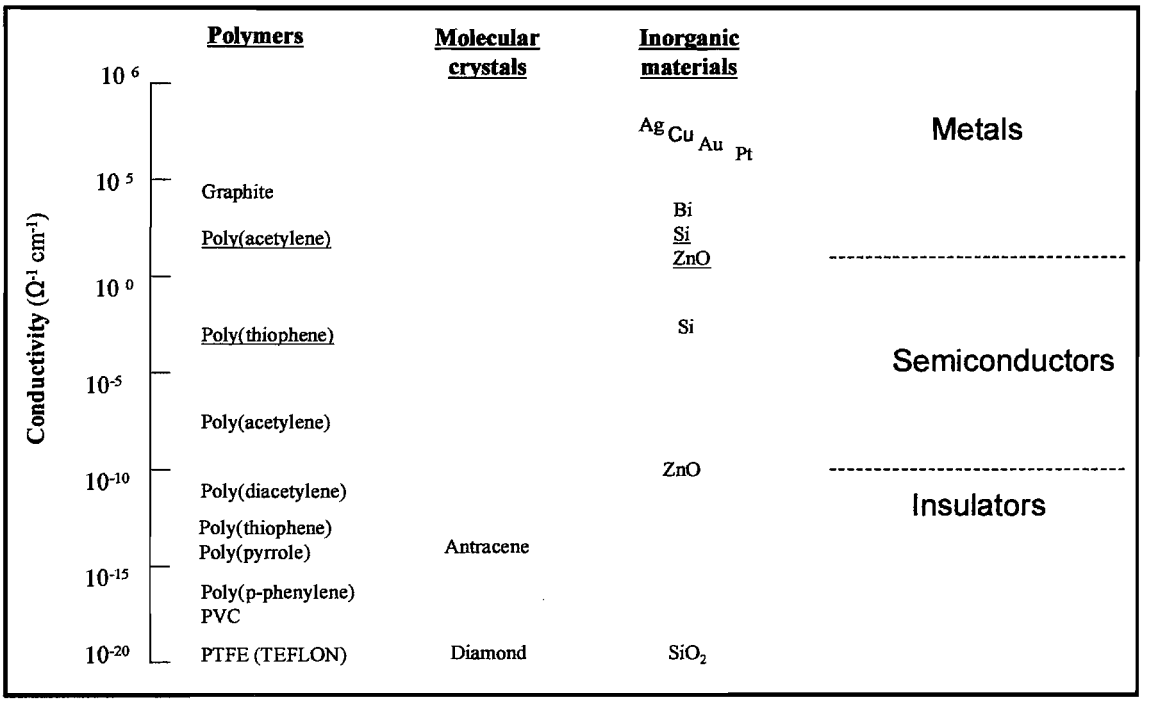

Figure 1.4. *Approximate conductivities of various organic and inorganic materials. Species that can be doped are listed in the undoped and heavily doped state (underlined)*[48].

The most well known conducting polymers are poly(thiophene), poly(pyrrole), PPy, and poly(aniline), PANi. The synthesis and characterization of electroactive polymers has become a most important area of research in polymer and materials science during the past two decades[49, 50]. Among these polymers, PANi has been of particular interest and is the main subject of this thesis.

1.5 Poly(aniline), PANi

PANi, differs from other conducting polymers because its conductivity depends on two variables; the degree of oxidation and the degree of protonation[51]. PANi can be synthesized chemically or electrochemically. Chemically, it is often synthesized by the oxidation of the aniline monomer, figure 1.5, with a chemical oxidant.

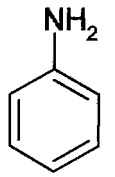

Figure 1.5 *Aniline monomer*

Polymerization is conducted in aqueous HCl, with ammonium persulfate as the oxidant[52-54]. Electrochemically, PANi synthesis is carried out by the electropolymerization of the aniline monomer. It can be carried out in three different ways; galvanostatic[55], applying a constant current for a certain time; potentiostatic[56], constant potential during fixed time; and potentiodynamic[57], potential is varied with time. PANi films can also be polymerized by autocatalytic electroless polymerization of aniline[58].

The synthesis of PANi films is normally carried out in acidic conditions[59], although PANi can also be electrodeposited at basic pH[60]. The conductivity of the polymer will strongly depend, among other factors, on the route of synthesis. Compared to the chemical route, the electrochemical procedure is preferred because no extraction from the solvent mixture is necessary and the thickness of the polymer film can be easily controlled by the charge passed.

PANi films have been electrochemically deposited on many different substrates, including Au[61], Pt[62], C[63], Ni[62], Ti[64], etc, and the electrochemical procedure used depends on the PANi application as its final morphology varies with the method applied, aniline concentration, substrate, counter ion and pH[53, 65-69].

1.5.1 PANi Electrochemistry

Figure 1.6 shows an experimental cyclic voltammogram of a PANi film in 1 mol dm^{-3} H_2SO_4, deposited at constant potential, $E = 0.90$ V *vs.* SCE, on a 2 μm diameter platinum disc electrode.

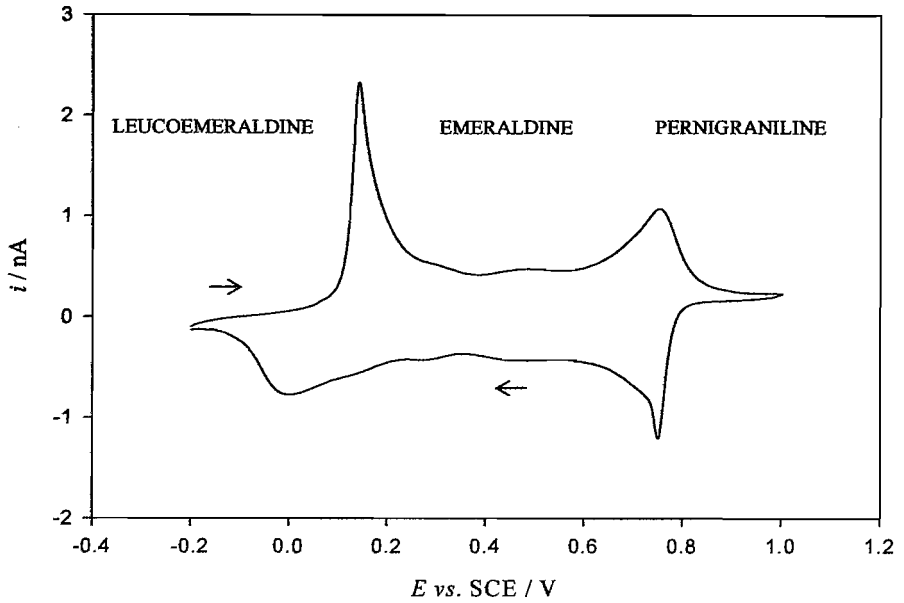

Figure 1.6. *Cyclic voltammetry of a PANi film in 1.0 mol dm^{-3} H_2SO_4, scan rate $v = 50\ mV\ s^{-1}$. Prior to acid cycling, the polymer was reduced at -0.20 V vs. SCE for 3 min. afterwards it was cycled from -0.20 V to 1.0 V vs. SCE. The first cycle is shown. The polymer was amperometrically deposited on a 2.0 μm diameter platinum disc microelectrode. E = 0.90 V vs. SCE for 120 s, 0.1 mol dm^{-3} aniline in 1 mol dm^{-3} H_2SO_4 solution. Charge passed through polymer deposited was 6.53 mC cm^{-2}. Solutions were degassed with argon for 15 min and temperature controlled at 25 ± 0.1 °C with a thermostatic bath.*

In acidic solutions, PANi shows three oxidation states and two redox processes. These are related to the change in the redox state, from its fully reduced state, leucoemeraldine, to its fully oxidized state, pernigraniline.

At -0.20 V *vs.* SCE the PANi film is in the reduced insulating state, known as leucoemeraldine. As the potential becomes more positive, the polymer starts to oxidize and at +0.20 V *vs.* SCE the transition from the insulating reduced state to the conducting half oxidized state of PANi, known as emeraldine, occurs. If the potential is increased, up to +0.80 V *vs.* SCE the transition from emeraldine to the second oxidation state known as pernigraniline occurs. The polymer film is then in its fully oxidized state and insulating.

Between these two transitions, a peak is found at ~ +0.50 V *vs.* SCE that has been attributed to degradation products of the film[55]. They were identified as benzoquinone and hydroquinone intermediates, (BQ/HQ), which are formed when PANi films are cycled to high anodic limits, up to the pernigraniline state.

This peak increases with the number of scans, indicating higher concentration of quinone units within the polymer chains as the film is cycled to high anodic potentials. This leads to an irreversible PANi chain breaking. If the polymer is cycled for longer times, it leads to the total disappearance of the redox peaks corresponding to emeraldine and pernigraniline transitions and the properties of the polymer are lost[57, 70].

This degradation process depends upon the acidic strength of the electrolyte and the composition of the PANi film. For instance, degradation of PANi in H_2SO_4 occurs faster than in HCl, at the same acid concentration and temperature[71]. Hence, the kinetics of polymer degradation in acidic solutions can be used as a parameter to establish the stability of the polymer film under study. During the course of this thesis, it will be shown that if the potential is reduced to +0.78 V *vs.* SCE, the presence of these degradation products can be avoided.

1.5.2 PANi and its different oxidation states

Fourier transform infrared (FTIR) , non-resonance FT-Raman, quartz crystal microbalance and XPS spectroscopy have been used to measure qualitatively the various intrinsic oxidation states of PANi[49]. The mechanism of PANi oxidation is shown in figure 1.7.

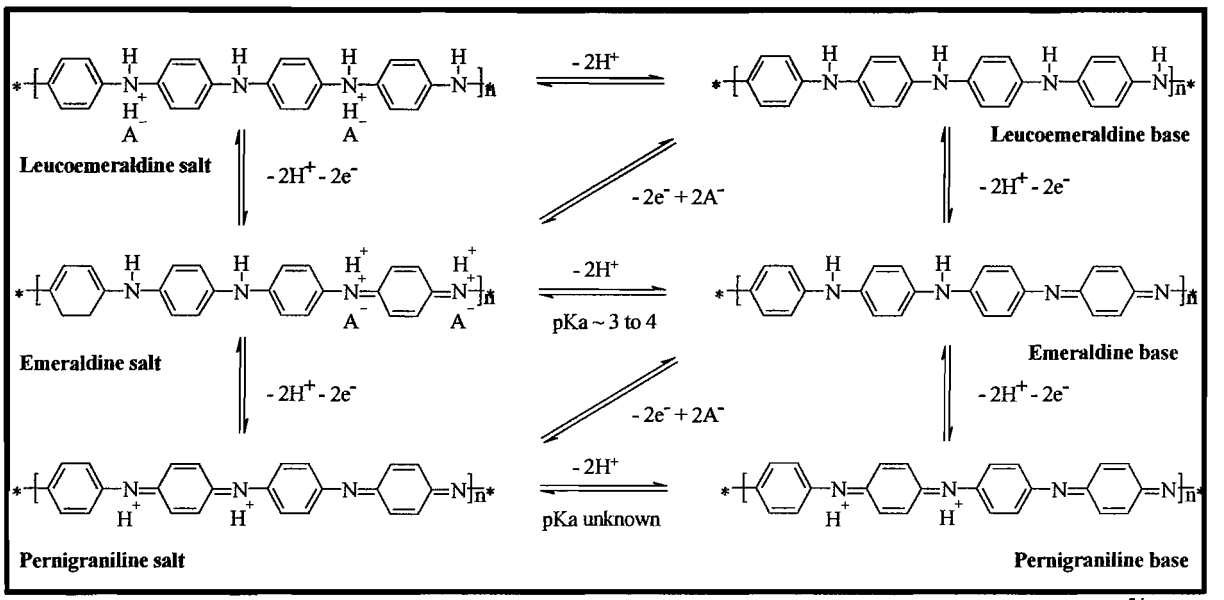

Figure 1.7. *Scheme of redox transformations and protonation equilibrium of PANi*[51].

PANi redox processes involve electron and proton transfers, whereas the salt/base equilibrium involve transfer of acid[72]. Emeraldine salt is conducting because of nitrogen protonation. The degree of protonation depends on the dissociation constant of the species and consequently varies with the pH and potential[73]. The emeraldine salt has a $pK_a \sim 3$ to 4, thus at pH above 4, the conducting emeraldine salt deprotonates giving the insulating emeraldine base[74]. This is just a salt/base equilibrium and no electrons are transferred.

It has been reported in the literature that deprotonation of PANi films can be lowered to some degree by working at high ionic strength[75]. This leads to a lowering of the ion concentration gradient across the film interface resulting in the system being closer to neutrality. The equilibrium electric potential difference within the polymer/solution interface can be also explained by the Donnan membrane equilibrium potential. Which explains the movement of ions within membranes[76-78].

The deprotonation of the emeraldine salt is a major problem when using PANi films in electrocatalysis as it leads to an electro-inactive polymer. Hence, there have been a large

number of publications looking at ways to minimize the deprotonation of PANi films at pH > 5. The next section discusses this issue in detail.

1.6 Conductivity at neutral pH; composite PANi films

The electrochemistry of PANi films above pH 5 shows only one broad peak which is the consequence of the overlap of the transitions between leucoemeraldine/emeraldine and emeraldine/pernigraniline[79]. Peter and Kalaji stated that the proton egress occurs faster than proton ingress and hence the polymer deprotonates upon cycling at neutral pH[80]. This is why the response of PANi films decreases upon cycling the potential at neutral pH. Therefore, in order to produce PANi films, which will remain conducting at neutral pH, it is necessary to find a method to avoid deprotonation of the emeraldine salt.

There are good reviews in the literature looking at different ways to overcome the main drawbacks of PANi and their applications as biosensors[81-83]. The most successful chemical and electrochemical approaches present in literature within the last few years, which follow on the initial work from Asturias[84] and Epstein[85] and coworkers are presented in figure 1.8 and now briefly discussed.

Barbero *et al.* successfully proposed that the quinoimine units are reactive towards different types of nucleophiles[86]. Sulphonates, thiols, esters, arylsulfinates or cyanides have been coupled to the polymer backbone[81, 86, 87]. This nucleophilic addition, which can be carried out either chemically or electrochemically, greatly modifies the properties of the original PANi. For instance, the coupling of sulphite units to the quinoimine rings allows PANi to retain its conductivity up to neutral pH[88]. The main risk of this method is that modification of the aromatic ring leads to an increase of polymer solubility at neutral pH and a careful control of the polymer modification is required.

Later on, Bartlett *et al.* introduced the idea of using large poly-anions, such as poly(vinylsulfonate)[89], poly(acrylate)[90] and poly(styrenesulfonate)[91, 92] with the PANi chains. The electropolymerization of aniline together with these polymer chains, containing sulphonate or carboxylate groups, leads to a composite polymer, as there is no

chemical bonding between the polymer chains. The poly-anion chains become trapped within the polymer. Therefore, the negative charge of the sulfonic or carboxylate groups being trapped will maintain electroneutrality with the positive charge of the oxidized polymer. These films were successfully applied to the detection of NADH and ascorbate[89, 92].

More recently, Battaglini *et al.* proposed a really novel and interesting approach[93]. They introduced an easy method to produce a PANi film which conductivity will not depend on polymer protonation. By chemical reaction of the unprotonated, reduced form of PANi, leucoemeraldine, with propanesultone, the protons on the nitrogen atoms are replaced by the sultone in an alkylation reaction. This idea relies on the same principle as those groups who decided to use alkylated aniline monomers, such as N-methyl or N-N-dimethyl poly(anilines)[94]. Battaglini's approach produces a polymer that is a mixture of an alkylated and non alkylated PANi film. Hence its conductivity is, at least, partially dependent on the percentage of polymer alkylation and protonation. The question here is whether the polymer solubility might be increased by the alkylation.

Finally, the most recent method developed by Knoll *et al.* also opened up an interesting new method of PANi modification[95]. PANi was doped with mercaptosuccinic-acid-capped gold nanoparticles by using the so called layer by layer method. This method consists of building layers of opposite charge on top of each other. The resulting multilayer film maintains polymer electroneutrality and therefore PANi conductivity can be shifted to neutral pH. A similar method has recently been used by Willner *et al.* and successfully applied for the detection of AA[96]. Summarizing, the literature provides a wide range of successful choices upon PANi modification. The method selected, with its advantages and disadvantages, will depend on the requirements of the application.

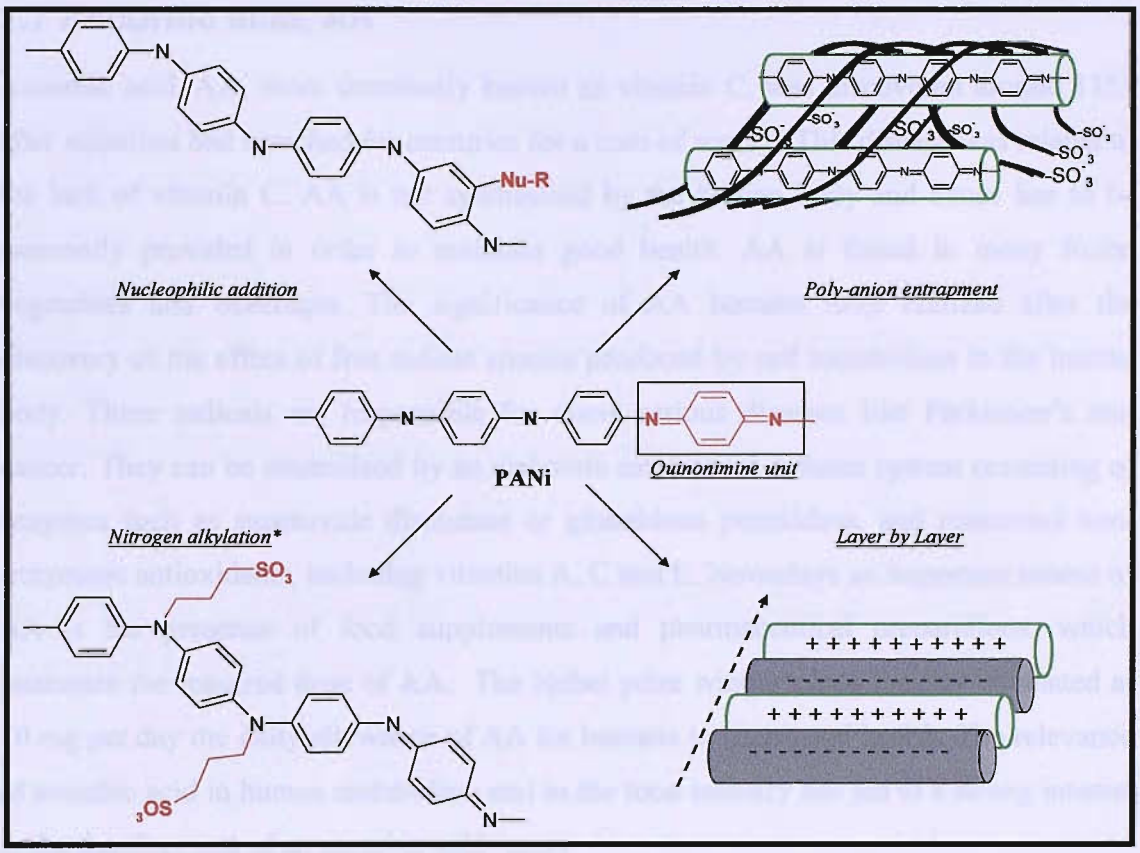

Figure 1.8. *Reaction schemes of the most successful approaches up to date to avoid PANi deprotonation.*

1.7 Ascorbic acid, AA

Ascorbic acid, AA, more commonly known as vitamin C, was discovered around 1753 after scientists had searched for centuries for a cure of scurvy. This disease was related to the lack of vitamin C. AA is not synthesized by the human body and hence has to be externally provided in order to maintain good health. AA is found in many fruits, vegetables and beverages. The significance of AA became fully realized after the discovery of the effect of free radical species produced by cell metabolism in the human body. These radicals are responsible for many serious diseases like Parkinson's and cancer. They can be neutralized by an elaborate antioxidant defence system consisting of enzymes such as superoxide dismutase or glutathione peroxidase, and numerous non-enzymatic antioxidants, including vitamins A, C and E. Nowadays an important source of AA is the presence of food supplements and pharmaceutical preparations, which guarantee the required dose of AA. The Nobel prize winner Linus Pauling estimated at 10 mg per day the daily allowance of AA for humans to keep good health. The relevance of ascorbic acid in human metabolism and in the food industry has led to a strong interest in the development of an ascorbic acid sensor.

1.8 AA oxidation at bare electrodes

The direct electrochemical oxidation of AA is possible but requires high overpotentials. AA posses two acidic protons (H_2A) with $pK_{a1} \sim 4.2$ and $pK_{a2} \sim 11.57$ [97]. Thus, in neutral solution AA exists as a monodeprotonated ascorbate anion, HA^-. The equilibrium potential of the couple is +0.06 *vs.* NHE but oxidation at bare glassy carbon or platinum electrodes requires potentials of +0.40 V or +0.60 *vs.* SCE, respectively[89, 98]. These high overpotentials lead to the generation of side reaction products, which are irreversibly adsorbed on the electrode surface, leading to electrode fouling. The fundamental electrode mechanism for AA oxidation has been examined at a number of metals electrodes. The electrochemical oxidation of AA has been investigated at carbon electrodes by Kuwana *et al.*[99] on platinum electrodes by Brezina *et al.*[97] and at mercury and gold electrodes by Aldaz *et al.* [100-108]

AA is oxidized to Dehydroascorbic acid (DHA), in the potential range of platinum oxide formation, figure 1.9. The adsorption of AA on Pt electrodes covers 68 % of the hydrogen adsorption sites[97]. It suppresses the hydrogen adsorption/desorption peaks, hindering complete activation of the electrode surface. This is probably the main disadvantage of metal electrodes. They perform well for mechanistic and kinetic investigations but are not suitable to be used as amperometric sensor devices due to poor selectivity in the presence of interferences due to the high overpotential required for its oxidation.

The overall reaction can be classified as an EEC process[98]:

$$AH_2 \rightleftharpoons A + 2H^+ + 2e^-$$

$$A + H_2O \rightleftharpoons B$$

Where AH_2, A and B correspond to ascorbic acid, dehydro-L-ascorbic acid and 2,3-diketogluconic acid.

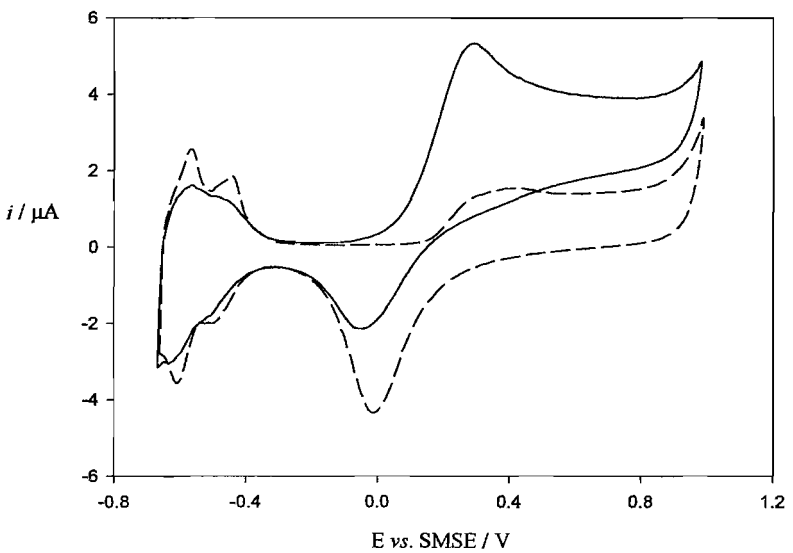

Figure 1.9. *Characterization of a Pt disc electrode, a = 250 μm, in 1M H_2SO_4, in the presence, solid line, and absence, dashed line, of 5mM AA. The electrode potential was swept from -0.60 to +1.0 V vs. SMSE at a scan rate of 50 mV s^{-1}. Solution was degassed with argon for 15 min and temperature controlled at 25±0.1 °C with a thermostatic bath.*

It is accepted in the literature that at low pH, the oxidation of AA to DHA proceeds via two consecutive one electron process involving the participation of a radical anion

intermediate. The ascorbate anion radical intermediate has a long half life and has been detected by Electron Spin Resonance/Electron Paramagnetic Resonance (EPR/ESR)[108-110]. The last product, DHA, undergoes fast hydration reaction characteristic of carbonyl groups to form the final electroinactive product, 2-3 diketogluconic acid[100, 111-113].

It has to be noticed that at pH values lower than the first pK_a value of AA, two protons are involved in the reaction whereas at neutral pH, the oxidation process will only involve the loss of a single proton owing to the fact that AA will be deprotonated as ascorbate, AH^-. Figure 1.10 shows the proposed reaction scheme.

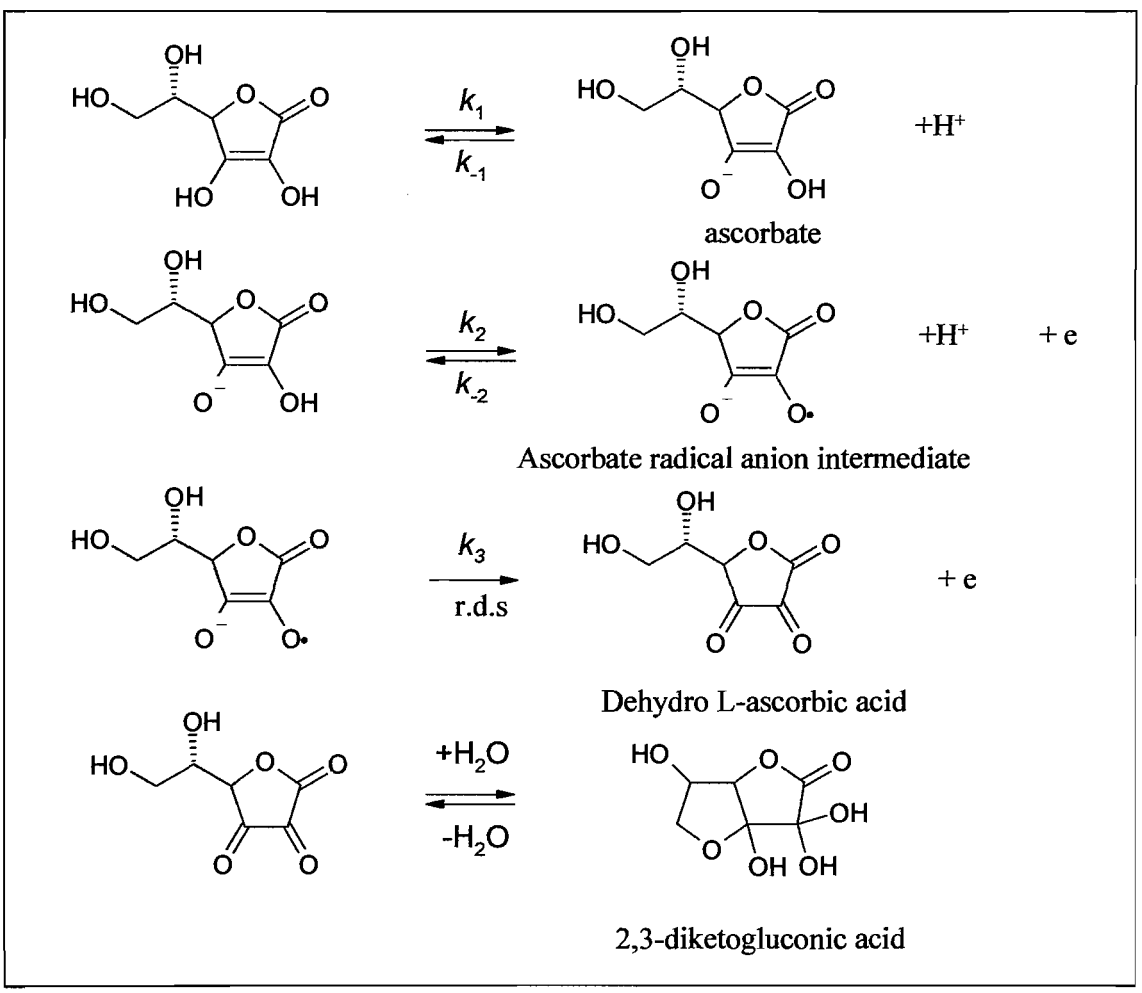

Figure 1.10 *Proposed reaction mechanism for ascorbate oxidation in acidic media*[97, 100, 101, 111]. *At low pH AA oxidation proceeds via two consecutive one electron processes involving the participation of a radical anion intermediate.*

k_1 and k_2 are assumed to be in rapid equilibrium and it is considered that the rate determining step, r.d.s., is given by k_3 in figure 1.10. Karabinas and Jannakoudakis extended Brezina's studies for AA oxidation on Pt electrodes giving a complete analysis of electrode kinetics in sulphuric acid solution[111]. At constant ionic strength in acidic solutions, AA oxidation showed a Tafel slope of 60-65 mV/decade, giving a reaction order of 0.95 respect to AA and a value of -1.90 with respect to H^+. These reaction orders are very close to their theoretical values 1 and -2.

FT-IR studies[108, 110] have shown that the presence of linearly bonded carbon monoxide, generated from the degradation of 2,3-diketogluconic acid, is the main adsorbate responsible for poisoning of the Pt surface[110]. Similar behaviour was observed at gold and mercury electrodes by Aldaz *et al.*[100, 113]. Due to carbon monoxide poisoning, the Pt electrode surface has been modified in many different ways in order to achieve a reliable response for AA oxidation. In the literature, electrocatalytic oxidation of AA at a CME has been extensively studied. Among all the diversity of CMEs, we want to emphasize in electrodes modified by conducting polymers. These methodologies are now discussed with reference to specific examples below.

1.9 AA oxidation at modified electrodes

The selective determination of AA is of much interest, especially in bioelectrochemistry. As described in the previous section, metallic electrodes are suitable for mechanistic and kinetic investigations, but do not perform well as materials in amperometric sensor devices. This is due to the irreversible adsorption products formed after AA oxidation. Only carbon electrodes appear to produce a better response if preteated[114].

In addition, the oxidation of AA at metal electrodes only occurs at high anodic potentials. Far above its redox potential. This is another disadvantage added to the electrode poisoning. At high anodic potentials, many organic molecules oxidize and this makes it difficult to achieve the selective oxidation of AA. Consequently, not even carbon electrodes are suitable materials for the selective oxidation of AA. There is a vast collection of good papers for modified Pt electrodes and their application to AA

oxidation present in literature. Due to the scope of this thesis, we will focus on Pt electrodes modified by redox or conducting polymers and its application to electrode kinetics.

Majda and Van Koppenhagen used heterogeneous poly(acrylamide) and acrylamide-vinylpyridine copolymeric gels containing ion exchanged ferricyanide ions as redox mediators[115, 116]. Convincing evidence for the mediated oxidation of ascorbic acid by ferricyanide ions, as well as the direct oxidation of the substrate at the Pt electrode is presented. The AA oxidation potential is also lowered to 0.20 V *vs.* Ag/AgCl relative to that for the direct reaction ~ 0.40 V *vs.* SCE. The kinetics of the mediation were examined in terms of the Andrieux-Saveant theory[117-123]. The mediation was found to be 'R+S', where the rate of the catalytic reaction and the rate of substrate diffusion jointly control the overall reaction rate.

The second and most common approach is using modified conducting polymers. Using conducting polymers for the detection of AA has many advantages. Firstly, it provides active groups, which can act as specific sites for the selective oxidation of AA. As AA in an analyte of interest in different areas such as, medicine, the food industry or physiology it is often necessary to measure AA in biological fluids. These fluids normally have pH values between 5 and 7. Some conducting polymers can become insulating at these pH. Among conducting polymers, a good discussion point in the literature is whether PPy or PANi films are best for AA oxidation.

Diaz *et al.* around 1979 introduced the excellent electrochemical properties of PPy and its application in electrocatalysis[40, 124-130]. Ewing and co-workers[131] were probably the first to use PPy films as electrocatalytic surfaces for AA oxidation. Although they did not carry out any kinetic analysis it is clearly presented that AA is oxidized at PPy films. The electrochemical response obtained is attributed to the fact that oxidized PPy films contain fixed cationic sites which minimized electrostatic repulsion between the ascorbate anion and the polymer surface[131].

It was a few years later when Lyons and Cassidy carried out an interesting analysis of the reaction kinetics between PPy and AA using a rotating disc electrode, RDE[98]. Their experiments carried out in 0.1 M NaCl solutions, showed that the voltammetric peak current varies in a linear manner with the square root of the scan rate, indicating rapid electrode kinetics. Consequently the oxidation is mass transport controlled[18]. It is significant to note that linear Koutecky-Levich plots (first order kinetics) displaying zero intercepts were obtained, regardless of the thickness of the different modified PPy films. It is also one of the first papers introducing a deep study of where the AA oxidation takes place in a PPy film. They concluded that the ascorbate reacts at the polymer/solution interface and not within the polymer matrix. The diffusion coefficient of AA in 0.1 M NaCl solution was estimated to be 5.5 x 10^{-6} and 6.6 x 10^{-6} cm^2 s^{-1} for PPy/Cl^- and PPy/DBS^- modified films respectively. This is somehow unclear, because if the reaction occurs at the polymer solution interface, the diffusion coefficient for AA should not depend on the type of polymer used.

Besides, this is an excellent agreement with the reference value obtained by Karabinas and Jannakoudakis, 6.5 x 10^{-6} cm^2 s^{-1} at bare Pt electrodes in acidic solutions[111]. From their RDE analysis the reaction order using PPy/Cl^- films was found to be 0.98 with respect to ascorbate and -0.94 with respect to H^+. Since in NaCl solution AA will be deprotonated as ascorbate, these values are a very good agreement with the theoretical values of 1 and -1 respectively.

However, in the case of PPy/DBS^- films the reaction order was 0.47 with respect to ascorbate and -1.09 with respect to H^+. This seems to be a bit puzzling as just the change in the counter ion from Cl^- to DBS^- make the reaction order for ascorbate differ by half of its value; even though, the reaction is happening at the polymer/solution interface for both polymers. In theory, this should not happen as the active sites for the reaction between PPy and AA will be exactly the same, and the only difference will be in the polymer morphology. Hence for two PPy films of the same thickness and different counter ion, one should expect the same response if the reaction is happening on the

polymer/solution interface. Lyons and Cassidy try to give an explanation to this unexpected response stating that AA oxidation takes place by a different reaction mechanism.

The main difference between the two mechanisms proposed lies in the ascorbate radical adsorption. The reaction order of 0.47 with respect to AA for PPy/DBS^- films is possibly due to a slow desorption of the ascorbate radical anion. Their analysis are based on a Temkin adsorption isotherm[132] which was also used by Conway *et al.*[133] with considerable success for hydrogen and oxygen evolution reactions, involving adsorbed intermediates.

Another approach to the study of AA electrocatalysis at modified Pt electrodes came around 10 years later by Bartlett and Wallace[89]. Due to the excellent results obtained with modified PANi films for the study of NADH oxidation[90-92] they decided to use the same modified films for AA oxidation. As for the PPy, films of Lyons and Cassidy, Bartlett and Wallace studied the oxidation of AA in citrate/phosphate buffer solutions on modified PANi films electrodeposited on a RDE. They obtained a diffusion coefficient of 5.0×10^{-6} cm^2 s^{-1} which is again in excellent agreement with the values obtained by Lyons and Cassidy[98] on PPy films and by Karabinas and Jannakoudakis[111] on bare Pt electrodes. Bartlett and Wallace also carried out a detailed RDE studies and established that oxidation of AA at modified PANi films occurs at the polymer/solution interface. It is interesting to see that two different and well known groups, using two different conducting polymers, agree with the location of the reaction, polymer/solution interface.

Considering how difficult is to obtain these results and seeing the extremely good similarities between Lyons and Bartlett it can be stated that AA oxidation at conducting polymers might occur at the polymer/solution interface. Bartlett and Wallace did not see any difference for the oxidation of AA between PANi/PVS and PANi/PSS films. We will go back to this point later on this thesis. Bartlett and Wallace carried out an excellent analytical study and showed that the reaction is mass transport controlled at low AA ascorbate concentrations, up to 5 mM, and that it becomes kinetically limited for higher

AA concentrations, 25 mM, which finally reach a saturated response similar to a Michaelis-Menten type mechanism. The Levich plots obtained in their initial analysis do not cross the zero origin suggesting the reaction may not follow a series of first order steps as normally considered[134].

It is proposed that the reaction may take place in a similar manner to that proposed for NADH oxidation at modified PANi films. As the oxidation of NADH is inhibited by the presence of NAD^+ they stated that NADH and NAD^+ compete for the active sites, which is certainly the case[92]. A nice experiment showing how the response of AA is suppressed by the presence of NAD^+, clearly suggest that AA reacts at the same sites as NADH. Hence, it can be suggested that both analytes might follow a similar reaction mechanism. They proposed that the reaction goes through an analogous reaction mechanism in which a complex is formed between the polymer and the ascorbate and that is followed by oxidation of bound ascorbate. The reaction mechanism presented is different to that proposed to Lyons *et al.*[98] for PPy films where no ascorbate anion radical intermediated are formed, figure 1.11.

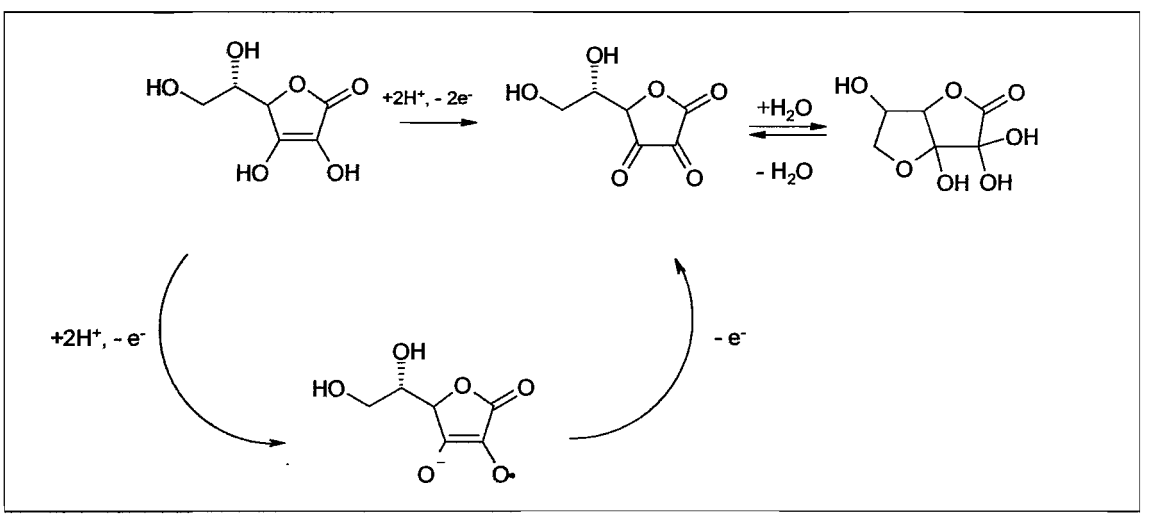

Figure 1.11. *Proposed reaction mechanisms for AA oxidation. At bare electrodes, AA oxidizes to DHA in a sequence of first order steps through an ascorbate radical intermediate*[100, 111-113].

Bartlett and Wallace[135] proposed that the ascorbate molecule attaches to the active sites of the PANi film and the oxidation occurs via a hydride transfer following a Michaelis-Menten type reaction mechanism, figure 1.12.

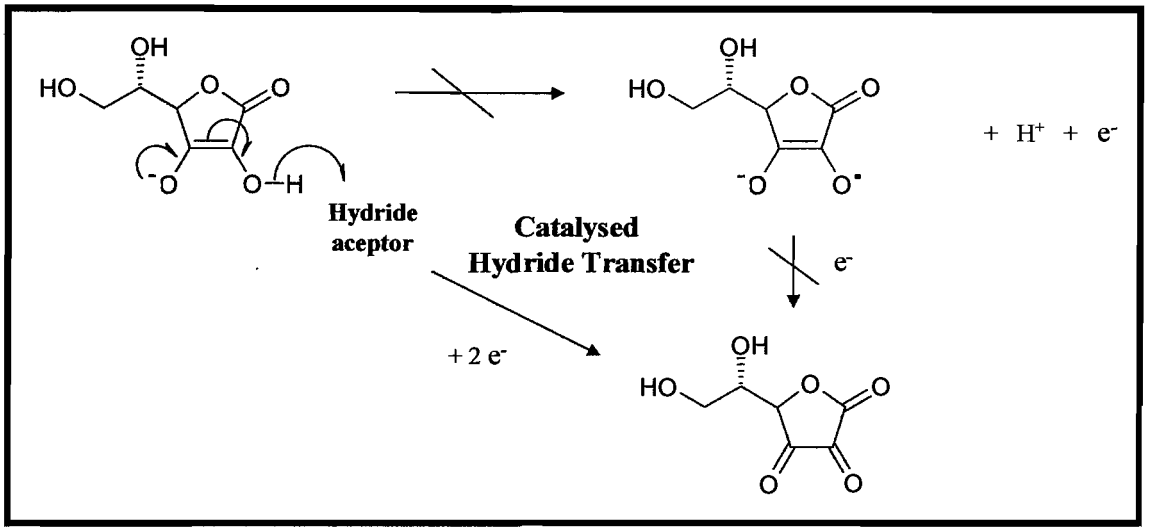

Figure 1.12. *Proposed mechanism for ascorbate oxidation in the presence of a hydride acceptor by Bartlett and Wallace*[135].

Their experimental data is analyzed using the theoretical model established in collaboration between Lyons and Bartlett for hydrated oxide layers[136]. The fitting of the experimental data with the theoretical model proposed is remarkable which is a good indication of the validity of the proposed model. If we believe that ascorbate oxidation may occur at the same PANi reactive sites as NADH does, the next reaction scheme, figure 1.13, can be adapted for the one proposed by Bartlett *et al*[91].

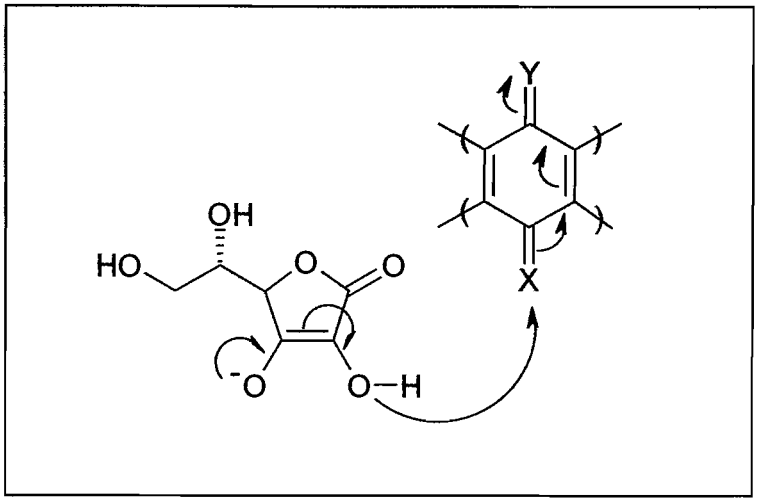

Figure 1.13. *Proposed reaction scheme for ascorbate oxidation by reaction with a redox mediator (adapted from Kitani et al.[137] and Bartlett et al.[91]). X is a group capable of accepting a hydride, Y is an electron deficient group.*

1.10 Enzyme Kinetics: Michaelis-Menten approximation

The first studies related to enzyme kinetics are attributed to Victor Henri in 1903 [138]. Henri proposed that the fundamentals accepted at that time for chemical catalysis were not applicable to enzyme catalysis. After years of discussion, in 1913 the ideas proposed by Henri were finally acknowledged due to the work published by Dr. L. Michaelis and Dr. Miss Maud L. Menten. The last authors following the work published by Henri studied a reaction catalyzed by an enzyme acting on a substrate. The experimental model used was the same as the one studied by Henri; the inversion of sucrose by invertase or saccharase. These studies led to the Henri-Michaelis-Menten equation, which is known as the Michaelis-Menten equation. Maybe, there is no other subject in biochemistry more discussed than the equation proposed by Michaelis and Menten.

Previous authors that studied the inversion of sucrose observed that at low concentrations of sucrose the initial rate of the reaction, V, was dependent on the concentration of substrate, [S]. However as the concentration of substrate increased the rate of the reaction decreased until the reaction is no longer dependent of the concentration of substrate, see figure 1.14.

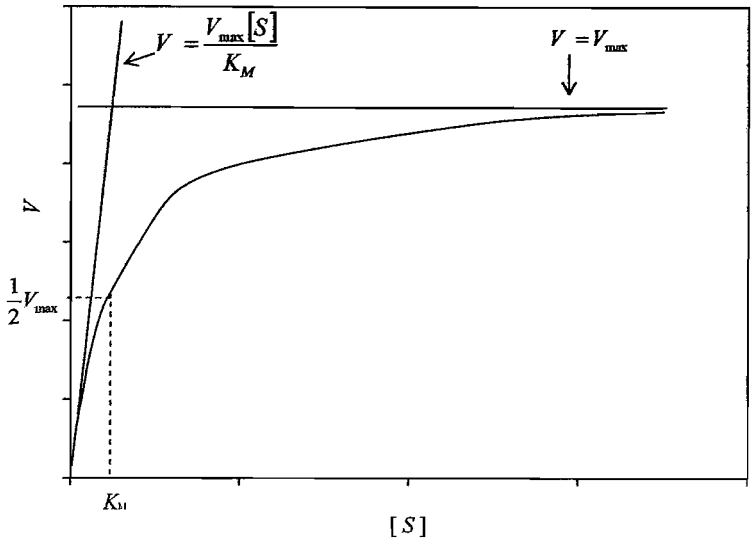

Figure 1.14. *Relation between reaction rate V and the concentration of substrate [S] defined by equation 1.9.*

Michaelis and Menten proposed that the enzyme [E] forms a complex [ES] with the substrate, [S], which decomposed to enzyme plus a product(s), [P].

$$[S] + [E] \underset{k_2}{\overset{k_1}{\rightleftharpoons}} [ES] \xrightarrow{k_{cat}} [E] + [P]$$

The total concentration of enzyme is given by $[E_T] = [E] + [ES]$ and the dissociative constant for the complex [ES] is specified by;

$$K_s = \frac{[E]\,[S]}{[ES]} = \frac{([E]-[ES])\,[S]}{[ES]} \quad (1.5)$$

Where $[E]$ and $[S]$ are the concentration of free enzyme and substrate respectively. Assuming that k_{cat} is the rate determining step and $k_{cat} << k_2$, the initial rate of the reaction is given by,

$$V = k_{cat}[ES] \quad (1.6)$$

Equation 1.6 shows that the rate of the reaction is determined by the complex enzyme-substrate [ES]. As $[ES]$ is difficult to obtain experimentally, a different expression is needed to obtain V_0. The rate of formation and decomposition for ES is given by;

Formation, $$\frac{d[ES]}{dt} = k_1 \left([E_T] - [ES] \right) [S] \quad (1.7)$$

Decomposition, $$\frac{d[ES]}{dt} = k_{-1} [ES] + k_2 [ES] \quad (1.8)$$

Considering the steady state approximation, Michaelis and Menten considered that the rate of formation and decomposition for the complex *ES* were equal.

$$k_1([E_T] - [ES])[S] = k_{-1}[ES] + k_2[ES]$$

From 1.5 and 1.6 we can obtain 1.9, known as the Michaelis-Menten equation;

$$V_0 = V_{max} \frac{[S]}{K_M + [S]} \quad (1.9)$$

Where V_{max} is the maximum velocity or maximum rate, see figure 1.14.

The equation proposed by Michaelis and Menten assumes:

a) Formation and fast equilibrium between the free enzyme and the initial substrate.
b) The concentration of the initial substrate is much higher then the concentration of enzyme. Therefore, [ES] is negligible compared to [E].
c) The rate of the reaction under considered is always the initial rate. V
d) $V = k_{cat}[ES]$
e) $k_{cat} << k_2$

where K_M is the Michaelis-Menten constant, $K_M = \frac{k_2 + k_{cat}}{k_1}$. Equation 1.9 is a conica of second order which graphic representation is shown in figure 1.14. The values for K_M range from 10^{-3}–10^{-6} M and represent the concentration of substrate at which, $V = \frac{1}{2} V_{max}$. However neither V_{max} nor K_M give an idea of the catalytic efficiency of an enzyme. As at low concentrations of substrate an enzyme shows its maximum efficiency,

$[S] << K_M$ Equation 1.9 can be expressed as; $V = \frac{k_{cat}}{K_M} [E] [S]$.

Where $\frac{k_{cat}}{K_M}$ is a rate constant and known as the specific constant. The value of $\frac{k_{cat}}{K_M}$ is in the order of 10^8 M^{-1} $s^{-1}$and it is used in biochemistry to compare the efficiency of different enzymes. Table 1.1 gives some representative values.

Enzyme	***Substrate***	k_{cat} (s^{-1})	K_M (M)	$\frac{k_{cat}}{K_M}$ (M^{-1} s^{-1})
Acetilcolinesterase	Acetylcholine	1.4×10^4	9.0×10^{-5}	1.6×10^8
ß-Lactamase	Benzilpeniciline	2.0×10^3	2.0×10^{-5}	1.0×10^8
Catalase	H_2O_2	4.0×10^7	1.1	3.7×10^7
NADH-deshidrogenase	NADH	43.0	4.3×10^{-5}	1.0×10^6

Table 1.1 *Representative values for different enzymes*[138].

1.11 General overview of thesis

The experimental results in this thesis are divided into four chapters. Chapter 3 focus on the electrodeposition and characterization of PANi films on Pt microelectrodes. Different parameters are presented such as the influence of the electrode roughness factor, electrolyte and methodology. In addition, the resulting modified microelectrodes are characterized under the electronic microscope, SEM. It is presented that flat PANi films can be obtained on small microelectrodes if the electrodeposition is controlled carefully by cyclic voltammetry. The shape of the polymer film is important to know in order to apply a kinetic model, which may give a better understanding of the analytical data obtained and improve the design of new coatings for ascorbate oxidation.

Chapter 4 shows the electroanalytical properties of the films produced as described in Chapter 3. It is presented that PANi conductivity can be successfully retained at neutral pH on modified microelectrodes by the incorporation of large counter anions such as PVS and PSS. In addition, alkylated PANi films are also presented as an alternative to PANi composites to retain polymer conductivity. The PANi films under study show good selectivity in relation to ascorbate in the presence of common interferences present in *in vivo* systems. Detection limit and reproducibility data is also presented.

Chapter 5 analyzes the analytical data obtained during Chapter 4 and a kinetic model will be proposed. It was found that PANi/PSS films presented half of the theoretical limiting currents for ascorbate oxidation. This interesting result was compared with the data obtained previously in our laboratories by Bartlett and Wallace[134] using a PANi/PVS rotating disc electrode.

Finally, Chapter 6 shows the experimental results in *in vivo* systems we obtained in collaboration with Dr. Janis Shute and Dr. Stefan Hanstein. PANi/PSS were used to measure ascorbate in low volume samples (100 μL) of human plasma. PANi/PVS were used to measure ascorbate in plant leaves. In both cases our results shows that the PANi films presented in this thesis can be used to measure ascorbate in *in vivo* systems.

Chapter 2

Experimental

2.1 Instrumentation

Electrochemical experiments were carried out either on a home made potentiostat or Autolab PGSTAT 30 (Utrecht, Netherlands). The electrochemical potentials are reported with respect to the saturated calomel (SCE) electrode or saturated mercury sulphate (SMSE) electrode in a two or three electrode configuration. Reference electrodes used in this work were homemade and built as described elsewhere[139]. A large area platinum gauze was used as the counter electrode, when needed. Platinum disc microelectrodes were home made by conventional methods[10]. Only the 2 and 5 μm Platinum disc electrodes were made by the Southampton glass blower, using Wollaston wire. Thomas Recording, GmbH, kindly supplied the needle type microelectrodes used in this work. All the electrochemical experiments shown in this thesis were carried out with the use of a Faraday cage. Electrochemical experiments were done in 25 mL Pyrex water-jacketed cells to control the temperature. Glassware was normally soaked in Decon solution diluted (1:10) with purified water and thoroughly washed at least three times. Scanning electron microscopy (SEM) analyses were performed on a Phillips XL30 ESEM TMP Scanning Electron Microscope (Phillips, The Netherlands).

2.2 Reagents

All aqueous solutions were freshly prepared using water purified using Whatman RO 50 and Whatman still plus systems. All reagents were commercially available and were employed as received, with the exception of aniline, which was purified either under vacuum or through a silica column, prior to use and stored in the fridge, in the dark and under argon atmosphere.

Aniline (99.5%, Aldrich), poly(vinylsulfonic acid), supplied as sodium salt solution in water (25 wt. % in H_2O) estimated molecular weight MW = 4000-6000 g/mol, Aldrich), poly(vinyl sulfate, potassium salt), supplied as a powder, estimated molecular weight

MW= 170,000 g/mol, poly(styrenesulfonic acid, sodium salt) supplied as powder, estimated molecular weight MW= 70,000 g/mol, Aldrich), ruthenium hexamine chloride, $Ru(NH_3)_6^{3+}$ (Aldrich), potassium chloride (AnalaR, Aldrich), propane sultone (99% and 98%, Aldrich), (+/-) camphorsulphonic acid, (98%, Aldrich), hydrochloric acid (AnalaR), sulphuric acid (98%, AnalaR), alumina (1.0, 0.3, 0.05 μm, Buehler), disodium hydrogen orthophosphate (99.5 % Aldrich), citric acid (99.5 %, Aldrich), uric acid (>99 % Aldrich), glutathione (>99 % Aldrich), vitamin E (α-tocopherol) (97% Aldrich), L-Histidine (>98 % Aldrich), acetic acid (>99 % Aldrich), lactic acid (85% Fluka), salicylic acid (>99% Sigma-ultra), maleic acid (99 % Aldrich), phenol (99 % Aldrich), albumin from bovine serum (BSA), pH ~7 (1 % (w/v) in H_2O), ≥96% (agarose gel electrophoresis), lyophilized powder (Sigma) and L-ascorbic acid (99.5%, Aldrich), were used in this work.

2.3 Microelectrode characterization and cleaning procedures

Platinum electrodes were hand polished directly prior to use with a slurry of 1.0, 0.3 and 0.05 μm alumina, Buehler. Afterwards they were washed with deionized water and alumina particles were removed from the surface by further microelectrode polishing on a wet polishing cloth, Buehler. In some cases, it was necessary to use concentrated sulphuric acid or sonication in distilled water for a better surface cleaning. Microelectrodes were washed with double deionized water and dried with a tissue paper, prior to experiments.

Microelectrode characterization was performed by standard electrochemical procedures. The microelectrode radius was calculated from the limiting current obtained from 5 mmol dm^{-3} ruthenium hexamine chloride, $Ru(NH_3)_6^{3+}$, in 0.25 mol dm^{-3} KCl by the diffusion limiting current equation for microelectrodes[140], $i = 4nFDCa$, where, i is the limiting current, n is the number of electrons involved, F is the Faraday constant, D is the diffusion coefficient for ruthenium hexamine (D = 8.8 x 10^{-6} cm^2 s^{-1})[141], C is the analyte concentration and a is the microelectrode disc radius.

Electrochemical cleaning procedures were performed by cycling the microelectrodes in 1 mol dm^{-3} sulphuric acid solution, between hydrogen and oxygen evolution, normally at a sweep rate of v = 200 mV s^{-1}. The electrode potential before and after acid cycling was kept at +0.20 V *vs.* SMSE, to ensure no modification on the electrode surface. Cycling in acid was stopped when resolved hydrogen adsorption/desorption peaks and well defined oxide formation and stripping were obtained.

2.4 Polymer deposition

2.4.1 Electrodeposition by cyclic voltammetry

PANi films were deposited on platinum microelectrodes by repeatedly cycling the potential at a scan rate, v = 50 mV s^{-1}, in an aqueous solution containing 0.1 mol dm^{-3} aniline and 1.0 mol dm^{-3} hydrochloric acid or 1.0 mol dm^{-3} sulphuric acid. The electrochemical deposition was started by sweeping the potential from -0.20 V to +0.90 V *vs.* SCE for the first scan, to initiate polymer growth, and then continuing cycling between -0.20 V and +0.80 V *vs.* SCE. Temperature controlled at 25 °C with the use of a thermostatic bath and degassed by bubbling Ar for 15 min.

Composite poly(aniline)-poly(vinylsulfonic acid), PANi-PVS, films were electrodeposited from a solution containing, 0.1 mol dm^{-3} aniline and 1.0 mol dm^{-3} hydrochloric acid or 1.0 mol dm^{-3} sulphuric acid and 22 % PVS. The electrochemical deposition was started by sweeping the potential from -0.20 V to +0.90 V *vs.* SCE for the first scan at v = 50 mV s^{-1}, to initiate polymer grow, and then continuing cycling between -0.20 V and +0.75 V *vs.* SCE. The temperature was controlled at 25 °C with the use of a thermostatic bath and degassed by bubbling Ar for 15 min.

When the counter ion, PVS, supplied as sodium salt solution in water (25 wt. % in H_2O) estimated molecular weight, MW = 4000-6000 g/mol, was passed through an ion exchange column, to eliminate Na^+ ions, the electrochemical deposition was started by sweeping the potential from -0.20 V to +0.90 V *vs.* SCE for the first scan at v=50 mV s^{-1}, to initiate polymer grow, and then continuing cycling between -0.20 V and +0.78 V *vs.*

SCE. Temperature controlled at 25 °C with the use of a thermostatic bath and degassed by bubbling Ar for 15 min.

Composite poly(aniline)-poly(vinyl sulfate, potassium salt), were electrodeposited identically as PANi-PVS, films.

Composite poly(aniline)- poly(styrenesulfonic acid), PANi-PSS, films were identically deposited from a solution containing, 0.1 mol dm^{-3} aniline and 1.0 mol dm^{-3} hydrochloric acid or 1.0 mol dm^{-3} sulphuric acid and 22 % PSS. The electrochemical deposition was started by sweeping the potential from -0.20 V to +0.90 V *vs.* SCE for the first scan at v=50 mV s^{-1}, to initiate polymer grow, and then continuing cycling between -0.20 V and +0.78 V *vs.* SCE. The temperature was controlled at 25 °C with the use of a thermostatic bath and degassed by bubbling Ar for 15 min.

Composite poly(aniline)-poly(vinylsulfonic acid)- poly(styrenesulfonic acid), PANi-PVS-PSS, films were electrodeposited from a solution containing, 0.1 mol dm^{-3} aniline and 1.0 mol dm^{-3} hydrochloric acid and 22 % PVS. The resulting PANi-PVS film was cycled between -0.20 and +0.50 V *vs.* SCE, v = 50 mV s^{-1}, for about 50 cycles, in a solution of 1.0 mol dm^{-3} hydrochloric acid and 22 % PSS, producing the desired PANi-PVS-PSS. The temperature was controlled at 25 °C with the use of a thermostatic bath and degassed by bubbling Ar for 15 min.

2.4.2 Electrodeposition by potential step

All PANi films were deposited on platinum microelectrodes by stepping the potential from 0.25 V to +0.90 V *vs.* SCE and held during different times in order to grow polymers of different thicknesses. The compositions of the solutions were the same as during the cyclic voltammetric experiments. The temperature was controlled at 25 °C with the use of a thermostatic bath and degassed by bubbling Ar for 15 min.

2.5 PANi alkylation

PANi films were electrodeposited by cycling voltammetry on Pt microelectrodes from a solution containing 0.1 M aniline monomer and 1M HCl, as the electrolyte. The potential was scanned from -0.20 V to +0.90 V *vs.* SCE for the first cycled at 50 mV s^{-1} and afterwards, the anodic potential was lowered to +0.80 V for the subsequent cycles. After polymer electrodeposition, modified electrodes were thoroughly washed with deionized water to remove any excess of the aniline monomer. PANi films were characterized in 1 M HCl solution by cycling the potential between -0.20 and +0.50 V *vs.* SCE at 50 mV s^{-1}. In all cases, films were reduced at -0.20 V *vs.* SCE for 5 min. Stable and reproducible voltammograms were obtained, indicating that the PANi films were well adhered to the microelectrode surface. Immediately after polymer characterization, PANi/Cl^- films were reduced electrochemically by applying a constant potential of -0.20 V *vs.* SCE for 10 min. Afterwards, polymer was washed with deionized water and the electrode body carefully dried with tissue paper. The electrodes were introduced in 2M sodium hydroxide aqueous solution, $T \approx 20$ °C, for 1 hr, in order to eliminate all protons within the PANi/Cl^- film.

Alkylation of the unprotonated reduced form of the PANi/Cl^- film was carried out by direct exposure overnight of the polymer film to neat propane sultone. At room temperature, T ≈ 15 to 20 °C, propane sultone (98 and 99% Aldrich) is a solid, although it melts with gentle heating. Consequently, electrodes were exposed to neat propane sultone and left inside an oven, overnight, at $T \approx 35$ to 40 °C. In all cases, after polymer exposure to neat propane sultone, the polymer film was thoroughly rinsed with deionized water in order to remove the excess of unreacted propane sultone. Microelectrodes were finally dried at room temperature and characterized in acid and neutral pH solutions.

2.6 Polymer characterization

2.6.1 In acid

After polymer electrodeposition, the resulting films were washed in acid solutions and then characterized using cyclic voltammetry by holding the potential at -0.20 V *vs.* SCE for 3 min to reduce the film fully. Afterwards films were characterized by cycling the potential between -0.20 and +0.50 V *vs.* SCE at v = 50 mV s^{-1} in 1 mol dm^{-3} acid solution. Stable and reproducible voltammograms were obtained, indicating that the PANi films were well adhered to the microelectrode surface. The temperature was controlled at 25 °C with the use of a thermostatic bath and solution degassed by bubbling Ar for 15 min. The charge passed during the deposition of the films and the charge passed during the characterization of the freshly deposited films in acid solution, were measured by introducing experimental data in a computer package Origin 6.0 and integrating the area under the emeraldine peak.

2.6.2 In buffer

After polymer characterization in acid solution, films were reduced at -0.20 V *vs.* SCE and then transferred to a 0.1 M citrate / 0.2 M phosphate solution, pH = 7. The polymer film was held at -0.20 V *vs.* SCE for 3 min prior to start the polymer characterization.

Composite PANi-PVS, were characterized between -0.20 and +0.30 V *vs.* SCE at v = 50 mV s^{-1}. Composite PANi-PSS, Composite PANi-PVS-PSS, and Composite poly(aniline)-poly(vinyl sulfate, potassium salt), were characterized between -0.25 and +0.50 V *vs.* SCE at v = 50 mV s^{-1}.

2.7 Analysis of interferences

Composite PANi films were exposed to different potential interferences. The polymer film was reduced at -0.20 V *vs.* SCE for 3 min. Afterwards, the potential was stepped from -0.20 to +0.10 V *vs.* SCE. The film was allowed to equilibrate for about 10 min. Once a stable background current was observed, a known amount of ascorbic acid was added to the solution. As soon as the current equilibrated, the following interferences

(0.20 M) were screened by holding the electrode potential at +0.10 V *vs.* SCE; glutathione, uric acid, acetic acid, lactic acid, salicylic acid, maleic acid, phenol and vitamin E. After the screening process, AA was added again to the solution, and the expected increase in current was obtained, indicating that the PANi film was not inhibited or modified in the presence of all these substrates.

2.8 HPLC analysis

A Shimadzu LC-10AD HPLC integrated with a Class-LC10 system was used with an UV-visible detector. For data acquisition, Shimadzu SPD-10A software was used. Separations were achieved using a 250 mm × 4.6mm Phenomenex LiChrospher®100–RP18 5μm C18 column. The LC-analyses were performed under isocratic mode at a flow rate of 1 ml min^{-1} with sample injections of 20 μL. Samples and standard solutions were chromatographed at ambient temperature (24.0±2.0 ◦C), using 0.2% metaphosphoric acid/methanol/acetonitrile (90:8:2, v/v/v) as the mobile phase (flow rate of 1.0mL min^{-1})

2.9 Blood Sample collection

Blood from 6 volunteers was collected by venipuncture into evacuated tubes and immediately centrifuged at 3000 rpm for 5 min at 25 °C. Plasma was mixed with an equal volume of 5% metaphosphoric acid (MPA) containing 1 mmol/L of EDTA. After this centrifugation step the supernatant was aliquoted and then stored at -10 °C.

2.10 Computer Software

The analysis of the experimental data has been carried out using a non-linear least squares fitting program supplied with the scientific graphic packages Sigma Plot 8.0. The curve fitting of the experimentally data obtained was carried out by entering the experimental values into the worksheet of the graphics package and plotted in an appropriate form so that the experimenter may approximate which factors limit the observed response, i.e. diffusion to the electrode, electrode kinetics, etc. This enables the experimenter to propose a mechanistic model of the system based on the observed behaviour. Once a model has been proposed, the equation that best describes the system behaviour is written as a curve fit and entered into the graphic package. The software

then iteratively determines the best values of the given parameter(s) in the equation to produce a theoretical curve as close to the experimental values as possible. It should be however be noted that the resulting parameters obtained after the curve fit are not unique, and incorrect choice of the starting parameter(s) can result in the program finding a false minimum. The amount of error in these experimental parameters is also calculated by the program using the standard deviation.

Chapter 3

Electrodeposition of PANi films on platinum microelectrodes

3.1 Objective

Our main interest through this Chapter is the production of stable and reproducible PANi films on small Pt microelectrodes, $12.5<a<1$ μm. The influence of the electrode roughness factor, microelectrode radius, aniline monomer concentration, electrolyte and coating method has been investigated. Some of the experiments have been done on ultra small needle type microelectrodes with elliptical or conical geometries. PANi coated microelectrodes were applied for the detection of AA in real systems and discussed through Chapter 6.

3.2 Introduction

It is apparent that the electrodeposition of a polymer film occurs by a process of nucleation and growth. Nuclei appear at active sites on the substrate and the growth occurs via the incorporation of further ions from the solution. The mechanism of the electrodeposition of polymers is similar but not identical to that shown by metals. According to Compton[142], nucleation and growth in metals can be broadly classified into two categories; 'interfacial (or charge) controlled', in which the nucleus growth rate is limited by the rapidity with which ions can be incorporated into the new phase, and 'diffusion controlled' in which the nucleus growth is limited by the rate at which material is transported through solution to the electrode surface. The first is favoured by high concentrations and low deposition overpotentials and the second is favoured by low concentrations and high overpotentials. Although certain systems also tend to one or the other. For instance, PbO_2 is usually deposited under charge control while Hg is a known example of diffusion control. Recommended reading related to the detailed mechanism of nucleation processes can be found in the work of Fletcher[143-146] and Fleischman[143, 145, 147, 148].

The morphology of the resulting film (metal or polymer) is highly influenced by numerous parameters such as electrolyte, counter ion, electrochemical method, etc. The morphology of the film is of vital importance for certain applications and therefore has to be controlled carefully. Pletcher *et al.*[149] have shown the importance of these parameters during the electrodeposition of mesoporous Pd films on Pt microelectrodes via hexagonal liquid crystal template for the detection of nitrite. On the other hand, Casella and Guascito[63] described how the morphology of PANi film electrodeposited on a glassy carbon electrode can affect the detection of AA.

With this in mind, this Chapter is an attempt to asses the right conditions to produce stable and reproducible PANi films on small Pt microelectrodes as electrocatalytic surfaces for AA. It has not been the aim, however, to go into deep detail of the mechanism of nucleation processes on Pt microelectrodes. The characterization and application of the resulting modified microelectrodes will be discussed in more detail through the rest of the Thesis.

3.3 Characterization of disc and elliptical Pt microelectrodes

The geometrical area of a microelectrode can be obtained electrochemically or by the use of an electron microscope. Electrochemically, the area of a microelectrode is calculated from the steady state limiting current obtained while oxidizing or reducing a redox couple, whose diffusion coefficient is well known. On the other hand, if the microelectrode area is known, the diffusion coefficient can be calculated from the steady state limiting current. As mentioned in section 1.1, the steady state limiting current for a microdisc electrode is given by equation (1.2). Bruckenstein and Janiszewska[150] have recently published the equation describing the steady state limiting current at an elliptical microelectrode, equation (3.1).

$$i_{elliptical} = 4nFDCaG(m)^{-1} \qquad \textbf{(3.1)}$$

Equation (3.1) is not far away from the equation (1.2) and only differs in the equivalent radius $r = a\,G(m)^{-1}$, established by the ellipse perimeter. This is calculated by an elliptical integral of second order given inside the term $G(m)$. In this case, a and b, are the major and minor semiaxes of the ellipse with area, $A_{ellipse} = \pi ab$. See Appendix A.1 for an

illustrative example. Steady state limiting current equations for different microelectrode geometries can by found at Oldham *et al.*[2] For a selection of articles related to the calculation of the diffusion coefficient of a redox couple by the use of a microelectrode see references [141, 151-154]. Figure 3.1, shows a scanning electron image, SEM, of a needle type elliptical platinum microelectrode used in this work.

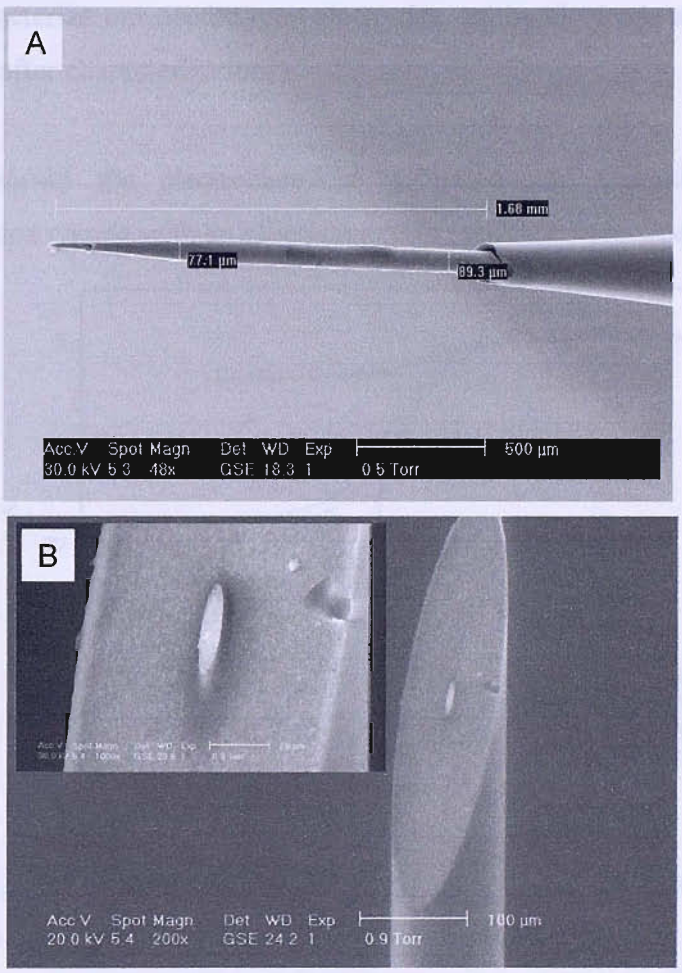

Figure 3.1 *Scanning electron image, SEM, of an elliptical needle type platinum microelectrodes supplied by Thomas Recording. Top figure shows the dimensions of the microelectrode glass body. Bottom figure and inset (B) shows a magnification of the microelectrode tip, presenting the elliptical platinum-tungsten (95/5)% core metal insulated by the glass body. Using the microscope software, the minor ellipse radius* $a = 3.29\mu m$ *and the larger ellipse radius* $b = 16.00\ \mu m$ *were determined.* $A_{ellipse} = \pi ab = 165.29\ \mu m^2$.

Needle type microelectrodes are very fragile and mechanical polishing is not possible. Within the redox couples available; $Fe(CN)_6^{4-}/Fe(CN)_6^{3-}$, $Ru(NH_3)_6^{3+}/ Ru(NH_3)_6^{2+}$, $IrCl_6^{2-}$ / $IrCl_6^{3}$ and the ferri/ferrocene redox couple. Pletcher *et al.*[141, 153] showed that the $Ru(NH_3)_6^{3+}/ Ru(NH_3)_6^{2+}$ redox couple undergoes electrochemical oxidation at the electrode surface without inhibiting electron transfer. Consequently, this is an excellent choice to characterize our needle type electrodes, as the electrode surface does not need to be polished after characterization.

Figure 3.2, shows the electrochemical reduction and oxidation of $Ru(NH_3)_6^{3+}/ Ru(NH_3)_6^{2+}$ redox couple with an elliptical needle type microelectrode.

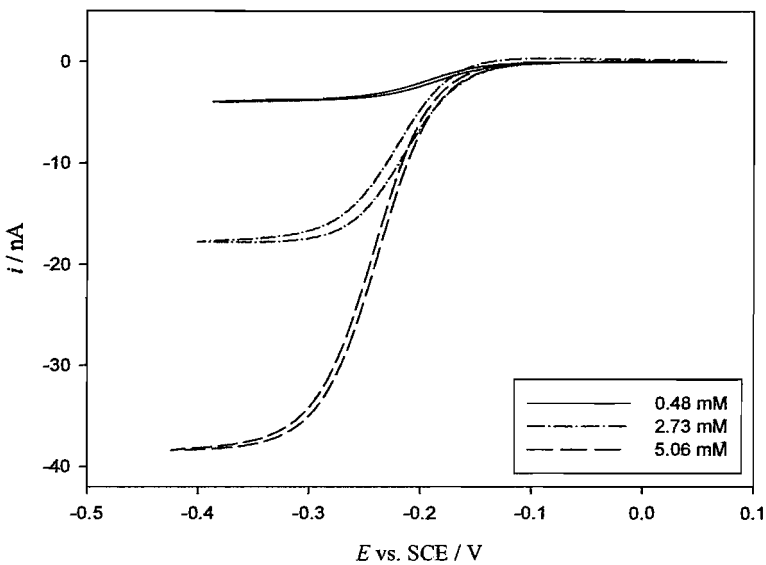

Figure 3.2 *Cyclic voltammograms obtained for a elliptical needle type platinum microelectrode similar as shown in figure 3.1. The potential was scanned at 5 mV* s^{-1} *from +0.05 V to -0.45 V vs. SCE in 0.48, 2.73 and 5.06 mM* $Ru(NH_3)_6^{3+}$ *in 0.25 M KCl as a supporting electrolyte. The third scan is shown. Major ellipse semiaxis, a=38.5 μm, minor semiaxis b = 12.9 μm. The term* $G(m)^{-1}$ *= 0.5562, calculated from equation 3.1. Solutions were degassed by bubbling Ar for 15min and temperature controlled at (25±0.1) °C with a water bath.*

As seen from figure 3.2, elliptical microelectrodes exhibit significant contributions from radial diffusion. Analogous to disc microelectrodes, the voltammetry present a sigmoidal

shape at low sweep rates, reaching a steady state value. The limiting current obtained is proportional to the electrode radius. The potential measured at $| E_{3/4} - E_{1/4} | = 60 \pm 2$ mV which agrees for a reversible one electron transfer process, n=1.

Therefore, knowing the values for the major and minor semiaxes (a,b) of the elliptical microelectrode, the term $G(m)^{-1}$ in equation 3.1 calculated from the table provided by Bruckenstein and Janiszewska[150], the diffusion coefficient for the $Ru(NH_3)_6^{3+}$/ $Ru(NH_3)_6^{2+}$ redox couple can be determined, table 3.1. See Appendix A.1 for an illustrative example.

$Ru(NH_3)_6^{3+}$ / mmol dm^{-3}	**i_{lim} / nA Electrode A**	**D_A / cm^2 s^{-1} x 10^{-6}**	**i_{lim} / nA Electrode B**	**D_B / cm^2 s^{-1} x 10^{-6}**
0.48	-3.94	9.5	-1.74	8.6
2.73	-17.8	8.6	-8.68	8.6
5.06	-38.4	9.3	-18.0	8.9
7.65	-57.6	9.3	-27.1	8.9
9.96	-73.9	8.9	-35.2	8.7

Table 3.1. *Steady state limiting current currents (i_{lim}) obtained from figure 3.1. The data here presented represent two elliptical needle type microelectrodes. The semiaxes of the ellipse were obtained by SEM. The diffusion coefficient, D, is calculated with equation 3.1. Electrode A; a=38.5 μm, b = 12.9 μm and $G(m)^{-1}$ = 0.5562. Electrode B; a = 21.35 μm, b = 5.0 μm and $G(m)^{-1}$ = 0.4892.*

The diffusion coefficient was obtained from the slope when representing the limiting current at different concentration; Electrode A, $D_A = 9.11 \times 10^{-6}$ cm^2 s^{-1} and electrode B, $D_B = 8.87 \times 10^{-6}$ cm^2 s^{-1}. These values are in good agreement with the one obtained by Pletcher and Beriet[141, 153] using Pt disc microelectrodes under similar conditions, $D_{Pletcher\ \&\ Beriet} = 8.8 \times 10^{-6}$ cm^2 s^{-1}.

The diffusion coefficient for $Ru(NH_3)_6^{3+}$/ $Ru(NH_3)_6^{2+}$ was also calculated using equation 3.1 by chronoamperometry (CA); stepping the potential from +0.05 to -0.45 *vs.* SCE and measuring the limiting current obtained at $t = 20$ s. The diffusion coefficient obtained by CA deviated 3 to 5 % depending on the electrode used when compared to CV.

Following the calculations described in this section, the area of the microelectrodes used in this work was calculated by equation 1.2 and 3.1 depending on geometry. The equation provided by Bruckenstein and Janiszewska[150] for an elliptical microelectrode was proven to be accurate either to calculate the diffusion coefficient of a reversible redox couple or to calculate the geometric area. This equation can be useful for small elliptical electrodes where the SEM may have difficulties providing accurate numbers. Microelectrodes used in this work were characterized as described in this section.

3.4 Electrodeposition of PANi on Pt microelectrodes

PANi films were produced by the electropolymerization of the aniline monomer in acidic conditions under potential sweep control. Figure 3.3 shows a typical voltammogram obtained when coating a platinum disc microelectrode, $a \approx 1.0$ μm.

In order to start the polymerization, the potential is scanned from -0.20 to 1.0 V *vs.* SCE during the first cycle, inset in figure 3.3. It can be seen that the current remains close to zero and increases sharply at around 0.80 V *vs.* SCE. The appearance of a loop in the voltammogram is attributed to nucleation on the electrode surface[51]. This is also observed on the electrodeposition of metal films. The peak current reached during the nucleation loop increased with the electrode surface area.

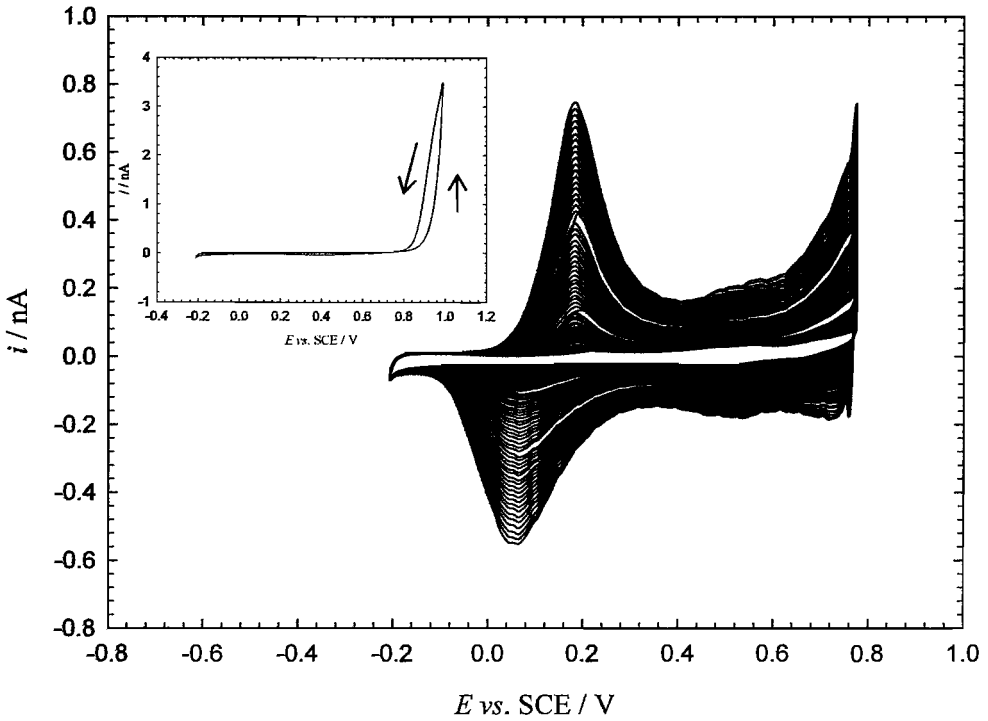

Figure 3.3 *PANi electrodeposition on a Pt disc microelectrode, a ≈ 1.0 μm in a solution of 0.1 M aniline in 1M HCl. The potential was scanned at 50 mV s^{-1} from -0.20 to +1.0 V vs. SCE for the first cycle, inset. Afterwards, the anodic potential was lowered to +0.78 V. Solution was degassed with Ar for 15 min and temperature controlled with a water bath at 25 °C. When the resulting polymer was characterized in oxygen free 1M HCl at 50 mV s^{-1} the charge density under the emeraldine reduced peak Q_{red} = 15.2 μC cm^{-2} which corresponds to an average thickness of the PANi film of ~0.76 μm. The thickness of the PANi film was calculated using the reduction charge measured under the emeraldine peak on a 20 mC cm^{-2} per 1 μm basis*[155].

The features seen in figure 3.3 are well known[39, 74]. The anodic and cathodic peaks at +0.20 V and +0.10 V belong to the oxidation/reduction of the leucoemeraldine / emeraldine redox state. The increase in current at approximately +0.6 V is due to the beginning of the oxidation to the second redox state emeraldine / pernigraniline. As the PANi film grows at around 0.50 V a small redox peak might appear. This peak can be used as a fingerprint to the formation of quinoimine units and it can be lowered or

eliminated by reducing the anodic limit. The influence of quinoimine units will be further discussed in section 3.5.

During the course of our experiments, the appearance of the first voltammogram, inset figure 3.3, was critical for a successful polymerization. In other words, by the look of the first voltammogram, the experimenter is able to asses if the electrodeposition will continue during the subsequent scans. If no nucleation loop is observed during the first cycle it is recommended to clean the electrode surface electrochemically or by mechanical polishing and possibly a fresh aniline solution is needed. This saves precious time as films not grown as described here resulted in irreproducible coatings and gave worse results when used as electrocatalytic surfaces for AA. In some cases, up to three nucleation cycles were needed to continue polymer growth. This effect was seen to be more important, somehow, as the microelectrode radius decreased.

In addition, the anodic limit was of critical importance for continued polymer growth. It has been reported in the literature that PANi nucleation and growth is related with the transition emeraldine / pernigraniline[156]. However, as already mentioned, cycling PANi to high anodic limits leads to polymer overoxidation[71]. Therefore the anodic limit has to be carefully controlled. This is due to the pH dependence of the last redox transition; Emeraldine $\leftrightarrow$ Pernigraniline + 2e + $4H^+$. Therefore the anodic limit at which the PANi is free of quinoimine units has to be characterized at the pH of the solution. In our case, pH=0, the anodic limit was maintained at +0.78 V *vs.* SCE after the first cycle. On the other hand, if the anodic potential is too low, $E < 0.60$ V *vs.* SCE no polymer growth is normally observed and if there is any, growth is slow. A careful control of this potential window 0.60 to +0.78 V *vs.* SCE is of critical importance to obtain a continued polymer growth with the desired morphology and free of quinoimine units.

3.4.1 Redox state of the electrodeposited PANi films

As can be seen from figure 3.3, the peak current for the different redox processes involved increases with the number of scans. This observation will only be possible if the PANi film is being deposited in its conducting state, emeraldine. This is a reasonable

assumption as the rate of film growth increases with film thickness. Whereas if the film was produced in the insulating state the rate of film deposition would decrease and eventually stop. Desilvestro *et al.*[157] developed a method to assess the polymer efficiency, meaning by polymer efficiency the rate of polymer growth. To determine the polymerization efficiency it is necessary to define two quantities; the overall charged passed at the end of each cycle (Q_i) and the charge passed during the reduction of the deposited film (Q_{red}). Desilvestro defined the ratio of Q_{red} to Q_i as the efficiency of polymerization, equation 3.2.

$$\frac{Q_{red}}{Q_i} = \frac{number\ of\ electrons\ required\ to\ reduce\ the\ polymer}{number\ of\ electrons\ required\ for\ electropolymerisation} \qquad (3.2)$$

From this ratio it is possible to determine which oxidation state the PANi has been deposited in. Previous work in our laboratories[134] (following the analysis proposed by Desilvestro) showed that PANi is electrodeposited in its conducting emeraldine state and reduced to leucoemeraldine during potential cycling. Our interest now, is to assess the conditions required to obtain a stable, reproducible and conducting film on small Pt electrodes.

3.4.2 Influence of the surface roughness; reproducibility

The reproducibility of the electrodeposition by cyclic voltammetry was studied. All the electrodes were characterized by cyclic voltammetry in 1 M H_2SO_4 before the experiment to evaluate the influence of the electrode surface state. The roughness factor, R_f, was calculated using the real surface area estimated from the charge under the hydrogen monolayer adsorption peaks using a conversion constant of 210 μC cm^{-2} [158]. The surface of the electrode surface was roughened to the desired R_f using SiC paper of different grades and alumina particle size. A low R_f value can be related to a smooth surface and vice versa.

Figure 3.4 shows the charge under the reduced emeraldine peak divided by the roughness factor R_f plotted versus the number of cycles during PANi electrodeposition at Pt disc microelectrodes, $a \approx 12.5$ μm, with different R_f.

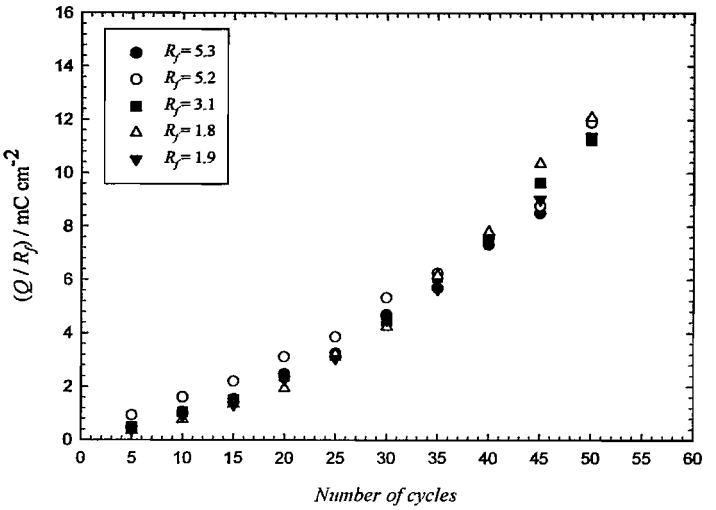

Figure 3.4 *Plot of the charge under the reduced emeraldine peak divided by the roughness factor with the number of cycles for PANi electrodeposition on a Pt disc microelectrode, $a \approx 12.5$ μm, with different roughness factor as indicated in the legend. PANi films were electrodeposited following the same procedure as figure 3.3 but in the presence of 1M H_2SO_4.*

After 50 cycles, the polymer film reached an approximate thickness of 3.25, 1.6 and 0.75 μm for R_f = 5.3, 3.1 and 1.8 respectively. The thickness of the PANi film was calculated using the reduction charge measured under the emeraldine peak on a 20 mC cm^{-2} per 1 μm basis[155].

Figure 3.4 shows that PANi growth is not dependent on the R_f and the reproducibility of the electrodeposition is consistent with the roughness factor.

The same trend as shown in figure 3.4 has been observed in the literature by different authors under similar conditions[157, 159]. It can be seen that after an induction period of about 5 to15 cycles the charge Q increased exponentially. This has been mentioned in the literature as two different growth processes. During the first cycles, induction period, a compact first layer of polymer film grows on top of the substrate. The faster growth rate observed afterwards is due to the growth on top of the existing film with a less dense structure. Both phases will present different polymer morphology and porosity.

Controlling the electrode roughness factor during our future experiments is essential to obtain the desired reproducibility, film thickness and morphology.

3.4.3 Influence of electrolyte and counter ion

In order to determine the influence of the electrolyte and counter ion on polymer growth the charge under the reduced emeraldine peak is plotted versus the number of cycles, figure 3.5.

The electrolyte and counter ion has a remarkable effect on the polymer growth. It appears that polymer growth is faster in H_2SO_4 than in HCl and growth rate decreases in the presence of PVS. The polymer film thicknesses after 20 cycles were approximately 0.4 μm for PANi/H_2SO_4, 0.29 μm for PANi/HCl, 0.15 μm for PANi/H_2SO_4/PVS and 0.05 μm for PANi/HCl/PVS.

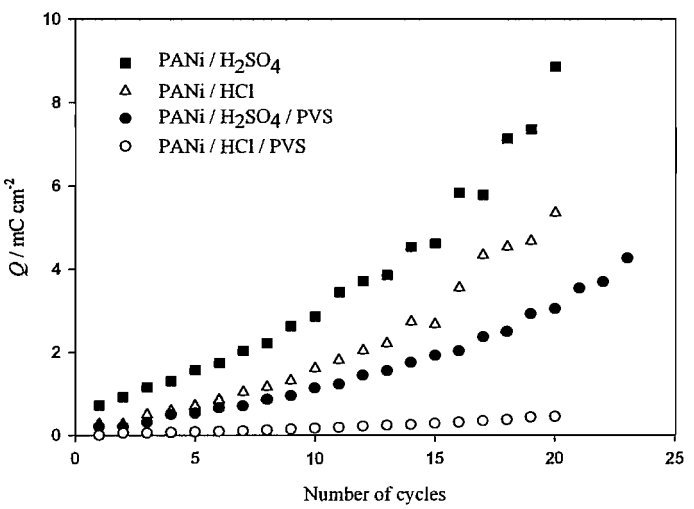

Figure 3.5 *Plot of the charge under the reduced emeraldine peak with the number of cycles for PANi electrodeposition on a Pt disc microelectrode, $a \approx 12.5$ μm, $R_f = 3.3$ in a solution of 0.1 M aniline in (A) 1M H_2SO_4, (B) in 1M HCl, (C) in 1M H_2SO_4 and 22% PVS and (D)1M HCl and 22% PVS. The electrodeposition procedure is the same as described in figure 3.3.*

It can be observed that after an induction period the charge Q increased exponentially for each case. It is generally agreed in the literature[157] that when using 0.1 to 0.2 mM aniline

and 1M electrolyte there is a dependence on the acid according to H_2SO_4 >> HCl > HNO_3 > $HClO_4$. There is still no clear explanation of the anion effect on aniline polymerization. Desilvestro *et al.* reported that the polymerization rate increases with increasing charge to ion size ratio of the anion and it is enhanced by increasing anion concentration[157]. Therefore, it seems that the anions participate specifically in the rate determining step of aniline polymerization in acidic solutions. For pH<1 aniline is fully protonated, pK_a = 4.63[157]. As protons are released during the formation of the dimer, one might expect that any anion acting as a proton scavenger may accelerate the PANi growth rate. However, the polymerization rates do not correlate with the values of the acidities.

Another interesting effect is the decrease of polymer growth rate by the addition of the PVS sodium salt. The addition of the PVS does not modify the solution pH = 0. When the PVS sodium salt was passed through an ion exchange column in order to exchange Na^+ for H^+ the growth rate was similar than without PVS. Exactly the same response was observed in the presence of PSS. Other authors in the literature reported either no difference[68] when PVS sodium salt is present or claim no influence[53] on the PANi growth rate in the presence of cations such as Li^+ or Mg^{+2}. FT-IR spectroscopical studies by Hyodo and Oomae[160, 161] confirmed that PVS or PSS are retained within the PANi film via potentiodynamic controlled polymerization. Further experimental and/or theoretical work is required in order to fully understand the mechanistic influence of anions on aniline polymerization.

3.5 Potentiostatic electrodeposition

In addition to potentiodynamically controlled polymerization the effect of constant potential upon film formation was studied. Figure 3.6 shows the experimental response obtained when stepping the potential from +0.20 V *vs.* SCE to +0.90 V in the absence (black lines) and presence of PVS (red dotted line)

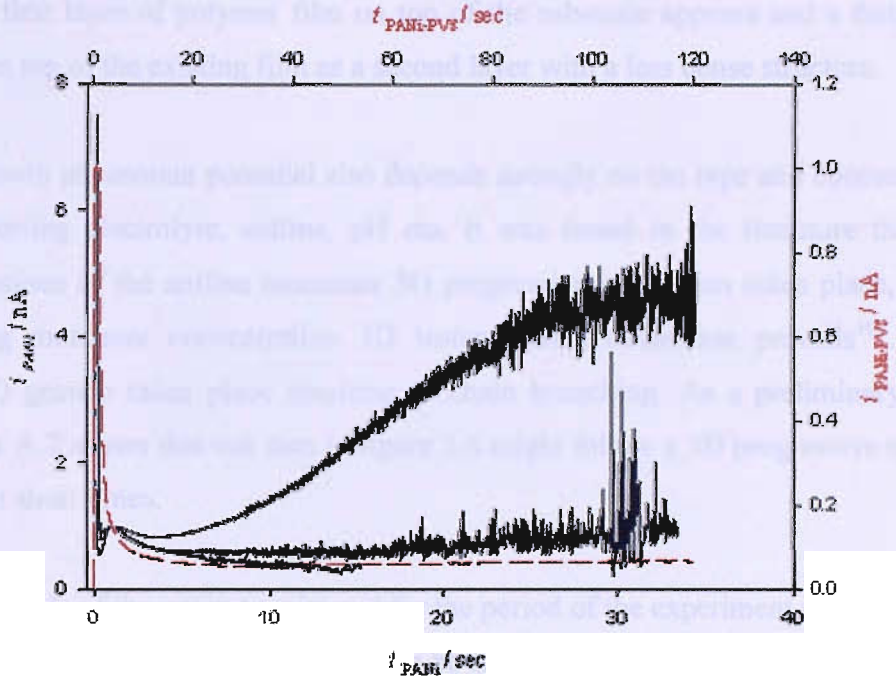

Figure 3.6. *Electrodeposition of 0.1 mM aniline and 1M H_2SO_4 in the presence (red dotted line) and absence (black solid lines) of 22% PVS sodium salt. Pt disc electrode radius $a \approx 12.5$ μm, $R_f = 1.8$. The electrode potential was stepped from +0.20 V to +0.90 V vs. SCE. Solution was degassed with Ar for 15 min and temperature controlled at 25 ° C.*

At time $t \approx 0$ min the sharp increase in the current is due to the double layer charging current and relaxation. It can be seen that the current transient for the three different electrodepositions of PANi/SO_4^{2-} (black solid lines) shows a broad peak with a current maximum at short times, t = 1.5min, and although the same potential is maintained during the experiment it is interesting to observe that in one case the current increases sharply at long times. This broad peak at short times was more difficult to observe in the presence of HCl but easier to spot for higher values of R_f.

The appearance of a current maximum in the course of a phase formation, t = 1.5min in figure 3.6, is usually associated with the processes of nucleation and growth of the new phase up to the formation of a full coverage layer[140]. Similar results were presented by Duic[162] and Tsakova[159] and the response obtained in fig 3.6 can be attributed to two growth processes. In a similar manner as under potentiodynamic polymerization a compact first layer of polymer film on top of the substrate appears and a further PANi growth on top of the existing film as a second layer with a less dense structure.

PANi growth at constant potential also depends strongly on the type and concentration of the supporting electrolyte, aniline, pH etc. It was found in the literature that at low concentrations of the aniline monomer 3D progressive nucleation takes place, and with increasing monomer concentration 3D instantaneous nucleation prevails[162]. At later stages 1D growth takes place resulting in chain branching. As a preliminary attempt, Appendix A.2 shows that our data in figure 3.6 might follow a 3D progressive nucleation process at short times.

The magnitude of the current registered for the period of the experiment is due to the high anodic potential E = 0.9 V *vs.* SCE. It can be seen that for longer times the experimental response becomes significantly noisy for all cases. Electronic noise was not observed in the presence of PVS or PSS. This effect has been reported in the literature and attributed to the accumulation of quinoimine units within the PANi film[55, 71]. Quinoimine units increase the film capacitance. After a certain time the current no longer increases and reaches a plateau. In this case, the film has reached a certain thickness and the resistance within the film is too high to allow further polymer growth.

Figure 3.6 also shows the current transient obtained during the electrodeposition of PANI/PVS/SO_4^{-2}, red dotted line. This time no peak maximum was observed and the electrodeposition time scale is much longer. The same effect was observed in the presence of PSS. The possibility to observe current maxima, indicating the particular nucleation process, depends on monomer concentration, on the potential of synthesis and on the counter ion present.

When the resulting PANi/H_2SO_4 films were characterized in 1M H_2SO_4 by cyclic voltammetry it was found that the charge under the reduced emeraldine peak was (180 ± 40) mC cm^{-2} which correspond to approximately (8 ± 2) μm film thickness. In the case of PANi/H_2SO_4/PVS it reached a film thickness of about 4 μm (80 mC cm^{-2}).

3.6 SEM characterization

3.6.1 Cyclic Voltammetry

Figure 3.7 shows a SEM image of a modified Pt microelectrode, a = 5.0 μm, where the polymer thickness was carefully controlled by cyclic voltammetry.

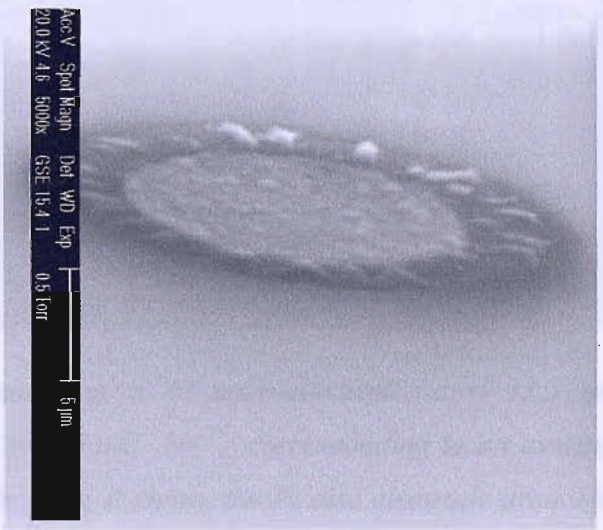

Figure 3.7 *Scanning Electron micrograph of a Pt disc microelectrode, radius, $a \approx 5.0$ μm, modified with a PANi/HCl/PSS film. The polymer film was electrodeposited from a solution containing 0.1 mol dm^{-3} aniline and 22% w/w PSS sodium salt in 1 mol dm^{-3} HCl solution in same manner as described in figure 3.3. Charge density under the emeraldine reduced peak $Q_{red} \approx 3.0$ mC cm^{-2}.*

The SEM image shows that the Pt microelectrode is clearly modified by the PANi film. It can be seen that small polymeric islands surround the electrode surface. This might be expected as the importance of radial diffusion increases as the microelectrode radius decreases[1]. To the best of the author's knowledge, figure 3.7 is the only SEM image available in the literature for a modified PANi microelectrode of such small dimensions.

As seen in figure 3.7 our controlled electrochemical method produces flat films whose thickness is much lower than the microelectrode radius. Indeed if the growth process continues, the polymer film will change to a mushroom shape morphology with considerable spill over. We will go back to the effect of the polymer morphology during the discussion of our kinetic model in Chapter 5.

3.6.2 Constant Potential

Figure 3.8 shows a SEM image when the PANi film was electrodeposited at constant potential, $E = 0.90$ V *vs.* SCE.

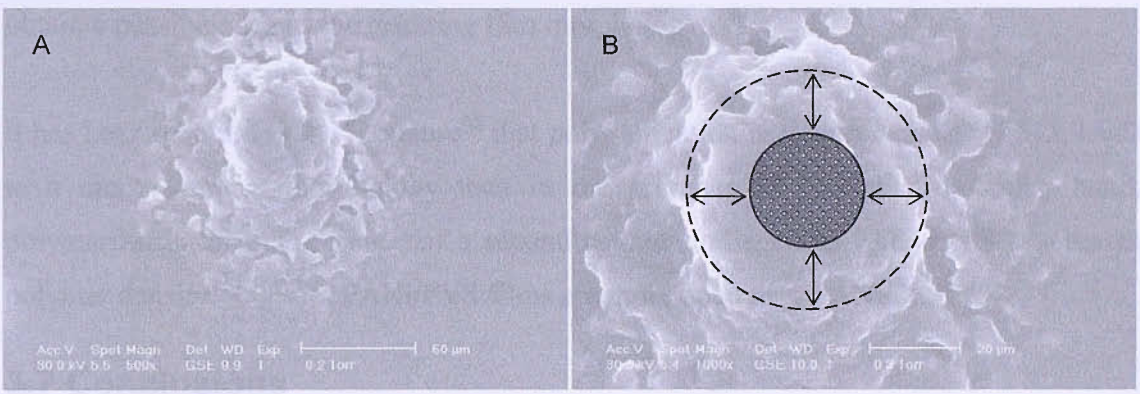

Figure 3.8 *SEM image of a Pt microelectrode, $a \approx 12.5$ μm, modified with a PANi/H_2SO_4 film, $Q = 180$ mC cm^{-2}, corresponding to an average thickness of 8 μm. The solid filled circle in fig B shows the Pt disc electrode area while the dashed circle tries to represent the limits of the PANi mushroom hemi-sphere. Experimental conditions as described in figure 3.6.*

Figure 3.8 shows that the PANi film has a hemispherical shape also mentioned as mushroom shaped in the literature. It is clear that the polymer film spreads considerably beyond the electrode radius. A magnification of the SEM image, figure 3.8.B the polymer film spreads more than twice the radius of the microelectrode. Polymer spill over can be controlled by the time of the polymerization.

It is difficult to find SEM images of modified PANi microelectrodes in the literature. A careful research shows that a recent publication by Caban *et al*[163]. also observed that

PANi films on a Pt microelectrode grow in the form of hemi-spherical micro deposits and their size exceeded three to six times the initial electrode disc radius, a = 11.5 μm. Depending on the time of electrodeposition the resulting films reached thicknesses ca. 50, 70 and 90 μm. This is not surprising as the lateral growth of PANi films has been observed even for different electrode geometries, specially for microband electrodes[164-167].

Out of many attempts, it was not possible however to obtain a clear definition of the polymer morphology on the nanometer scale. We have no choice than to speculate and follow previous studies in our laboratories and in the literature with bigger electrodes to obtain a possible idea of the resulting film morphology.

It has been reported in the literature[65] that polymerization in the presence of H_2SO_4 leads to a more compact morphology than in the presence of HCl. On the other hand, polymerization in the presence of a second counter ion such as PVS or PSS increases polymer density[134, 168, 169]. PANi/PVS films are more open than PANi/PSS[134].

3.7 Conclusions

Stable PANi films were successfully electrodeposited on small Pt microelectrodes. The electrode surface roughness factor, R_f, does not affect the PANi electrodeposition. Thinking of a possible scale up to produce a needle type microelectrode for AA analysis it is recommended that the electrode R_f has to be known for manufacturing purposes. The influence of the electrolyte and second counter ion produces significant differences on the polymer growth rate. There is still work to be done to fully understand the differences observed. The morphology and thickness of the resulting PANi film can be carefully controlled under potentiodynamic control. The data obtained from the SEM shows that flat PANi films with thickness much lower than the microelectrode radius can be obtained on small Pt microelectrodes. Potentiodynamic aniline polymerization is a useful technique to control polymer thickness and spill over. Better resolution of the SEM images may be obtained by gold sputtering of the PANi film as described by Desilvestro[157].

On the other hand, at constant potential, PANi morphology and spill over were more difficult to control and in our experience, less reproducible coatings were obtained. Although further work is needed to improve polymerization under constant potential. Rajendran and Tsakova used the pulse potentiostatic method[170] with good results and it is worth investigating in future work.

Based on our experience we believe that the desired PANi morphology, flat film or mushroom shape, can be controlled much better under potentiodynamic control when using small microelectrodes. The anodic limit has to be carefully selected to allow a continued polymer growth in the absence of quinoimine units. With the support of the information obtained in the literature it was determined that our PANi films will be produced under potentiodynamic control in the presence of 0.1 mM aniline and 1M HCl and PVS or PSS. The rest of the thesis is now organized to characterize the PANi films produced as described in this Chapter towards the oxidation of AA in real systems.

Chapter 4

Electrochemical characterization of modified PANi microelectrodes

4.1 Objective

The electroanalytical properties of PANi films with large counter anions such as PANi-PVS and PANi-PSS will be characterized. In addition, alkylated PANi films are studied as an alternative to PANi composites to retain polymer conductivity. Their interesting analytical properties such as stability, durability, detection limit, etc will be discussed in detail in relation to AA oxidation.

4.2 Introduction

As described in Chapter 1, section 1.6, the conductivity of PANi depends on two variables; the degree of protonation and its oxidation state. Different studies have shown that PANi films deprotonate above pH 5, and consequently it turns into an insulating polymer.

Asturias, Epstein and Doblhofer showed that the incorporation of polyanions during film growth produces a composite film which remains conducting at neutral pH[84, 85, 171-180]. The primary difference between PANi and PANi-polyanion films is the mobility of the counter ions. In the case of PANi, the counter ions are free to diffuse into, out and within the film whereas in the modified case they are fixed.

Figure 4.1 shows a cartoon representing the diffusion of the counter ions between the polymer and solution for a PANi-polyanion film.

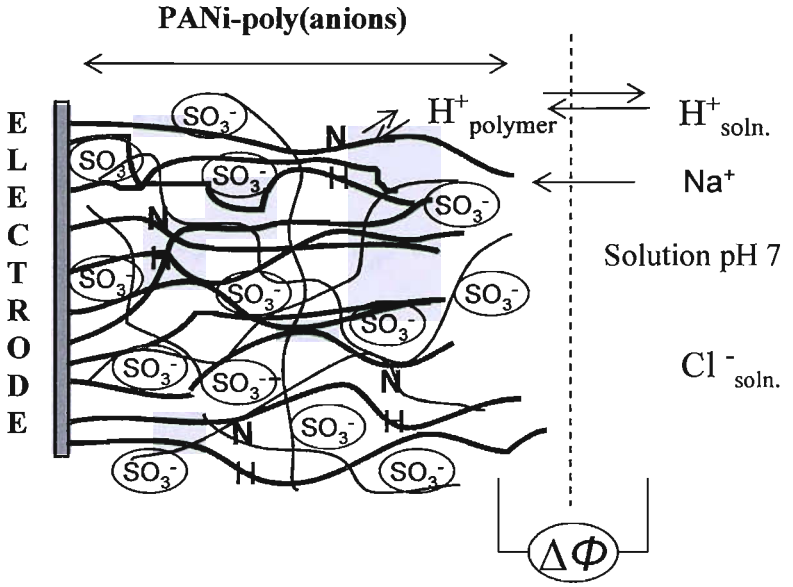

Figure 4.1. *Co-immobilisation PANi-poly(anions) to preserve emeraldine protonation at neutral pH. The black chains with SO_3^- groups attached represent a polyanion trapped within the PANi matrix represented by the green chains.*

Assuming that a PANi film behaves in a similar manner to a membrane; when a membrane is immersed in an aqueous electrolyte solution, there is a clear discontinuity in the environment of all charged species at the membrane solution interface on a molecular scale. This will lead to a potential difference at the interface and to the presence of a double layer. The potential difference is known as the Donnan Potential[181].

$$\Phi_{Donnan} = \Phi_{mem} - \Phi_{sol} \quad (4.1)$$

Deprotonation of PANi is a consequence of the pK_a of the isolated chain. Therefore, the Donnan potential for the polymer film can shift this value and retain polymer conductivity.

In our situation, we need to consider H^+ equilibrium inside and outside the film. On the one hand we have the internal equilibrium between the PANi nitrogen groups and the protons within the film; $N + H^+ \leftrightarrow =N^+H$. On the other hand, the equilibrium between the Cl^- ions in solution and H^+ those are free to move.

The Donnan potential across the interface can affect the concentration of ions in the film because the electrochemical activity of H^+ and of Cl^- individually must be balanced inside and out and this has concentration, activity and potential terms. The H^+ chemical potential is given by equation 4.2;

$$\tilde{\mu}_{H^+} = \mu^{\circ}_{H^+} + RT \ln a_{H^+} + nF\Phi_{Donnan} \qquad (4.2)$$

Where $\tilde{\mu}_{H^+}$ is the electrochemical potential, $\mu^{\circ}_{H^+}$ is the chemical potential of H^+ in the standard state, a_{H^+} is the activity and Φ_{Donnan} the potential difference between the film and the solution. *R, n and T* have their usual meaning.

Then inside the film PANi + H^+ = (PANi-H^+). Protonation equilibrium is set up. Hence, both H^+ film and (PANiH^+) are inside the film so there is no effect from Φ_{film}. The equilibrium is just driven by the concentration (activity). The presence of SO_3^- groups within the polymer means that more H^+ move into the film to neutralize or partially neutralize the charge. Thus, the concentration of H^+ in the film is higher than in the solution.

If $\Phi_{Donnan} = \Phi_{(film)} - \Phi_{(sol)}$,

In solution; $\tilde{\mu}_{H^+(sol)} = \mu^{\circ}_{H^+} + RT \ln a_{H^+(sol)} + nF\Phi_{(sol)}$ (4.3)

In the film; $\tilde{\mu}_{H^+(film)} = \mu^{\circ}_{H^+} + RT \ln a_{H^+(film)} + nF\Phi_{(film)}$ (4.4)

at equilibrium the next relation applies: $\tilde{\mu}_{H^+(film)} = \tilde{\mu}_{H^+(sol)}$, and assuming that at equilibrium the chemical potential of H^+ in the standard state is the same in the film and in the solution, $\mu^{\circ}_{H^+}(film) = \mu^{\circ}_{H^+}(sol)$ we obtain;

$$\Phi_{Donnan} = \frac{RT}{nF} \ln\left(\frac{a_{H^+_{(sol)}}}{a_{H^+_{(film)}}}\right) \qquad (4.5)$$

Equation 4.5 gives the Donnan potential to retain PANi conductivity. One of the aims in this Chapter is to develop this concept using large negatively charged counter ions, such

as PVS and PSS to maintain polymer conductivity on a small scale. In addition, Battaglini *et al.*[93] recently proposed an interesting approach to retain polymer conductivity. His idea of an alkylated PANi film was briefly explained in Chapter 1, section 1.6.

In this Chapter we now describe the different PANi-polyanion films and alkylated PANi films electrodeposited on small Pt microelectrodes and their application as electrocatalytic surfaces for AA at neutral pH.

4.3 PANi-PVS and PANi-PSS characterization

In Chapter 3, we discussed the electrodeposition of a PANi film in the presence of large counter ions such as PVS and PSS. It was shown how the growth rate was affected by the counter ion. It is now our interest to establish if these modified PANi films retain polymer conductivity at neutral pH.

4.3.1 Effect of the counter ion on polymer stability at neutral pH

Figures 4.2 and 4.3, shows the characterization at neutral pH of a PANi-PVS, and a PANi-PSS, film, respectively. Although the charge density passed during the electrodeposition was similar for both polymers, we can appreciate that the counter ion produces a clear difference when the modified PANi is characterized at neutral pH.

In the case of PANi-PVS, figure 4.2, the potential was held at -0.20 V for 3 min to fully reduce the polymer and afterwards the potential was cycled from -0.25 to +0.30 V *vs.* SCE. If this polymer is cycled above +0.30 V *vs.* SCE it leads to an irreversible loss of its conductivity, resulting in an insulating polymer[89]. This is because, at pH 7, cycling the PANi-PVS film above +0.30 V, the polymer oxidizes to its pernigraniline form. It is known that overoxidation of PANi leads to irreversible degradation of the polymer film. This is clearly visible in acidic pH and its also possible at pH 7, but degradation will occur more slowly[57, 71].

From figure 4.2, we can see that the current decreases within the first five scans until it reaches a stable value for the subsequent scans. Similar behaviour was observed for thin PANi-PVS films electrodeposited at larger electrodes[89]. This decrease in response is probably due to polymer deprotonation. The protons that are not electrostatically retained by the SO_3^- anions could diffuse from the polymer network to bulk solution.

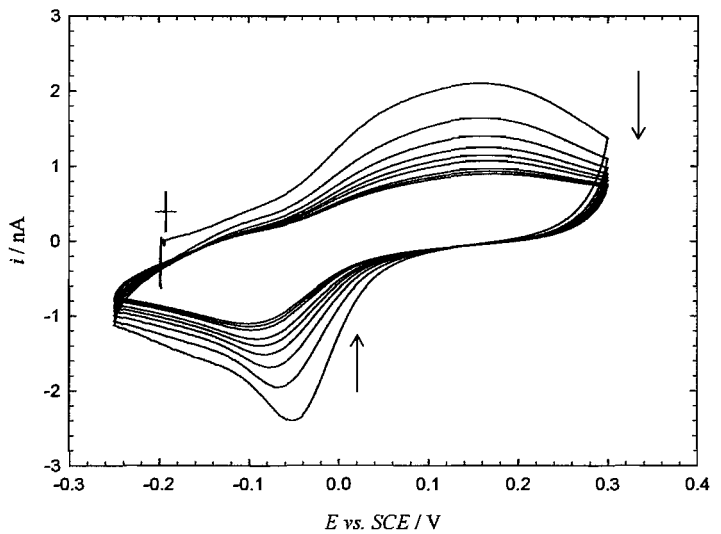

Figure 4.2 *Characterization at neutral pH, of a PANi-PVS film (deposition charge density Q = 2.80 mC cm^2, a = 12.5 μm) during repeated cycling. The film was held at -0.20 V for 5 min. prior to being cycled from -0.20 to +0.30 V during ten consecutive scans at 50 mV s^{-1}, in a 0.1 M citrate / 0.2 M phosphate buffer, pH 7, oxygen free solution at 25 °C. The molecular weight of the counter ion, Na^+PVS^-, is MW ≈ (4000 – 6000) g mol^{-1}, monomer MW [-$CH_2CH(SO_3)Na$-] = 130.10 g mol^{-1} . The arrows in figure show the direction of the decrease in the current registered through subsequent scans.*

In the case of PANi-PSS films, figure 4.3, the potential was held at -0.20 V for 3 min to fully reduce the polymer and afterwards the potential was cycled from -0.25 to +0.50 V *vs.* SCE. It is shown that PANi-PSS offers a more stable response over a wider range of potentials, compared to PANi-PVS.

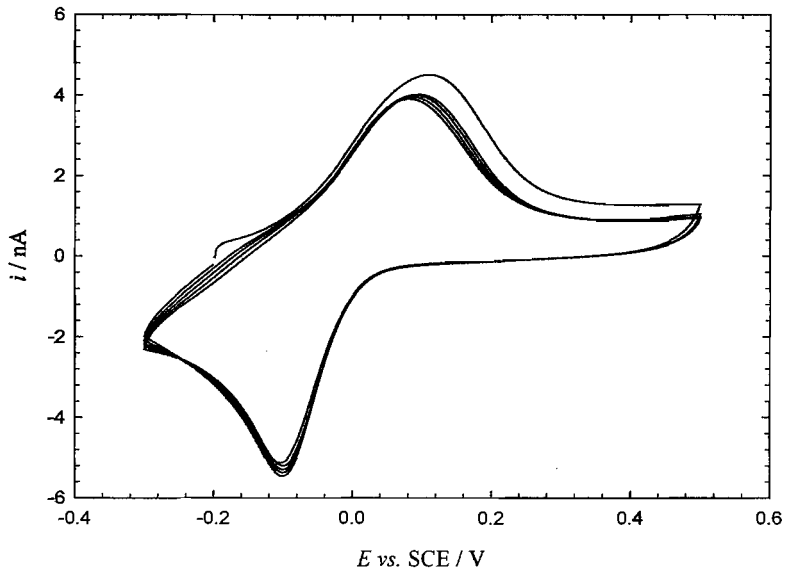

Figure 4.3 *Characterization at neutral pH, of a PANi-PSS film (deposition charge Q = 2.72 mC cm^2, a = 13.0 μm) during repeated cycling. The film was held at -0.20 V for 5 min prior to be cycled from -0.25 to +0.50 V during five consecutive scans in a 0.1 M citrate / 0.2 M phosphate buffer, pH 7, oxygen free solution at 25 °C. The molecular weight of the counter ion, Na^+PSS^- is MW ≈ 70,000 g mol^{-1}, monomer MW* [-$CH_2CHPh(SO_3)Na$-] = *207.20 g mol^{-1}.*

From the voltammogram in figure 4.3, it can be seen that there is only a small difference from the first cycle to the subsequent ones. Indicating that PSS as a counter ion retains protons in a different manner as PVS. The electrochemical characterization shows the excellent properties of our PANi-PSS microelectrodes. This result was observed through different replicates at different electrodes.

The difference between PANi-PVS and PANi-PSS, could be due to the molecular weight or chemical structure of the counter ion. Looking in the literature for these counter ions in particular, PVS, $[\text{-}CH_2CH(SO_3)Na\text{-}]_n$, and PSS, $[\text{-}CH_2CHPh(SO_3)Na\text{-}]_n$, Barbero *et al*[66]. and Desilviestro *et al*[65]. have shown that the counter ion plays a crucial role in determining the morphology of the PANi films. More precisely increasing the molecular weight of the counter ion leads to a more dense and compact polymer structure[65, 168, 169]. Bruckenstein[182], using tetrafluoroborate and hexafluorophosphate as counter ions with a

poly(vinylferrocene) (PVF) film has demonstrated that the resulting polymer can be more or less rigid, which leads to the entrapment of smaller numbers of water molecules within the polymer film. This clearly modifies the response obtained[182].

Bearing in mind that large counter anions with high molecular weight lead, somehow, to a more stable response we decided to use as the counter anion, poly(vinylsulfate, potassium salt), $[-CH_2CH(OSO_3)K-]_n$, with a molecular weight MW = 170,000. This polymer has a similar chemical structure as our previous PVS, $[-CH_2CH(SO_3)Na-]_n$, MW = 400 – 6000, but a much longer polymer chain.

Figure 4.4, shows the response of PANi- poly(vinylsulfate), film at neutral pH. This polymer was treated identically as our previous PANi-PVS film, shown in figure 4.2.

It can be observed that, similarly to our previous observations, there is a difference between the first and subsequent scans. However, it is now clear that the response attains a stable value right after the first scan. Therefore, it seems that increasing the molecular weight of the counter anion within the PANi film is better retained. Although the counter ion affects the gross morphology, at the micrometer level, of the polymer film, as will be discussed in Chapter 5, it seems to affect also in the molecular level.

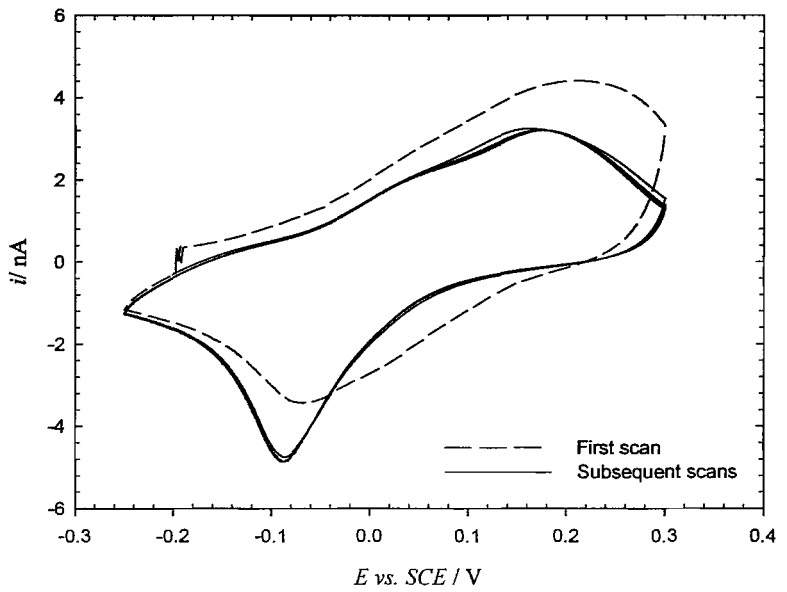

Figure 4.4 *Characterization at neutral pH, of a poly(aniline)-poly(vinylsulfate), PANi-PVS*, film (deposition charge density Q = 2.42 mC cm^2, a ≈ 12.5 μm) during repeated cycling. The film was held at -0.20 V for 5 min. prior to be cycled from -0.20 to +0.30 V during ten consecutive scans in a 0.1 M citrate / 0.2 M phosphate buffer, pH 7, oxygen free solution at 25 °C. The molecular weight of the counter ion, potassium poly(vinylsulfate), K^+PVS^- is MW ≈ 170,000 g mol^{-1}, monomer MW* [-$CH_2CH(OSO_3)K$-] = *174.22 g mol^{-1}.*

Therefore, from the experimental results, longer PVS chains seems to retain polymer stability better but PSS still presents the best response. Taking into account the molecular weights of the polymer in relation with their monomer we can calculate de degree of polymerization, *DP*;

$$DP = \frac{\mathrm{MW}_{polymer}}{\mathrm{MW}_{monomer}} \qquad (4.6)$$

$DP_{\text{Na-PVS}} = 38$, $DP_{\text{K-PVS}} = 956$ and $DP_{\text{Na-PSS}} = 338$. It is likely that a high value on the degree of polymerization will lead to longer chains and therefore to a denser polymer. In addition, the main difference between PVS and PSS is the aromatic rings present in the later, which may interact with the PANi, and this aids the stability. However, no evidence for this assumption has been found.

4.4 PANi-PVS and PANi-PSS as electrocatalytic surfaces for AA oxidation

The voltammetric response of PANi-PVS and PANi-PSS films electrodeposited on a Pt microelectrode, in the absence and presence of AA at neutral pH, is presented in figures 4.5 and 4.6, respectively. As shown during the previous section, these polymers show stable voltammetry at neutral pH if the potential window is carefully controlled for each case. It is clear from both figures that our electrodeposition method on small microelectrodes produces stable PANi films, which are excellent electrocatalytic surfaces for ascorbate oxidation at neutral pH.

In both cases, the electrocatalytic current starts at approximately similar potentials, $E \approx 0.0$ V *vs.* SCE. Having an electrocatalytic surface capable of oxidizing AA at low potentials has an enormous potential advantage. As at higher potentials many organic molecules oxidize, this makes it difficult to achieve the selective oxidation of AA. Therefore, PANi-PVS and PANi-PSS microelectrodes are excellent choices for AA oxidation at neutral pH, which makes them of potential of use for application in real systems.

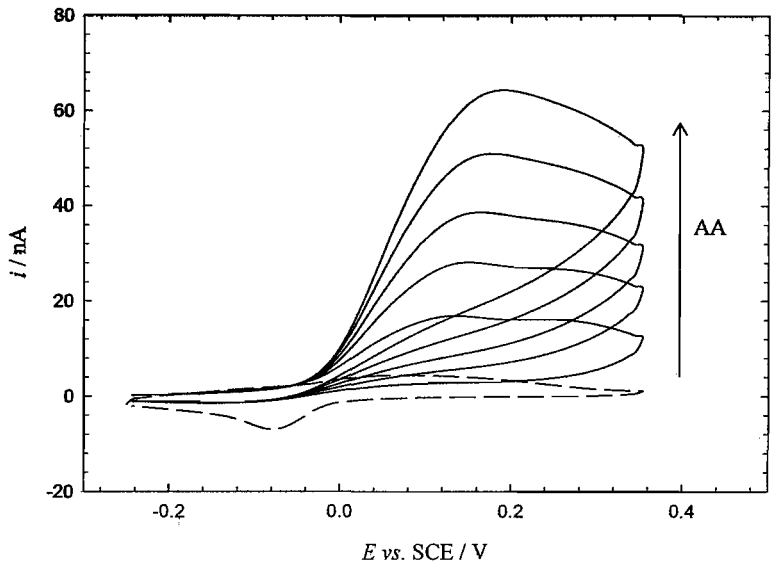

Figure 4.5 *Characterization at neutral pH, of a PANi-PVS film, MW_{PVS} = 4000-6000 g mol^{-1} (deposition charge density Q = 2.80 mC cm^2, a ≈ 12.5 μm) in the absence, dashed lined, and presence of different amounts of AA. For each voltammogram, the PANi-PVS film was held at -0.20 V for 5 min prior to being cycled from -0.20 to +0.38 V. In the absence of AA, dashed line, the second cycle is shown. In the presence of AA, solid lines, the first cycle is shown. Each increase in the current was brought about by the addition of 5 mM AA to the solution. Experiments were done in a 0.1 M citrate / 0.2 M phosphate buffer as the supporting electrolyte at pH in oxygen free solution at 25 °C.*

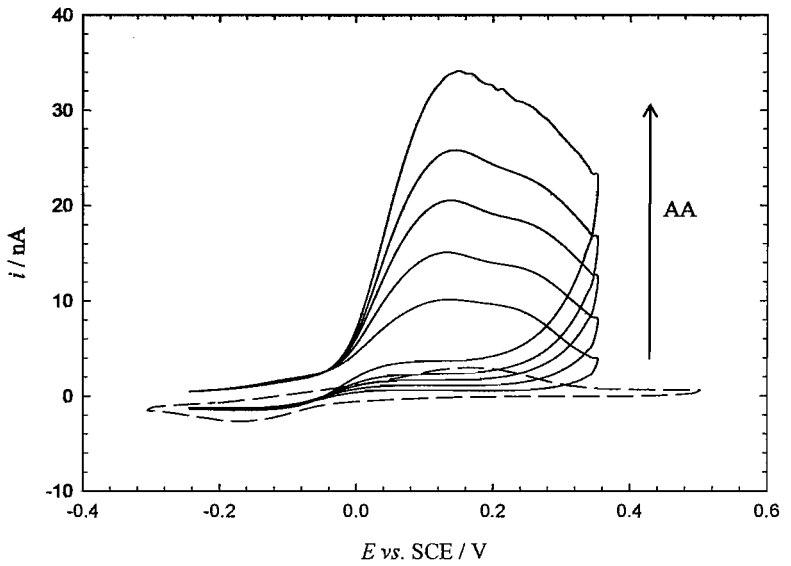

Figure 4.6 *Characterization at neutral pH, of a PANi-PSS film, MW_{PSS} = 70,000 g mol^{-1} (deposition charge Q = 2.72 mC cm^2, $a \approx 13.0$ μm) in the absence, dashed lined, and presence of different amounts of AA. Same details as in figure 4.5 apply.*

Before going further, we want to point out a curious effect. On closer inspection of figures 4.5 and 4.6, it can be seen that PANi-PVS show higher electrocatalytic currents towards AA oxidation compared to PANi-PSS. Figure 4.6, plots the current obtained at E = 0.10 V *vs.* SCE for both PANi composites. It is clear that PANi-PVS gives twice as much current as PANi-PSS.

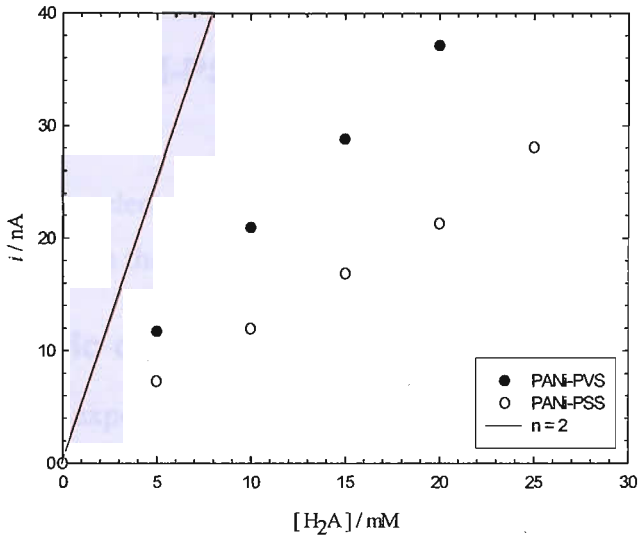

Figure 4.7 *Limiting currents obtained during consecutive additions of AA, from figures 4.5 and 4.6, for a PANi-PVS, film, MW_{PVS} = (4000 – 6000) g mol^{-1} and a PANi-PSS, film, $MW_{PSS} \approx$ 70,000 g mol^{-1}. The background current was subtracted. The red solid line is the solution for mass transport limited current, described by i=4nFDCa, considering n = 2, $D_{AA} = 5 \times 10^{-6}$ cm^2 s^{-1}.*

The red solid line in figure 4.6 is the theoretical response expected for a modified microelectrode using equation 1.2. Although this equation only applies for steady state limiting currents registered under pure mass transport control, it is included here as a guide. This difference in response between PVS and PSS PANi films was observed during the course of many experiments and by different collaborators within this project. This result is much unexpected as in theory the counter ion should not make any difference to the AA oxidation. As shown in figure 4.1, the function of the counter ion is to retain polymer conductivity at neutral pH, the PANi active sites are independent of the counter ion. This effect will be discussed in much greater detail in Chapter 5, when a kinetic model for the reaction will be proposed.

4.5 PANi-PVS and PANi-PSS as amperometric sensors for ascorbate oxidation

Our modified PANi microelectrodes were used as amperometrical sensors for ascorbate oxidation at neutral pH with the intention to measure rapid changes in AA concentration.

4.5.1 Amperometric detection of AA at neutral pH

Figure 4.8 shows the experimental response obtained for a PANi-PSS film. After equilibrating the PANi film for 10 min, AA was added to the bulk solution. After each addition, the solution was stirred for a few seconds with the use of a Teflon coated follower. The switching on/off of the magnetic stirrer produced an electrical spike on the recorded signal but was necessary to attain a homogeneous solution and did not otherwise affect the measurements. The stirrer was isolated from the mains between measurements; otherwise, the electromagnetic field affects the experimental response.

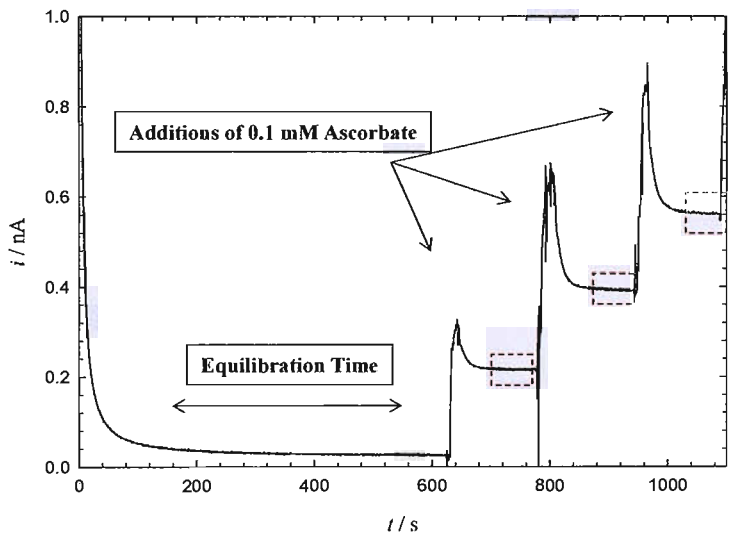

Figure 4.8 *Amperometric responses for a PANi-PSS film, MW_{PSS} = 70,000 g mol^{-1} (deposition charge density Q = 3.32 mC cm^2, a ≈13.0 μm). The PANi composite was held at -0.20 V for a minimum of 3 min to ensure fully reduction of the film, not shown in the figure. Afterwards, the potential was stepped to +0.10 V, and held at this constant potential for 30 min. Each increase in the current corresponds to an addition of 0.1 mM AA. Experiments were carried out in 0.1 M citrate / 0.2 M phosphate buffer as a supporting electrolyte, pH 7, oxygen free solution at 25 °C. The red dashed rectangles in figure show the range of data averaged to get the experimental limiting currents.*

As seen from figure 4.8, the addition of 0.1 mM AA clearly gives an increase in the current, due to the oxidation of ascorbate on the PANi film. The response reaches a stable limiting current in the range of seconds. The time to reach a stable value can be affected by the mixing of the solution. Attaining a fast response is due to radial diffusion present in microelectrodes. Bartlett and Wallace, with the use of the RDE, reported response times in the range of minutes[134]. As seen from figure 4.8, successive additions of AA produce an increase in the limiting current; therefore, PANi-PSS microelectrodes can be used as amperometric sensors for AA at neutral pH. The red dashed rectangles in figure 4.8 show the range of data averaged to get the experimental limiting currents, so a calibration curve can be built.

When PANi-PVS films were used as amperometric sensors for AA at neutral pH, similar response were observed as for PANi-PSS. The current increased sharply after each addition of AA and reached a steady state response in a few seconds. However, as seen during the voltammetric characterization figures 4.5 and 4.6, the limiting currents obtained were double the value when compared for PANi-PSS. This effect was seen throughout the course of different experiments and will be discussed in the following Chapter.

4.5.2 Reproducibility and stability

In order to study the reproducibility and stability of our modified PANi microelectrodes calibrations curves were plotted for successive replicates. Figure 4.9 plots the experimental currents obtained for a PANi-PSS film during ascorbate oxidation at E = 0.10 V *vs.* SCE, pH=7. The limiting current increases linearly with the concentration of AA, but the response deviates from linearity above 20 mM and reaches a saturation value above 60 mM. This is a consequence of the kinetics involved in the electrochemical reaction and will be explained in detail in Chapter 5.

Figure 4.9 plots the response for five consecutive calibration curves, showing almost identical response. This clearly shows the good reproducibility of the PANi-PSS microelectrodes. However, these films are stable up to a limit. The red triangles in figure

4.9 shows the response obtained after using the same PANi-PSS after 5 consecutive replicates for ascorbate oxidation, at pH = 7. It is clear that the limiting currents are considerably lower compared with the previous response. This response was observed during the course of different experiments and was also observed for PANi-PVS modified microelectrodes. PANi-PVS presented significant decrease from the initial response after two or three calibrations curves for ascorbate.

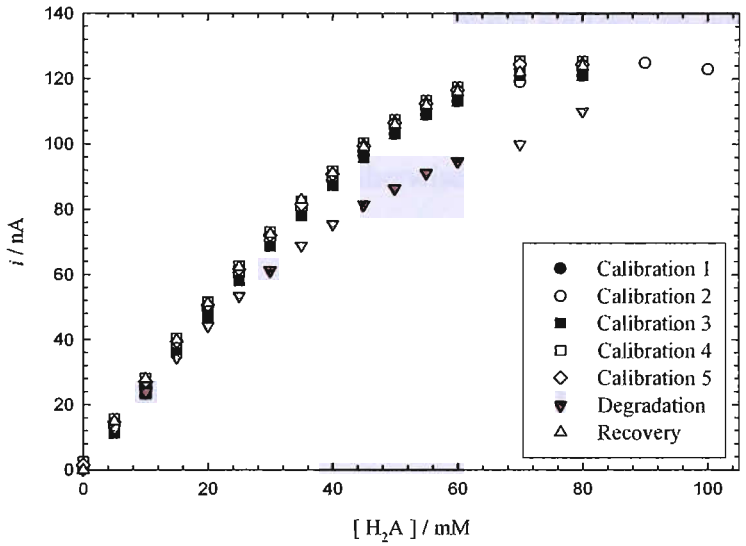

Figure 4.9 *Amperometric response at E = 0.10 V vs. SCE, for the same PANi-PSS film (deposition charge density Q = 2.72 mC cm^2, a ≈ 13.0 μm), during successive additions of AA at neutral pH. The PANi-PSS film was reduced by holding the electrode potential at -0.20 V for 5 min to ensure the full reduction of the polymer film. Afterwards the potential was stepped to +0.10 V for the oxidation of ascorbate. The electrolyte solution is 0.1 M citrate /0.2 M phosphate buffer, pH 7, 25 °C, degassed with Ar for 15 min. The red triangles show the response obtained after five successive calibration curves. The yellow triangles shows how the response can be recovered after seeing degradation by cycling the resulting PANi-PSS in a solution containing 1 M HCl and 22% PSS, cycled between -0.20 and +0.50 V vs. SCE for approximately 50 cycles.*

In order to study if the decrease in response was due to PANi dissolution, the charge under the anodic emeraldine peak in acidic pH was compared before and after exposure to ascorbate. No significant decrease in the peak area was observed before and after

exposure to AA in buffer solution on the same day of analysis. This observation indicates that PANi is not being dissolved after exposure to ascorbate in neutral pH.

It is believed that PANi films expand when they are switched from reduced to oxidized form in solution, or viceversa[183]. In a similar way that a dry sponge expands or contracts as water is added or removed to it. Therefore, it could happen that after long time exposure of these PANi-PSS films in buffer solution applying an anodic potential, and due to the stirring of the solution each time AA is added, the polymer network may expand in a way that facilitates polymer deprotonation. The implication of PANi deprotonation is linked to loss of PSS. Otherwise if H^+ egress another cation such as Na^+ has to come in order to retain charge balance.

However, from the data obtained, it could be due to a combination of both effects; loss of PSS counter anion and/or polymer deprotonation. Further work needs to be done to clarify this question. Maybe ion chromatography of the buffer solution before and after analysis could be used to detect PSS in solution and possibly clarify this question.

If PSS is leached out to the solution, it can be a potential problem for *in vivo* applications. Nevertheless, the response of the PANi-PSS film can be fully recovered if the PANi-PSS film is cycled in an acidic solution contained PSS. Following the procedures proposed by Barbero *et al.*[169] and by Hyodo and Oomae[160, 161]. They showed that the counter ion can be introduced by different methods within PANi films. It can be done at the time the film is deposited in acidic solution containing the aniline monomer and the desired counter ion. Alternatively, the PANi film can be first electrodeposited on the electrode and afterwards exposed to an acidic solution containing the new counter ion. Both mechanisms are believed to introduce the counter ion within the PANi film.

Consequently, the resulting degraded PANi-PSS film was cycled in a acidic solution containing the PSS anion, and cycled from -0.20 to +0.50 V *vs.* SCE at 50 mV s^{-1}. The properties of the polymer film are fully recovered and this is shown in figure 4.10, yellow triangles. Again, the recovery in response could be due to a recovery in polymer

protonation and not be due to PSS leaching. Because by cycling the polymer in acidic solution the PANi film expands and contracts as it being oxidized and reduced together with the intake and spelling of cations and anions at the same time.

An exactly similar problem was observed for PANi-PVS, and this film also had a limited life. The limiting currents started to decrease after 3 to 4 calibrations curves. The response of the polymer film was also recovered by cycling the degraded polymer in acidic solution containing PVS between -0.20 to +0.50 V *vs.* SCE at 50 mV s^{-1}.

When PANi-PSS and PANi-PVS were reconditioned, the initial response was recovered for all cases. In this way, the modified microelectrode remained stable for weeks and can be kept at room temperature without further degradation. This results may suggest that in order to obtain a robust electrode the PANi film has to be cross-linked with the counter ion in a way that the counter ion cannot leach out of the composite film.

4.5.3 Selectivity

As we are aiming for the application of these modified PANi microelectrodes for the detection of AA *in vivo*, a screening for common interferences was carried out in the presence of AA. The concentration of the interferences tested was always higher than the concentration of AA. Some of the experimental results are presented in figure 4.11.

If the film is electroactive for any of the substrates added at the potential of the measurement, the current registered will increase with its concentration. However if the film is inhibited for the substrate the current registered will decrease with time. In the case that the film is electroinactive for the compound under study, no change in the steady state current will be observed.

As seen from figure 4.11, the limiting current increased when 0.15 mM AA was added to the solution. Afterwards different potential interferences, which might be present in human plasma or physiological fluids, were analysed.

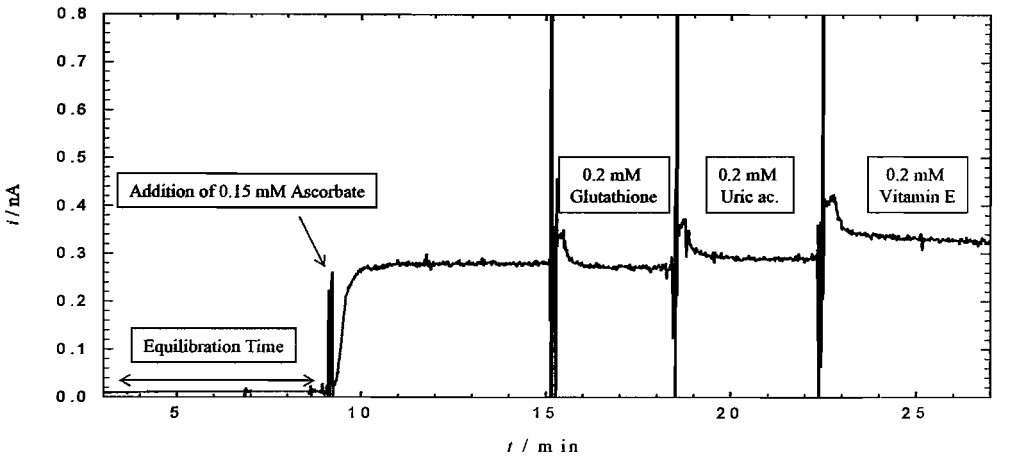

Figure 4.11 *Screening for common interferences using PANi-PSS (deposition charge density Q = 2.75 mC cm^2, a ≈ 13.0 μm) modified microelectrodes. Prior to the experiment the PANi-PSS film was reduced by holding the electrode potential at -0.2 V for 5 min to ensure the full reduction of the polymer film. Afterwards the potential was stepped to +0.10 V vs. SCE. The film was equilibrated for approximately 10 min, by applying a constant potential of +0.10 V. The first increase in the current corresponds to the addition of 0.15 mM AA into the bulk solution. When the response was stable, potential interferent species were added at higher concentration, 0.2 mM, using the same procedure. The electrolyte solution is 0.1 M citrate /0.2 M phosphate buffer, pH 7, 25 °C, degassed with Ar for 15 min.*

The next sequence of interferences were screened, giving a negative result; glutathione (GSH), uric acid (UA), acetic acid, lactic acid, salicylic acid, maleic acid and phenol. The only potential interference for this PANI-PSS film in the presence of AA was vitamin E, but as seen from figure 4.11, the response to Vitamin E is small. After the screening process, AA was added again to the solution, and the expected increase in current was obtained, indicating that the PANi-PSS was not inhibited or modified in the presence of all these substrates.

PANi-PVS were screened against glutathione, uric acid and salicylic acid giving no interference.

4.5.4 Detection limit

The minimum concentration of ascorbate which can be measured at pH=7 by our PANi-PSS was investigated. Figure 4.12 shows the experimental response obtained at low ascorbate concentration. It is clearly seen that PANi-PSS films show extremely good activity for low ascorbate concentrations. A clear increase from the background current is observed after the addition of 1.0 μM AA. If we define the detection limit as three times the standard deviation of the background current we can see that the detection limit for PANi-PSS microelectrodes is below 1.0 μM AA. This is a clear advantage for further applications in real systems. The background current might depend on the matrix; therefore, it can be different in buffer than in human plasma or physiological fluid and this can affect the detection limit.

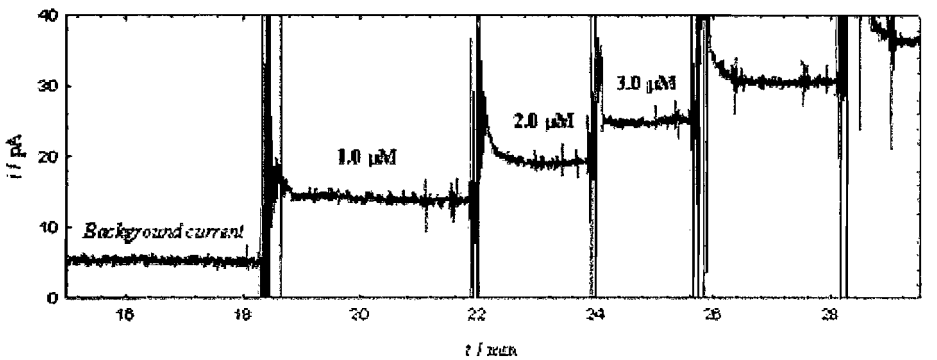

Figure 4.12 *Detection limit for PANi-PSS (Deposition charge density Q = 2.75 mC cm^2, a ≈ 13.0 μm) modified microelectrodes. Prior to the experiment the PANi-PSS film was reduced by holding the electrode potential at -0.20 V for 5 min to ensure the full reduction of the polymer film. Afterwards the potential was stepped to +0.10 V vs. SCE. The film was equilibrated for approximately 18 min, by applying a constant potential of +0.10 V. The increase in the current corresponds to additions of 1.0 μM AA into the bulk solution. When the response was stable, successive additions were made. The solution was stirred with the help of a magnetic stirrer, using a Teflon coated follower inside the solution. The electrolyte solution is 0.1 M citrate /0.2 M phosphate buffer, pH 7, 25 °C, degassed with Ar for 15 min. The vertical lines, between additions of AA correspond to electrical noise coming from the switching on/off of the magnetic stirrer to homogenise the solution.*

4.6 Alkylated PANi microelectrodes for ascorbate measurements

As briefly discussed at the beginning of this Chapter, alkylation of PANi is a different approach to avoid polymer deprotonation and retain polymer conductivity at pH > 5. The idea is particularly interesting as an alternative to PANi-poly(anion) entrapment and this section is aimed at PANi alkylation on really small microelectrodes.

4.6.1 Electrochemical Characterization of alkylated PANi films

When the modified PANi film was cycled in HCl solution, the response obtained is almost the same as for an unmodified PANi film. No significant difference in the charge under the anodic or cathodic peaks is observed before and after exposure, indicating that none of the polymer was dissolved through the alkylation reaction. Figure 4.13 shows a typical response obtained for a PANi film after exposure to neat propane sultone, at neutral pH, see section 2.5 for the experimental details.

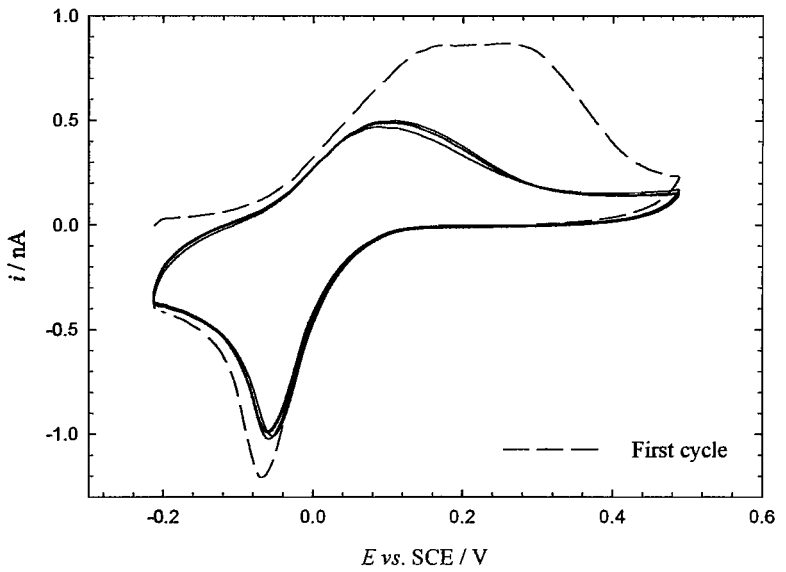

Figure 4.13 *Cyclic voltammograms of an alkylated PANi/Cl⁻ film (deposition charge density Q = 4.25 mC cm^2, a ≈ 1.0 μm) after direct exposure to neat propane sultone, see detail in the text. Alkylated PANi films were first reduced at -0.20 V vs. SCE and thereafter the potential was scanned from -0.20 to +0.50 V at 50 mV s^{-1}. Dashed line shows the response of the first cycle and solid lines are the subsequent 10 continuous cycles. Solution was degassed with Ar for 15 min and temperature controlled at 25 °C.*

As seen from figure 4.13, it is evident that a stable voltammogram over a wide range of potentials is obtained, which resembles the response obtained with our PANi/PSS microelectrodes, figure 4.3. The first scan clearly differs from the subsequent ones. However, no decrease in either the anodic or the cathodic peaks is observed with continuous scans. This difference in response might be expected as probably not all the polymer is being modified. Therefore, the first scan will show the electroactivity of the whole film, and any protons within the PANi will diffuse to the bulk solution. This is observed as a stable response during the second and subsequent cycles and represents the response of the modified portion of the PANi film. This is clear evidence that the PANi film has been successfully modified. To the best of the author's knowledge this is the first time PANi has been successfully alkylated on such a small microelectrode, a = 1.0 μm. Also, when comparing our results to those published by Battaglini *et al.*[93] it is clear that careful attention to the reaction temperature clearly improves the response obtained.

In order to quantify how much of the polymer was modified, the responses at neutral pH and in acidic conditions were compared. Analyzing the charge under the anodic peaks in 1M HCl and at neutral pH we can estimate that approximately ~30 % of the polymer film remains conducting at neutral pH. Assuming that the charge obtained in 1M HCl represents a 100% conductive polymer. This percentage was not increased by a second exposure of the alkylated PANi to fresh propane sultone.

4.6.2 Raman spectroscopy of PANi films

In order to verify if propane sultone really attaches to the nitrogen atoms of the PANi chain, as shown in figure 4.14, Raman spectroscopy was carried out on the electrode surface before and after exposure.

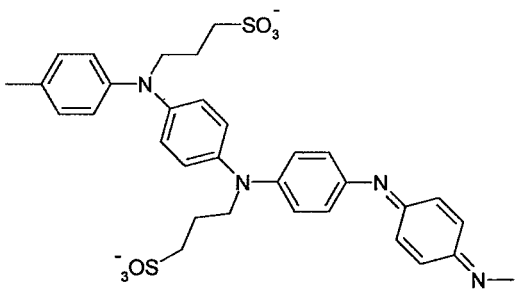

Figure 4.14. *Proposed chemical structure for a sultonated PANi*[93]. *Alkylation of the PANi atoms is achieved by direct exposure of the reduced PANi form to propane sultone.*

It is clear that it is impossible to carry out the study on such small microelectrodes because the Raman laser spot is much larger than the extent of the PANi film. Consequently we were forced to carry this analyses at Pt disc electrodes, a = 3.5mm. Exactly the same procedures for polymer electrodeposition and exposure to propane sultone were followed as used for the microelectrodes, and described in detail in the previous section.

Figure 4.15 shows the experimental response obtained for a PANi/Cl^- film before, black solid line, and after exposure to neat propane sultone, red dashed line. The dotted blue line is the subtraction of the red and black lines shown to highlight the differences.

The Raman spectra obtained show many features characteristic of PANi like films[184, 185]. The reduced PANi/Cl^- film, solid black line, shows characteristic features in the region between 1000 and 1700 cm^{-1}. The Raman bands observed could be ascribed to definitive vibrations based on known assignments. For both cases, a strong band appears at 1172 cm^{-1} which can be attributed to bending C-H vibration mode of quinoid-like rings[81].

Bands between 1300-1400 cm^{-1} belong most probably to polarons, C-N^{+}[185]. The most striking effect appears at 1468 cm^{-1}, which is intense for PANi/Cl^{-} after being exposed to neat propane sultone, red dashed line. This band is attributed to C=N stretching[81, 186].

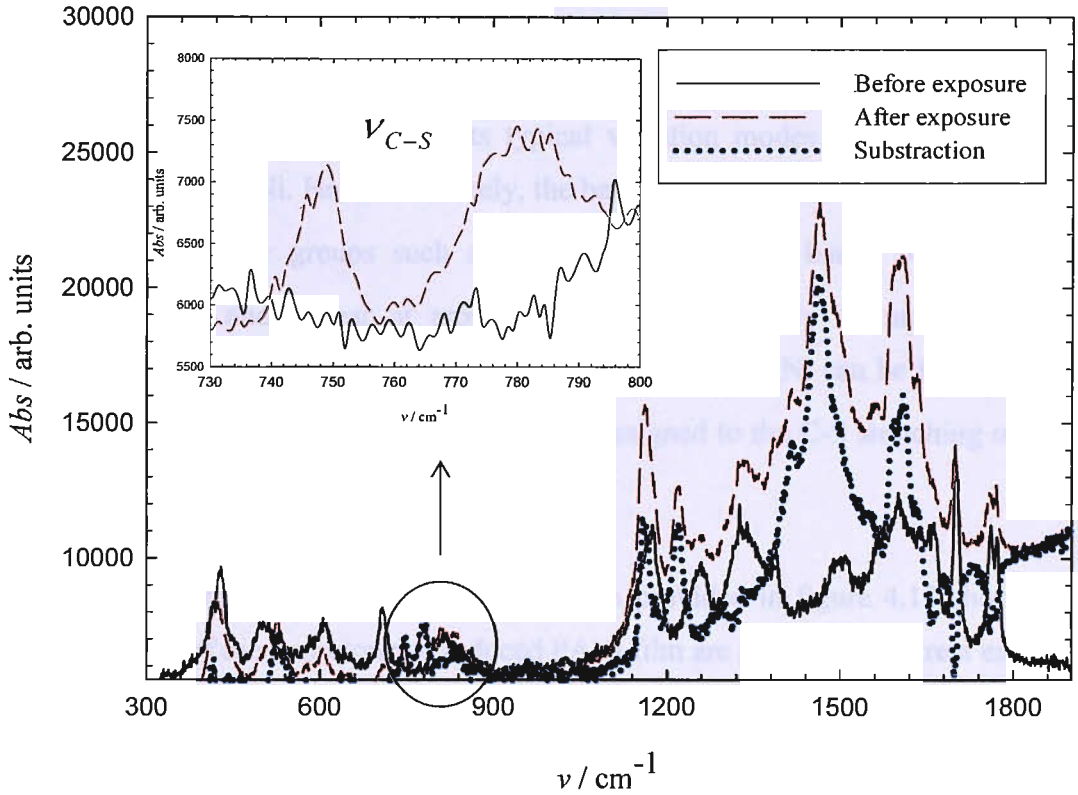

Figure 4.15. *Raman spectra of a PANi film, (deposition charge density Q = 83.25 mC cm^2, a = 3.5 mm before, solid black line, and after exposure to neat propane sultone, dashed red line. The dotted blue line is the spectra obtained from the subtraction before and after exposure. The spectra was recorded using a Remishaw system 2000 Raman microscope fitted with a x10 objective in a 90° scattering geometry and the laser beam (633 nm) power was limited to 20 mW. All experiments were recorded at room temperature.*

The absence of this band in the reduced form, solid black line, and a clear intense peak after exposure to propane sultone, clearly shows that the PANi has been oxidized, and the signal for the presence of the double bond C=N appears, as seen in figure 4.14. Although PANi oxidation can also be due to the presence of oxygen.

The band appearing at 1607 cm^{-1} is difficult to assign and there is disagreement in the literature. Some authors state that this band can be attributed to C=C stretching vibrations of the quinoid rings present in the oxidized PANi form[187, 188]. Also the absence of this band in the spectrum of the reduced form, indicates that this band is a feature of an oxidized form. The dotted blue line in figure 4.16 is obtained by subtraction of spectra before and after exposure. It presents typical vibration modes characteristic for more oxidized form of PANi. Hence it is likely, the band appearing at 1607 cm^{-1} belongs to the oxidized form. Polar groups such as SO_3^- give strong IR bands but weak Raman stretching bands and appear at around 1035 cm^{-1}. The only feature which can be attributed to the presence of sulfur compounds within the PANi can be found as a weak band at 750 cm^{-1}, inset figure 4.16, and can be assigned to the C-S stretching of C- SO_3^- bond[189, 190].

This data together with the electrochemical data provided in figure 4.13 show that the nitrogen atoms of the unprotonated reduced PANi film are alkylated by direct exposure to neat propane sultone.

4.6.3 Electrochemical stability at different pH

The properties of our alkylated PANi film were studied at different pH. Figure 4.16 shows the experimental results obtained for a alkylated PANi film electrodeposited on a Pt disc electrode, a = 2.5 μm. Each graph plots five continuous scans over the potential window presented.

It can be seen that stable responses upon polymer cycling are clearly obtained. This indicates the good properties of the modified PANi films. Also, considering that we are presenting the response of the same polymer film exposed at different pH and that almost no decrease in the response is seen, shows that alkylated PANi microelectrodes have really good stability and are promising materials to be used at neutral pH.
Furthermore, it can be appreciated that the anodic and cathodic redox peaks shift with pH. This is expected as the PANi oxidation and reduction processes depend on pH[191].

Therefore, as the pH is decreased from pH=7 to acidic conditions, a higher percentage of PANi becomes electroactive, increasing the charge below the anodic and cathodic peaks. The slope of potential as a function of pH is about 64 mV/pH, which is close to the theoretical expected 59 mV/pH, for a one proton one electron reaction.

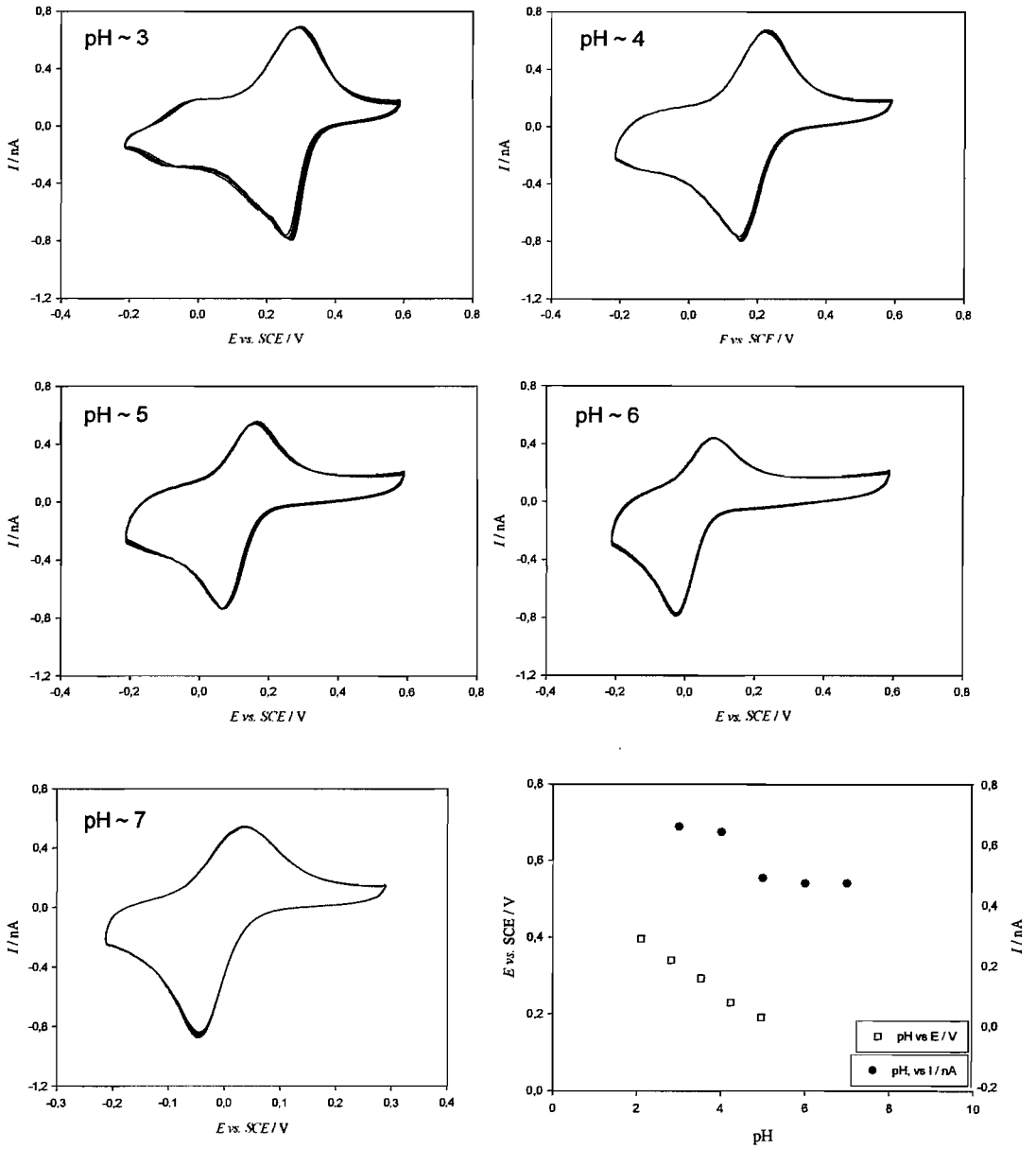

Figure 4.16 Characterization of a *PANi film (deposition charge Q = 4.57 mC cm^2, a = 2.5 μm) after direct exposure to 1,3-propane sultone. The polymer film in phosphate buffer solutions of different pH was first reduced at -0.20 V vs. SCE for 3min and thereafter the potential was scanned at 50 mV s$^-$ between -0.20 and +0.60 vs. SCE for 5*

consecutive cycles. Solutions were degassed with Ar for 15 min and temperature controlled at 25 ± 1 °C.

4.6.4 Alkylated PANi microelectrodes as electrocatalytic surfaces for ascorbate oxidation at neutral pH

In the previous section we have shown how alkylated PANi films offer great stability at neutral pH, hence they are promising materials as electrocatalytic surfaces for AA oxidation at neutral pH. Figure 4.17 shows the response of an alkylated PANi film at neutral pH in the absence, solid line, and presence of different amounts of AA.

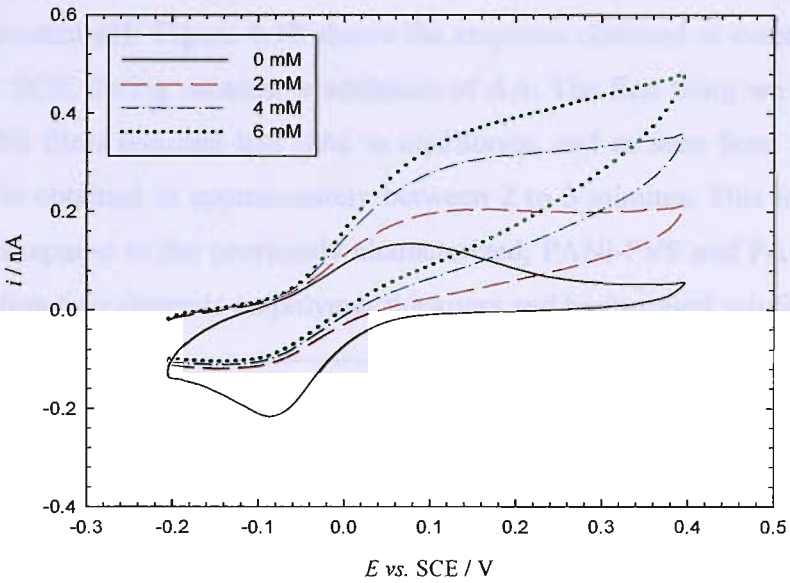

Figure 4.17 *Electrochemical characterization of an alkylated PANi film (deposition charge Q = 1.87 mC cm^2, a = 2.5 μm) at neutral pH, in the absence, solid black line, and in the presence of 2 mM AA, dashed red line, 4mM AA, dashed dotted blue line, and 6 mM AA, dotted green line. Alkylated PANi films were first reduced at -0.20 V vs. SCE for 3 min and thereafter the potential was scanned at 50 mV s^{-1} from -0.20 to +0.40 V in the absence and presence of AA. Solution was degassed with Ar for 15 min. and temperature controlled at 25 ± 1 °C.*

As can be seen, the addition of AA to the solution makes the anodic current increase, starting at approximately +0.00 V *vs.* SCE. The reduction peak current decreases on the

return scan. The fact that the reduction peak decreases or disappears, in the presence of ascorbate indicates that the polymer film is reduced because of the reaction with AA. As the polymer is already reduced by the reaction with the ascorbate molecules, the electrochemical reduction of the PANi is not observed on the return scan. The same effect is observed during successive additions of AA to the solution. Therefore, alkylated PANi films are an excellent surface for AA oxidation at neutral pH.

4.6.5 Alkylated PANi film as amperometric sensor for AA

Following the same approach used for the previous modified PANi microelectrodes, section 4.4, alkylated PANi were characterized as potential amperometric sensors for ascorbate at neutral pH. Figure 4.18 shows the response obtained at constant potential, E=0.10 V *vs.* SCE, during successive additions of AA. The first thing we notice, is that alkylated PANi films required less time to equilibrate, and as seen from figure 4.18, a stable signal is obtained in approximately between 2 to 3 minutes. This is considerably faster when compared to the previously characterized, PANi-PVS and PANi-PSS films. The equilibration time depends on polymer thickness and background solution.

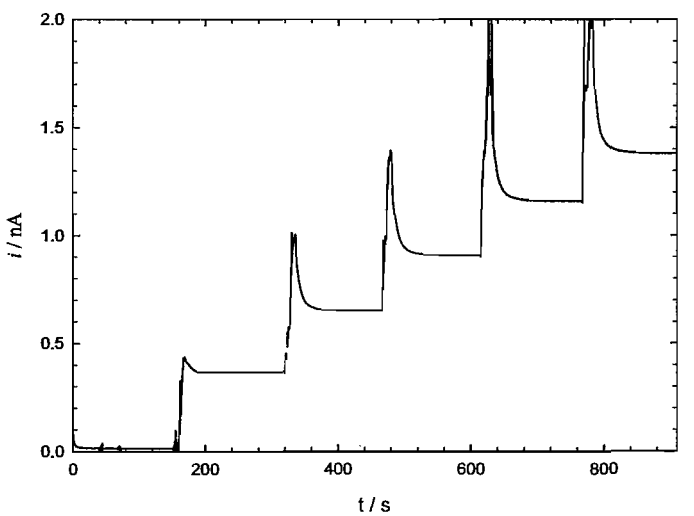

Figure 4.18 *Amperometric response, E = 0.10 V vs. SCE, for an alkylated PANi film, (deposition charge Q = 1.82 mC cm^2, a = 2.5 μm). The alkylated PANi was first reduced at -0.20 V vs. SCE for 3 min and thereafter the potential was stepped from -0.20 to +0.05 V in the absence and presence of AA. Each increase in the current corresponds to an addition of 1.0 mM AA. Solution was stirred for a few seconds with a magnetic.*

Experiments were carried out in 0.1 M citrate / 0.2 M phosphate buffer as a supporting electrolyte, pH 7, oxygen free solution at 25 °C. Electrical noise produced from the magnetic stirrer was eliminated from the graph.

The limiting currents obtained were plotted versus the ascorbate concentration and a linear trend was seen for the range of concentrations shown in figure 4.18. The response follows the expected slope of $n = 2$. This result agrees with our PANi-PVS films, but differs from those observed for PANi-PSS films, which presented lower limiting currents. This interesting observation will be discussed in Chapter 5.

4.6.6 Stability for alkylated PANi microelectrodes

Although alkylated PANi offers great properties when characterized at neutral pH and as electrocatalytic surface for ascorbate oxidation, there are some problems with the stability of the films. Successive calibrations for ascorbate yielded lower responses with each replicate. It is known that PANi films become more soluble after polymer alkylation[192]. Therefore, the problem with stability could be due to some loss of the alkylated portion of the polymer film, after long exposure to the buffer solution. When the films were characterized by cyclic voltammetry in HCl, no significant loss of the anodic charge was observed. However, when characterized at pH=7, after the calibration curves a clear reduction of the anodic and cathodic currents was observed and in some cases, a total loss of the initial properties. It was found that the response was recovered to a certain extent if the film was treated to a second alkylation process suggesting loss of alkylated link after exposure to buffer solution.

4.7 Conclusions

Throughout this chapter, we have presented different methods to retain PANi conductivity at neutral pH on small microelectrodes. The stability of the modified PANi depends on the counter ion introduced and the methodology adopted. The counter ion seems to play an important role to retain polymer conductivity. For all cases presented, excellent results were obtained towards our final applications. PANi/PSS films presented the better analytical properties for our final target as they remain stable for longer time compared to PANi-PVS.

The reason of the decrease in polymer stability is worth of further analytical study. Presumably, PANi expands when it is oxidised and this could aid PSS or PVS from the outer layer of the PANi composite to leach out into the solution. Mechanical stirring of the solution between additions of AA can also help to the loss of the counter ion. If this happens, charge balance between H^+ and SO_3^- groups will be different after long time exposure in buffer solution and therefore the response for ascorbate oxidation will differ from the initial. Analysing the charge under the emeraldine anodic peak before and after exposure to buffer solution shows that no PANi is being loss. Nevertheless, PVS seems to be lost faster than PSS. This is probably due to the density of the PANi composite chains being higher for PANI/PSS as it presents a higher degree of polymerization. The better stability present for PANi/PSS could be also due to a better interaction of the aromatic rings present in PSS with the PANi chains.

In addition, the experimental evidence that the PANi composite initial response in buffer pH can be recovered if the polymer is cycled in PSS or PVS with the corresponding acid suggest that PSS or PVS is lost from the outer later of the polymer film, after long time exposure to buffer solution.

When these films were used as electrocatalytic surfaces for ascorbate, the limiting currents obtained for PANI/PSS were half of the value compared to PANi/PVS and alkylated PANi films. There could be the possibility that PSS chains deposit preferentially in a way that reduces the PANi active sites available at the surface. If this is the case the PANi film will behave identically as a PANi-PVS film but with somehow with half of the reaction sites. Nevertheless, this observation is extremely curious and it is worthily of further study. Our results indicate that AA oxidation involves the transfer of two electrons.

Previous work by Bartlett and Wallace[134], using PANi-PVS modified RDE, have shown that the reaction of ascorbate at composites PANi films is of Michaelis-Menten type

mechanism. They showed that the ascorbate binds to the active PANi sites, in a similar way as enzyme-substrate complex, and a precise kinetic model was proposed.

Therefore, we were curious to see if the oxidation of AA at PANi-PSS microelectrodes follows a similar mechanism as for PANi/PVS modified RDE. Whether or not this is the case, it is believed that a deeper study of the electrode kinetics will help to provide a better understanding to our experimental results. The next chapter addresses this difficult question.

Chapter 5

A kinetic model for ascorbate oxidation at modified PANi microelectrodes

5.1 Objective

In this Chapter, we will determine with the help of mathematical models the precise operational characteristics of the modified electrode when operated in the steady state mode. This approach has the advantage that the model proposed will enable us to predict the optimum conditions, such as polymer thickness, counter ion, electrode potential, pH, etc, for an optimum operation.

In the next sections, we will introduce the concept of the kinetic model proposed by Bartlett and Wallace[135] for PANi composites on the RDE but now applied to microelectrodes. It has been our hope to obtain a deeper understanding of the reaction kinetics at PANi composites for ascorbate oxidation. The curious difference seen in Chapter 4 between PANi-PVS and PANi-PSS towards the oxidation of AA will be discussed in detail. Therefore, kinetic data will be compared between the RDE and the microelectrode for different PANi composites and our analysis will be summarized in a set of case diagrams. This Chapter aims to clarify this difficult question, and it is the first time in the literature to attempt such comparison for AA.

5.2 Introduction

Theoretical models describing mediated electron transfer at modified electrodes relevant to our work have been provided by Albery *et al.*[193-199], and by Andrieux and co-workers[118-120, 123, 200, 201]. In both approaches, planar diffusion of the substrate to the polymer matrix is considered. Lyons and Bartlett together or independently, have recently extended these theoretical models[51, 91, 98, 135, 202-213]. Careful consideration is required if these theoretical models are to be applied to microelectrodes. Lyons *et al*[210,

[214, 215]. and Dong and Che[216-223] have developed further the models provided for the electrocatalysis at hydrated polymer layers and applied to modified microelectrodes.

Reaction and diffusion at a polymer modified microelectrode is more complex than the corresponding process at a chemically modified macroelectrode, since both planar and radial diffusion must be considered[1]. The balance between radial and planar diffusion within the polymer film will alter depending on the ratio of the radius of the inlaid microdisc to the thickness of the overcoating polymer film[214]. For instance, if we define $\xi = \frac{a}{\ell}$ as the ratio between the electrode radius, a, and the polymer thickness, ℓ, then following Lyon's[214] analysis, radial diffusion will become important when the thickness of the polymer is comparable to the microelectrode radius. On the other hand, planar diffusion within the polymer will dominate when the thickness of the polymer is much lower than the microelectrode radius. This is a key question when approaching a theoretical model for modified microelectrodes.

As stated by Lyons *et al.*[210, 214, 215] and by Dong and Che[220-223] the question of polymer geometry will play a crucial role prior to the development of a theoretical model. On the one hand, modified macroelectrodes present planar shapes because no radial diffusion is present. However, modified microelectrodes may present planar or mushroom shapes. The three possible geometries most likely to be present at a modified microelectrode disc are sketched in figure 5.1.

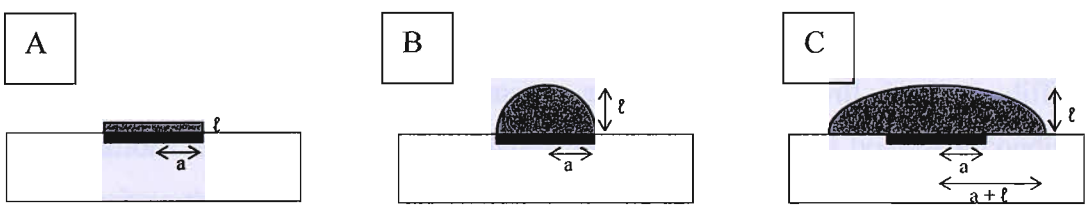

Figure 5.1. *Cartoon representing the three possible geometries of a polymer electrodeposited on a microelectrode; a, defines the microelectrode radius and, ℓ, defines the polymer thickness.*

The lack of data in the literature makes the problem of polymer geometry at a microelectrode still unresolved. This is probably difficult to believe as modified microelectrodes are used by many groups for numerous applications.

A different question to answer before establishing a model is whether the polymer film spreads out beyond the inlaid microdisc increasing the microelectrode radius, as shown in figure 5.1.c. It is commonly the case that for a macroelectrode the polymer film spreads over the conducting substrate and no spillover is observed and if there is any, it is insignificant compared to the electrode radius. However, when considering microelectrodes, the conducting polymer may spread outside the metal area, meaning that the polymer spreads a distance comparable to the microelectrode radius.

Caban *et al*[163]. showed that PANi films on a Pt microelectrode grow in the form of hemi-spherical micro deposits and their size exceeded three to six times the initial electrode disc radius, a = 11.5 μm. Depending on the time of electrodeposition the resulting films reached thicknesses ca. 50, 70 and 90 μm. So that the final polymer shape is similar to the one sketched in fig 5.1.c. This is not surprising as the lateral growth of PANi films has been observed even for different electrode geometries, specially for microband electrodes[164-167]. The reason for PANi lateral growth is subject to discussion and it is likely that film growth is based on progressive nucleation with the three-dimensional diffusionally-controlled growth of the nuclei[163, 224].

These two separate parameters, geometry and spill over, will lead to different approximations as they give rise to different sets of mathematical boundary conditions and necessitate the use of different distance normalization schemes when the equations quantifying transport and kinetic processes within the layer are solved[214].

Lyons *et al.*[210, 214, 215] and by Dong and Che[220-223], have reported interesting theoretical approaches to develop the equations which describe the overall current at polymer modified microelectrode for the case of first order reaction kinetics. They have considered the two possible situations; the polymer may spillover the conducting support,

or the polymer may not spillover. In both cases, they consider a mushroom shape after electropolymerization, figure 5.1.b and c. When the spillover is considerable, meaning that the polymer spreads a distance comparable to the microelectrode radius, a more complicated coordinate system is needed. Instead of spherical coordinates, it is necessary to use an oblate spheroidal coordinate system. This change of coordinates substantially complicates the mathematics involved.

Their studies show extremely good agreement when comparing between experiment and theory. However, their results are always based on first order reaction kinetics. The case for second order reaction kinetics remains unresolved. In this case the set of coupled non-linear differential equations becomes really complicated and nobody has solved them to date[215]. Therefore, the analysis of our experimental results becomes quite complicated. As we believe that the reaction of AA at modified PANi/PVS films might follow non-linear Michaelis-Menten reaction kinetics[89].

Summarizing, if we want to compare the previous mechanism proposed for AA oxidation at the modified RDE with our current modified microelectrodes, we need to consider the case where planar diffusion dominates with respect to radial diffusion at microelectrodes. This will only happen when the thickness of the polymer is much lower than the radius of the microelectrode. Only in this situation, can we use the current equations obtained for a non-linear Michaelis-Menten second order reaction kinetics, and applied to planar macroelectrodes for our modified microelectrodes.

5.3 Shape of the electrodeposited polymer film

In Chapter 3, we presented a study of controlled electrodeposition of PANi films at Pt microelectrodes. Cyclic voltammetry is a useful technique to control polymer thickness and avoid considerable polymer spill over and uncontrolled growth, which may produce anomalous morphologies. The electrodeposited PANi films had a thickness much lower than the microelectrode radius and with a really low degree of spillover, figure 3.7, section 3.6. Only in this situation, the kinetic models based on planar diffusion will apply for a microelectrode.

5.4 Kinetic Model

In the previous section, we discussed the different factors that lead to the initial boundary conditions when proposing a kinetic model. In addition to these variables, we now need to consider where the reaction takes place.

In the simplest case, the electrochemical reaction could occur at three different places; at the polymer/solution interface, within the polymer or at the electrode/polymer interface. In all cases, the kinetics of the reaction will be determined by;

1) Mass transport of the substrate from the bulk solution to the polymer surface.
2) Diffusion of the substrate within the polymer.
3) Binding of the substrate to the oxidized and active polymer sites. If a Michaelis-Menten mechanism is followed.
4) Electron or proton transfer. We consider that electron or proton movement is fast within these polymers.
5) Detaching of the oxidized product from the reduced and now inactive polymer sites.
6) Diffusion of the oxidized product within the polymer.
7) Mass transport of the reaction product to the bulk solution.

Lyons *et al.*[98] and Bartlett and Wallace[135] showed that the oxidation of AA at modified PPy or PANi is independent of polymer thickness. The reaction seems to occur at the polymer/solution interface. Considering the results of Bartlett and Wallace for RDE experiments[135], we believe that the oxidation of AA at PANi composites will follow a Michaelis-Menten type mechanism. Lyons and Bartlett[136] were pioneers introducing the concept of comparison between the electrochemical kinetics of heterogeneous redox catalysis at oxide layers with the mechanism occurring at enzyme electrodes. They developed a mathematical model describing heterogeneous redox catalysis at hydrated oxide layers. The theoretical model is applied to the electro oxidation of formate at RuO_2 electrodes in alkaline solutions. In this paper, it is proposed that the conversion of the substrate to the product occurs via a Michaelis-Menten type mechanism in the hydrated oxide layer. The effect of concentration polarization is also discussed. As it is relevant to

this thesis, a brief explanation of the mathematical approach is outlined and discussed together with its application to modified microelectrodes.

The reader can refer for further analysis to Lyons *et al*[210]. and Dong and Che[222] publications and references therein, where they have developed interesting mathematical equations to calculate the limiting currents for a modified microelectrode of different radius. However, their assumptions are based on a reaction mechanism occurring within the polymer film with a first order kinetics. Their equations are not applicable to our case, as we believe that ascorbate oxidation at modified PANi microelectrodes, occurs at the polymer/solution interface following a Michaelis-Menten type mechanism. This will be further discussed at the end of this chapter.

5.4.1 Theoretical model for heterogeneous redox catalysis at a thin hydrated oxide layer by Lyons and Bartlett[136]

A schematic representation of the theoretical model with the proposed reaction mechanism is shown in fig 5.2. AA represented as H_2A, has two ionizable protons, $pK_{a1} \sim 4.2$ and $pK_{a2} \sim 11.57$ [97]. At neutral pH, AA will be deprotonated, and represented in our case as $[AH^-_{bulk}]$, (units of mol cm^{-3}). Assuming that the oxidation of AA at modified PANi films occurs at the polymer/solution interface, the next sequence of steps is proposed.

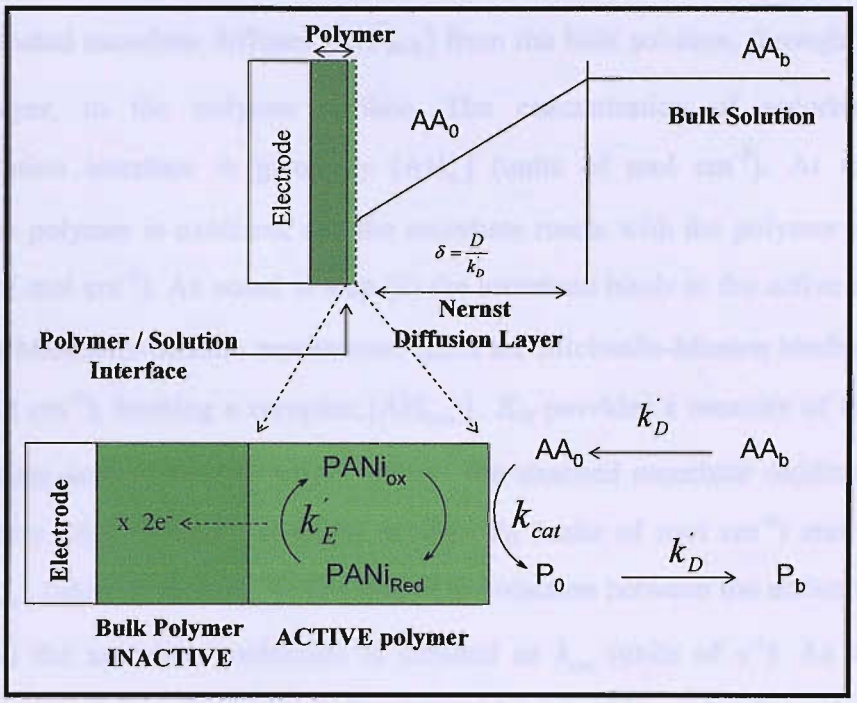

$$AH^-_{bulk} \xrightarrow{k'_D} AH^-_0 \qquad (1)$$

$$[\text{sites}]_{ox} + AH^-_0 \underset{}{\overset{K_M}{\rightleftharpoons}} (AH^-)_{complex} \qquad (2)$$

$$(AH^-)_{complex} \xrightarrow{k_{cat}} [\text{sites}]_{Red} + P_0 \qquad (3)$$

$$[\text{sites}]_{Red} \xrightarrow{k'_E} [\text{sites}]_{ox} + 2\,e^- + H^+ \qquad (4)$$

$$P_0 \xrightarrow{k'_D} P_{bulk} \qquad (5)$$

Figure 5.2 *Proposed reaction mechanism for the oxidation of ascorbate at modified PANi films, introduced by Bartlett and Wallace*[134]*. The reaction mechanism is slightly modified from the one proposed by Lyons and Bartlett*[136].

The deprotonated ascorbate diffuses [AH^-_{bulk}] from the bulk solution, through the Nernst diffusion layer, to the polymer surface. The concentration of ascorbate at the polymer/solution interface is given by [AH^-_0] (units of mol cm^{-3}). At the applied potential, the polymer is oxidized, and the ascorbate reacts with the polymer active sites Γ_{ox} (units of mol cm^{-2}). As noted in step (2) the ascorbate binds to the active sites of the polymer via Michaelis-Menten mechanism. K_M is the Michaelis-Menten binding constant (units of mol cm^{-3}), forming a complex, [AH^-_{bulk}]. K_M provides a measure of the strength of the substrate-active site interaction. Next, the attached ascorbate oxidizes with the polymer active sites, giving a reaction product P_0 (units of mol cm^{-3}) and a reduced polymer Γ_{red}, (units of mol cm^{-2}). The rate of the reaction between the active sites of the polymer and the ascorbate molecules is denoted as k_{cat} (units of s^{-1}). As the overall reaction is driven by an applied anodic potential at the electrode, the polymer is re-oxidized after reaction with AA.

Hence, the rate of polymer electro-regeneration is defined as k_E' (units of s^{-1}). Where k_E' depends on the electrode potential. We assume that charge propagation through the polymer film itself is rapid. Finally, the reaction product P_0 diffuses away to the bulk solution, P_{bulk}. It is assumed that the mass transport rate constant k_D' (units of cm s^{-1}) for the substrate and product are the same.

Assuming there is no inhibition by the reaction product and considering concentration polarization, the flux j (units of mol cm^{-2} s^{-1})for the reaction is described by[205];

$$\frac{1}{j} = \left(1 - \frac{j}{k_D'\,[AH^-_{bulk}]}\right)\left(\frac{1}{k_E'\,\Gamma_{sites}} + \frac{1}{k_{cat}\,\Gamma_{sites}}\right) + \frac{K_M}{k_{cat}\,\Gamma_{sites}\,[AH^-_{bulk}]} + \frac{1}{k_D'\,[AH^-_{bulk}]} \quad \textbf{(5.1)}$$

where

$$k_{cat} = \left(\frac{1}{k_2} + \frac{k_{-2}}{k_2\,k_3} + \frac{1}{k_3}\right) \textbf{(5.2)} \quad \text{and} \quad K_M = k_{cat}\left(\frac{1}{k_1} + \frac{k_{-1}}{k_1\,k_2} + \frac{k_{-1}\,k_{-2}}{k_1\,k_2\,k_3}\right) \textbf{(5.3)}$$

The significance of k_i and k_{-i} rate constants in (5.2) and (5.3) has been discussed by Albery and Knowles in the context of enzyme kinetics[225]. As the overall flux j measured will be determined by the limiting step of the reaction, equation 5.1 can be simplified for each case. When mass transport to the electrode surface is rate limiting, the term $k_D^{'}$ will be dominant. The reaction can be also limited by the binding constant between the ascorbate and the product and the reaction flux will be governed by K_M and k_{cat}. The term $\frac{1}{k_{cat}\ \Gamma_{site}}$ will dominate if there is saturated catalysis; the active sites of the polymer could be saturated due to high ascorbate concentrations in the vicinities of the polymer/solution interface. The term $\frac{K_M}{k_{cat}\ \Gamma_{site}\ [\mathrm{AH^-_{bulk}}]}$ will dominate for unsaturated catalysis. Furthermore, the reaction can be limited by the rate of the regeneration of the polymer actives sites, $k_E^{'}$. Therefore, the term $\frac{1}{k_E^{'}\Gamma_{\mathrm{site}}}$ will dominate.

Next, using the relationship between the current and the flux[17], i = nFAj, and assuming that catalysis at thin polymer layers present similarities to enzymatic catalytic systems, Lyons and Bartlett applied the approach by Albery and coworkers[197, 198] to obtain equation 5.4.

$$i_{overall} = n\ F\ A\left[\frac{k_{ME}^{'}\ K_{ME}\ [AA_{bulk}]}{K_{ME} + AA_{bulk}\left(1 - \frac{i}{n\ F\ A\ k_D^{'}\ [AA_{bulk}]}\right)}\right] \quad \textbf{(5.4)}$$

Where $K_{ME} = \left(\frac{K_M}{k_{cat}} + \frac{\Gamma_{site}}{k_D^{'}}\right)\left(\frac{1}{k_E^{'}} + \frac{1}{k_{cat}}\right)^{-1}$ **(5.5)** and $k_{ME}^{'} = \left(\frac{K_M}{k_{cat}\Gamma_{site}} + \frac{1}{k_D^{'}}\right)^{-1}$ **(5.6)**

The term K_{ME} (units of mol cm^{-3}) is related to the Michaelis-Menten rate constant and $k_{ME}^{'}$ (units of cm s^{-1}) represents the effective electrochemical rate constant for the thin

polymer film at low ascorbate concentrations. The term $\left(1-\frac{i}{nFAk_D'[AA_{bulk}]}\right)$ in equation 5.4 is due to the effect of concentration polarization[205].

Equation 5.4 can be rearranged to give a quadratic for i;

$$\frac{1}{nFAk_D'}i^2-(K_{ME}+[AA_{bulk}])+nFAk_{ME}'K_{ME}[AA_{bulk}]=0 \qquad (5.7)$$

Which is easily solved to give:

$$i=nFA\frac{k_D'}{2}\left[(K_{ME}+[AA_{bulk}])\pm\sqrt{(K_{ME}+[AA_{bulk}])^2-\frac{4k_{ME}'K_{ME}[AA_{bulk}]}{k_D'}}\right] \qquad (5.8)$$

The term ± will give two possible solutions. Plotting the limiting current i versus AA_{bulk} for substrate concentrations in the milimolar range we obtain the theoretical response represented in graph 5.3.

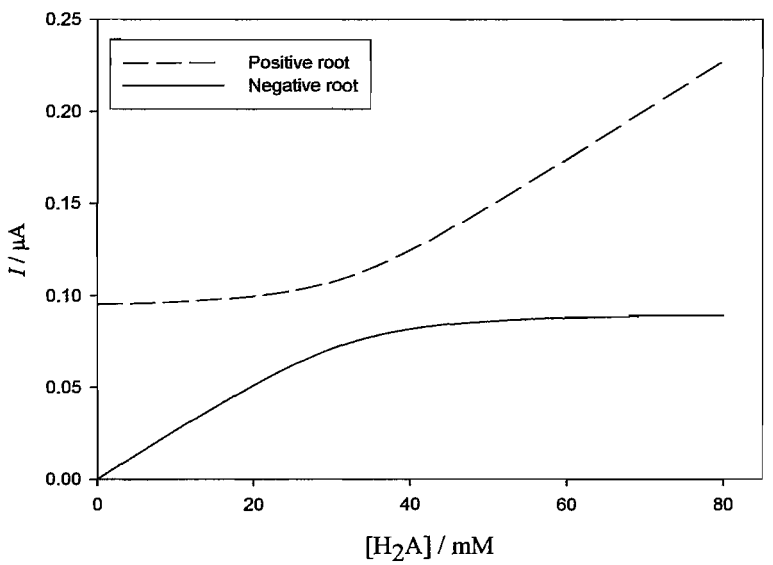

Figure 5.3 *theoretical solutions for the positive and negative square root of equation 5.8. Assuming, D = 5.0 x 10^{-6} cm s^{-1}, a = 12.5 µm, n = 2, K_{ME} = 3.43 x 10^{-2} mol cm^{-3} and k_{ME}' = 2.82 x 10^{-4} cm s^{-1}.*

Analyzing the solution for the negative root. At low substrate concentrations, the response is linear, following a pure mass transport control. In this region, the overall

current will be predicted by equation[17] $i=nFAkC$. As the ascorbic acid concentration increases, the reaction becomes kinetically limited and the currents registered will be lower than for a pure mass transport control. At high AA concentrations, the current reaches a saturation level, where the current no longer increases. It is clear from figure 5.8 that the solution for the positive root has no physical meaning and is discarded. Therefore, the overall current will be determined by equation 5.9.

$$i = nFA\left[\frac{k_D^{'}}{2}\left\{\left(K_{ME}+[\mathrm{AH^-_{bulk}}]\right)-\sqrt{K_{ME}+[\mathrm{AH^-_{bulk}}]-\left(\frac{4\ K_{ME}\ k_{ME}^{'}\ [\mathrm{AH^-_{bulk}}]}{k_D^{'}}\right)}\right\}\right]$$

(5.9)

Equation 5.9 represents the overall current for the electro-oxidation of a substrate at a thin polymer layer. It also considers the effect of concentration polarization and assumes there is no inhibition by the reaction product.

The overall current given by equation 5.9 depends on the reaction kinetics and therefore, is dependent on the potential applied. Equation 5.9 has four possible limiting cases:

Case IA. *Mass transport kinetics*

When the process is mass transport control, the term $k_D^{'}$ is the main term in equation 5.1. Hence, the current is determined solely by the rate of transport of AA to the polymer/solution interface. In this case, the rate of the catalytic reaction is faster than the rate of mass transport of the substrate to the polymer surface. In this case, $[AA_{bulk}] << K_{ME}$ and $\frac{k_{cat}\Gamma_{sites}}{K_M} >> k_D^{'}$. In addition, the potential applied is high enough to make the rate of electrocatalytic regeneration of the polymer active sites, $k_E^{'}$, fast. Equation 5.9 can then be simplified to give;

$$i_l = nFAk_D^{'}[AA_{bulk}] \quad \textbf{(5.10)}$$

This equation gives the current for a process under mass transport control. Hence for a RDE this equation is equivalent to the Levich equation[17];

$$i_l = 1.54nFD^{\frac{2}{3}}\upsilon^{\frac{-1}{6}}c^{\infty}W^{\frac{1}{2}}, \quad \textbf{(5.11)}$$

where, ν is the kinematic viscosity, W is the rotation rate in Hz, and the other values are as previously defined. For a microelectrode[1] the equivalent expression is;

$$i = 4nFDCa \quad \textbf{(5.12)}$$

Case II. *Unsaturated reaction kinetics*

The overall current is determined by $\frac{k_{cat}}{K_M}$, which is a rate constant and known as the specific constant. Because K_M determines in a way the bond strength between the ascorbate and the active sites of the polymer, it is used to compare the efficiency of different enzymes.

In this case, the rate of the electrocatalytic reaction is slower than the rate of mass transport. As we are still at low ascorbate concentrations and the rate of regeneration of the polymer active sites will be fast enough so as not to be rate limiting, the overall current will be given by;

$$i_{II} = \frac{nFAk_{cat}\Gamma_{site}[AA_{bulk}]}{K_M} \quad \textbf{(5.13)}$$

Overall, the reaction is second order being both first order in the concentration of sites and first order in ascorbate concentration.

Case III. *Reactivation of the polymer active sites,* $k_{sites}^{'}$.

Now the concentration of ascorbate at the polymer surface is high enough to saturate the polymer active sites, $[AA_{bulk}] >> K_{ME}$. In this situation, the rate of mass transport $k_D^{'}$ and the rate of the catalytic reaction k_{cat} are both much higher than the rate of electro-regeneration of the polymer active sites, $k_E^{'}$. Therefore, the overall current is given by;

$$i_{III} = nFAk_E^{'}\Gamma_{sites} \quad \textbf{(5.14)}$$

Case IV. *Saturated reaction kinetics.*

Again the concentration of ascorbate within the Nernst diffusion layer is high enough to saturate the polymer active sites, $[AA_{bulk}] >> K_{ME}$. But now the rate of the electro-

regeneration of the polymer active sites and the mass transport are higher than the rate of the catalytic reaction. The overall current is given by;

$$i_{IV} = nFAk_{cat}\Gamma_{sites} \quad \textbf{(5.15)}$$

Figure 5.4 plots equation 5.9 using the rate constants obtained by Bartlett and Wallace[135] using the RDE. The rate constants are calculated fitting the experimental data using a non linear least mean square program[134]. It can be seen that the electrode potential has a significant effect on the response obtained. In the next sections, our experimental data will be plotted in the same form and different kinetic parameters will be obtained.

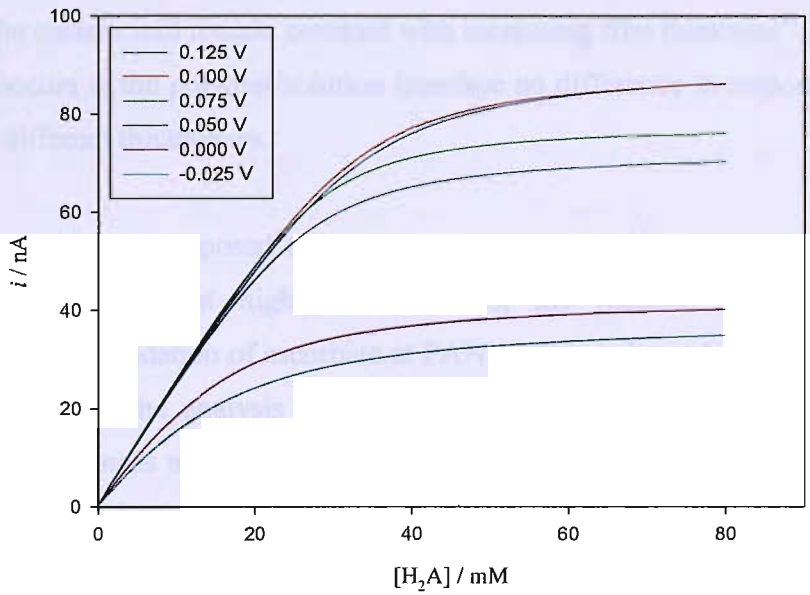

Figure 5.4 *Plots of current as a function of AA concentration for different electrode potentials calculated by equation 5.9 for a = 12.5 μm and using the rate constants* K_{ME} *and* $k_{ME}^{'}$ *obtained by Bartlett and Wallace using the RDE*[135] *and equation 5.9.*

5.5 Effect of film thickness

Previously we showed that our modified microelectrodes present planar geometry with low degree of polymer spillover beyond the metal disc. In order to apply the kinetic model proposed for the oxidation of ascorbate at modified Pt microelectrodes, we need to establish where the reaction takes place. As mentioned before, in the simplest case, the reaction could occur at the electrode/film interface, through the polymer or at the polymer/solution interface. If the reaction occurs at the electrode/film interface, the response would decrease with film thickness if transport through the film is slow. Moreover, if the reaction occurs through the whole of the film, the response to a constant concentration of ascorbate will initially increase with film thickness until there are enough reactive sites within the polymer to consume all the ascorbate diffusing into it, after which the current will remain constant with increasing film thickness[91, 92]. Finally, if the reaction occurs at the polymer/solution interface no difference in response should be observed for different thicknesses.

According to the model proposed at low ascorbate concentrations the response is mass transport controlled and at high concentrations, the reaction is kinetic limited. Consequently, if the oxidation of ascorbate at PANi-PSS is independent of film thickness we need to carry out the analysis under the conditions where the reaction kinetics is limiting rather than mass transport. In order to answer this question, we prepared two Pt microelectrodes coated with significantly different PANi-PSS thickness films. Figure 5.5 shows the values of the experimental limiting currents obtained for each film during ascorbate oxidation at neutral pH for a broad range of AA concentration.

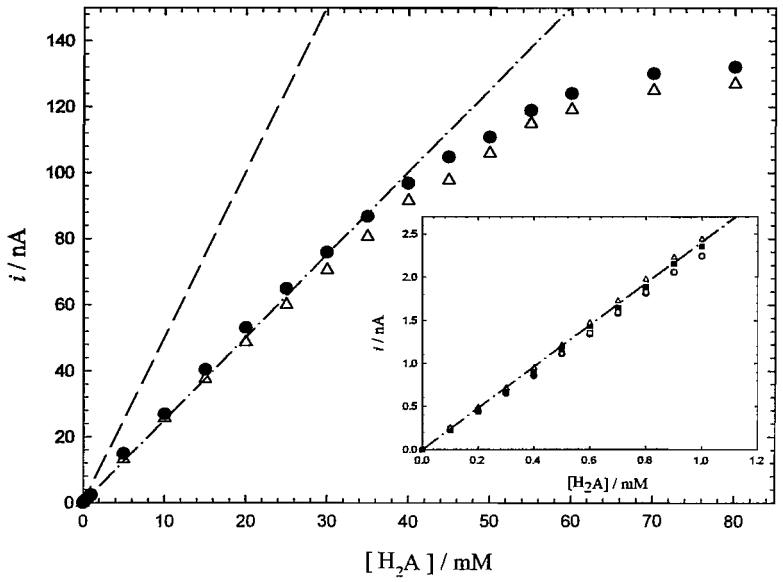

Figure 5.5 *Plots of the current at 0.10 V vs. SCE as a function of ascorbate concentration for a Pt disc microelectrode, a ~ 13.0 μm, potentiodynamically coated with two different film thicknesses of PANi-PSS,* • *12 mC cm*$^{-2}$ *and* Δ *3 mC cm*$^{-2}$*. Inset on figure shows the response for four different PANi-PSS of different thicknesses at low ascorbate concentration, deposition charges;* • *12 mC cm*$^{-2}$*,* ○ *7.8 mC cm*$^{-2}$*,* ■ *5.3 mC cm*$^{-2}$ *and* Δ *3 mC cm*$^{-2}$*. The dashed and dashed dotted lines represents the theoretical solution of eqn. 5.12, considering n = 2 and 1 respectively. Assuming D = 4.8 x 10*$^{-6}$ *cm*^{2} *s*$^{-1}$ *and a = 13.0 μm. The electrolyte solution was 0.1 M citrate / 0.2 M phosphate buffer, pH 7, temperature controlled at 25 °C and solution degassed with Ar for 15 min. The background current was subtracted from the experimental data.*

The inset in figure 5.5 shows the response obtained for another four Pt electrodes coated with PANi-PSS of different thicknesses for the concentrations of interest towards *in vivo* applications.

It can be seen that the current increases linearly with the ascorbate concentration for low ascorbate concentration and saturates at high concentrations. According to our model, this response will be expected as for low substrate concentrations no saturation of the polymer active sites is observed and the current is mass transport limited. In other words, the rate of electroregeneration of the polymer active sites, $k_E^{'}$, is much faster than the rate

of mass transport, k_D' . Inset on figure 5.5 clearly shows that for low ascorbate concentrations the response is not dependent on polymer thickness because the process is under mass transport control. The small deviations observed are believed to be due to small differences in the electrode area being larger for thicker polymers. It is clear that in this region we cannot assess where the reaction takes place.

At high ascorbate concentrations, we can see that two PANi-PSS of different thicknesses present quite similar response. The response deviates from linearity and the current is not dependent on ascorbate concentration. In this situation, the concentration of ascorbate at the polymer/solution interface is high and the polymer active sites do not regenerate fast enough. Therefore, the response is kinetically limited. If the reaction occurs through the polymer film, the experimental response will differ between films. Since we obtained similar response this is an indication that oxidation of ascorbate at PANi-PSS may occur at the polymer/solution interface.

Our current results agree with the results in the literature. Lyons *et al.*[98] at PPy films and Bartlett and Wallace[135] at PANi modified RDE also confirmed that ascorbate oxidation is thickness independent and occurs at the polymer/solution interface.

5.6 Number of electrons involved in the reaction

In the case of a microelectrode, equation 5.9 can be simplified to equation 5.12. This defines the current under mass transport control, which depends on the microelectrode radius, the diffusion coefficient, the concentration of AA and the number of electrons. Therefore, the experimental results were compared with the predicted theoretical response. The dashed and dashed dotted lines in figure 5.5 represent the theoretical solution of equation 5.12 considering the number of electrons, $n = 2$ or 1.

As seen from figure 5.5, our results indicate that the oxidation of ascorbate at PANi/PSS microelectrodes, surprisingly, may follow a one electron process instead of the expected two electron process. It is generally believed that the oxidation of ascorbate involves two electrons and depending on the pH, one or two protons transfer [111]. It has been reported in

the literature that electroinactive species can build up within the Nernst diffusion layer hindering the electrocatalytic reaction[98]. As the solution was stirred between the successive additions of AA, this effect can be neglected.

This unexpected result was observed during the course of many experiments and by different collaborators within this project. Dr. Stefan Hanstein and Dr. Paul Kilmartin applied our PANi/PSS microelectrodes for the oxidation of ascorbate in plants leaves and in wine beverages respectively, obtaining the same results as ours. Previous experience in our laboratories[134] with PANi-PVS modified RDE, applied ascorbate oxidation, gave the expected two electron process. At this stage, it was surprising for us to think that the counter ion within the polymer affects the number of electrons involved in the reaction. This curious and unpredicted observation is now further discussed.

5.7 Effect of the counter anion for the oxidation of ascorbate at modified PANi microelectrodes

Desilviestro and Scheifele[65] clearly showed how the growth mechanism and the final polymer morphology are influenced by the electrochemical method used and the experimental conditions, such as aniline concentration, counter ion, pH, etc.

We have attempted many times to obtain SEM images for these PANi microelectrodes, but our best results are shown in figure 3.7. We had no success obtaining a higher resolution image to find out the polymer morphology at the polymer/solution interface.
Bartlett and Wallace[134] showed that the electropolymerization of PANi films in the presence of PVS MW $\approx$ 4000-6000, produced an open structure. However, when using PSS, MW $\approx$ 70,000, as the counter ion, the film is more dense and compact in appearance. Similar data for PANi-PVS[92, 169] and PANi-PSS [92, 168, 226] films is available in the literature. Although the same solution composition and scan rate was used for the PANi electrodeposition at the RDE and the microelectrode, the diffusion of intermediates away from the electrode is much more rapid at the microelectrode. Therefore, we might expect differences in morphology for each case. The only situation were both

morphologies will be comparable is when the rotation rate of the RDE is fast enough to achieve similar mass transport as the microelectrode under study.

Although the counter ion affects the gross morphology of the polymer on the micrometer scale, it should not affect the details of the reaction mechanism on the molecular level. It is believed that the active sites of the PANi film, the diimine units within the polymer[134], will be the same and accessible independently of the counter ion. As in theory, the counter ion is present just to retain proton conductivity at neutral pH[89-91].

In order to clarify this difficult question a composite polymer containing both counter ions, PVS and PSS was prepared following the procedures proposed by Barbero *et al.*[169] and by Hyodo and Oomae[160, 161]. They showed that the counter ion can be introduced by different methods; it can be done from the same acidic solution containing the aniline monomer and the desired counter ion, or the PANi film can be first electrodeposited on the electrode and afterwards exposed to an acidic solution containing the new counter ion.

Figure 5.6 compares the response for ascorbate oxidation at low ascorbate concentrations for three modified PANi films, with different counter ions. The response plotted clearly shows that the counter ion present within the PANi film alters the limiting currents obtained for ascorbate oxidation.

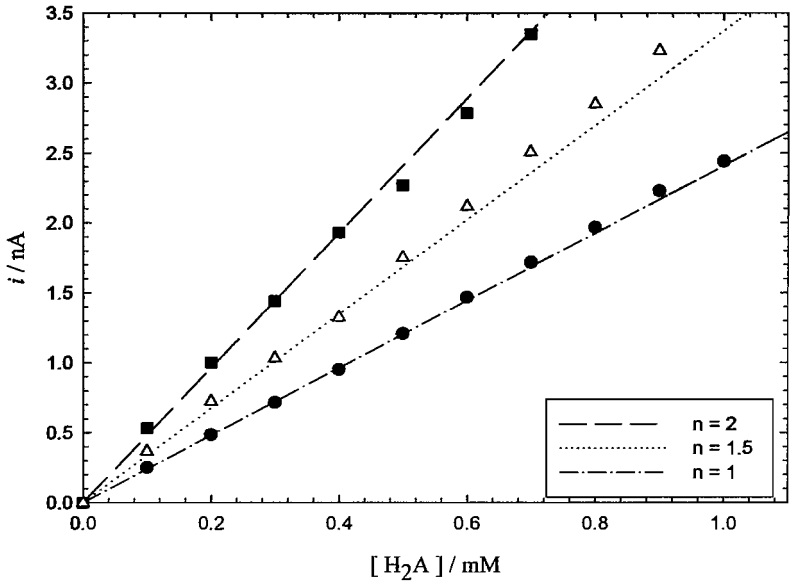

Figure 5.6 *Plots of the current at 0.10 V vs. SCE as a function of ascorbate concentration for a Pt disc microelectrode, A = 4.91 x 10^{-6} cm^2, potentiodynamically coated with three different PANi films.* ■ *PANi/PVS,* •*PANi/PSS, and PANi-PVS-PSS. Approximated deposition charges, Q = 3.5 ± 0.3 mC cm^{-2}. The dashed, dotted and dashed dotted lines represent the theoretical solution of equation 5.12, for n = 2, 1.5 and 1 respectively. Experimental conditions are as described in figure 5.5.*

The experimental results for PANi-PVS, ■, match closely the predicted response, dashed line, for $n = 2$. This result agrees with the response obtained by Bartlett and Wallace[135] at the PANi/PVS modified RDE. There, they suggested that ascorbate may oxidize at the polymer/solution interface through a hydride transfer mechanism, according to $n = 2$.

PANi-PSS, •, present lower limiting currents, and the predicted response matched the experimental values for $n = 1$. Consequently, the reaction mechanism at PANi/PSS microelectrodes has to be different to that occurring at PANi/PVS. The reaction mechanism could be different to the one proposed in figure 5.2. In this case, ascorbate oxidation seems to occur through the generation of an ascorbate radical intermediate, in a similar manner to bare Pt electrodes. However, this radical anion intermediate, if produced, is not oxidized to DHA. It can be suggested that the ascorbate radical

intermediate diffuses to the bulk solution before is further oxidized. Hence, the second electron is not produced and the limiting currents registered only show a one electron process, $n = 1$.

In the case of the PANi/PVS/PSS copolymer, it can be seen that the response obtained lies exactly in between the other two composites films. The experimental response matches the theory when $n = 1.5$. This experiment shows that when the PSS chains are introduced within the PANi/PVS are packed in a way that affects the mechanism for ascorbate oxidation. However, obtaining limiting currents in between both cases is even more surprisingly.

Our problem could be similar but certainly not comparable to the oxygen reduction reaction at bare platinum microelectrodes. Kucernak *et al*[227]. have demonstrated that the oxygen reduction mechanism follows a different number of electrons depending on the electrode radius. They clearly showed that, hydrogen peroxide, H_2O_2, the intermediate in oxygen reduction, diffuses fast before is further reduced to H_2O, for microelectrodes. So the number of electrons changes from $n = 4$ for a macroelectrode to $n = 2$ or lower for a microelectrode. However, in our case we see values for n in between 1 and 2, which is puzzling.

A careful review within the literature shows that Lyons *et al.*[98] observed something similar during the oxidation of ascorbate in NaCl at modified PPy films with DBS^- (dodecylbenzene sulphonate) or Cl^- as the counter ions. There they saw higher limiting currents for PPy/ DBS^- films. However, the differences in the limiting currents observed are not double or half the value as in our case. The reaction or with respect to $[H^+]$ was -0.94 and -1.09 for PPy/Cl and PPy/DBS respectively, as it was expected. However, the reaction order with respect AA was 0.98 and 0.47 for PPy/Cl and PPy/DBS respectively. Lyons proposed a different adsorption of the ascorbate intermediate radical for each polymer, considering the first electron transfer step (generation of the radical anion), step 2 in figure 1.11, as the rate determining step for PPy/Cl. The fractional order with respect

to AA found for PPy/DBS was attributed to a slow desorption of the radical anion intermediate.

More recently Willner *et al.*[96] presented a PANi-PSS film containing gold nanoparticles that produced higher electrocatalytic currents compared to PANi-PSS, for ascorbate oxidation. Regrettably, no discussion in terms of mechanistic study is given. Thus, our results are not as unexpected as we initially thought. Something seems to be happening that is related to the choice of counter ion within the polymer film, which is in addition to the polymer gross morphology.

Unfortunately, at this stage of the Chapter we can not provide a final answer to this question. The effect of the counter ion will be further discussed during the conclusions at the end of this Chapter.

5.8 Effect of ascorbate concentration for PANi-PVS and PANi-PSS composites

Figure 5.7 plots the experimental limiting currents obtained at 0.10 V *vs.* SCE at different ascorbate concentrations, for PANi-PVS and PANi-PSS composites with similar electrodeposition charges. As we can see, PANi-PVS films present higher limiting currents across the whole range of concentrations studied. Dashed and dashed dotted lines in figure 5.7 plot the theoretical solution of equation 5.12. for $n = 2$ and $n = 1$ respectively.

Using a commercial non-linear least mean squares program, we can fit our experimental data to the proposed model. The dotted lines in figure 5.7 are the best fits obtained between the experimental data and the Lyons equation (5.9). See Appendix A.1. for further details.

Number of electrons	K_{ME} / mol cm^{-3} PANI-PVS	$k_{ME}^{'}$ / cm s^{-1} PANI-PVS
2	(3.93 ± 0.08) X 10^{-5}	(4.61 ± 0.02) X 10^{-3}

Table 5.1. *Best fit parameters, considering number of electrons n = 2 and D = 4.8 x 10^{-6} cm^2 s^{-1}, from the analysis of the current for ascorbate oxidation at PANi-PVS modified electrode using equation 5.9 for the data shown in figure 5.7 In each case the number of points considered during the fitting was λ = 15.*

Number of electrons	K_{ME} / mol cm^{-3} PANI-PSS	$k_{ME}^{'}$ / cm s^{-1} PANI-PSS
2	(5.81 ± 0.20) X 10^{-5}	(3.01 ± 0.04) X 10^{-3}
1	(5.31 ± 0.10) X 10^{-5}	(4.62 ± 0.02) X 10^{-3}

Table 5.2. *Best fit parameters, considering different number of electrons n = 2 or 1 and D = 4.8 x 10^{-6} cm^2 s^{-1}, from the analysis of the current for ascorbate oxidation at PANi-PSS , modified electrode using equation 5.9 for the data shown in figure 5.7 In each case the number of points considered during the fitting was λ = 15.*

5.9 Effect of electrode potential

Assuming the oxidation of ascorbate at modified PANi films occurs at the polymer/solution interface, we can analyze the electrochemical response for a single film thickness but this time at different potentials. The potential applied will have a strong influence on the concentration of polymer active sites, Γ_{sites}, and the rate of the polymer electro-regeneration of active sites, $k_E^{'}$.

Therefore, by studying the ascorbate oxidation at PANi for different potentials and concentrations we will be able to asses the influence of these 3 important parameters; Γ_{sites}, $k_E^{'}$ and K_M. This information will produce a better understanding and establish the validity of the proposed model.

It is known that within the potential range -0.10 and 0.15 V *vs.* SCE these PANi composites are in the emeraldine state and therefore, conducting[89, 91, 92]. For that reason, ascorbate oxidation at modified PANi-PSS microelectrodes was studied between -0.025 and +0.125 V volts. These will produce a broad potential range where significant differences may be observed. Figure 5.8, plots the experimental measured current versus ascorbate concentration for a single film thickness but at different electrode potentials.

It is clear that the potential applied affects the limiting currents obtained. The responses deviate from linearity and reach saturation level at all of the potentials applied. It is interesting to note that the deviation from linearity and the saturation level are reached at different ascorbate concentration depending on potential applied.
This is a consequence of the concentration of polymer active sites, Γ_{sites}, which strongly depends on the potential applied. Although it is still not clear to us but the applied potential may also affect the adsorption of [HA^-] species into the polymer and therefore affect the strength of the attachment between substrate and ligand, K_M.

Out of these experimental results, it was considered that a potential in between 0.075 and 0.125 V *vs.* SCE would give the optimum value for ascorbate oxidation at neutral pH on PANi-PSS films.

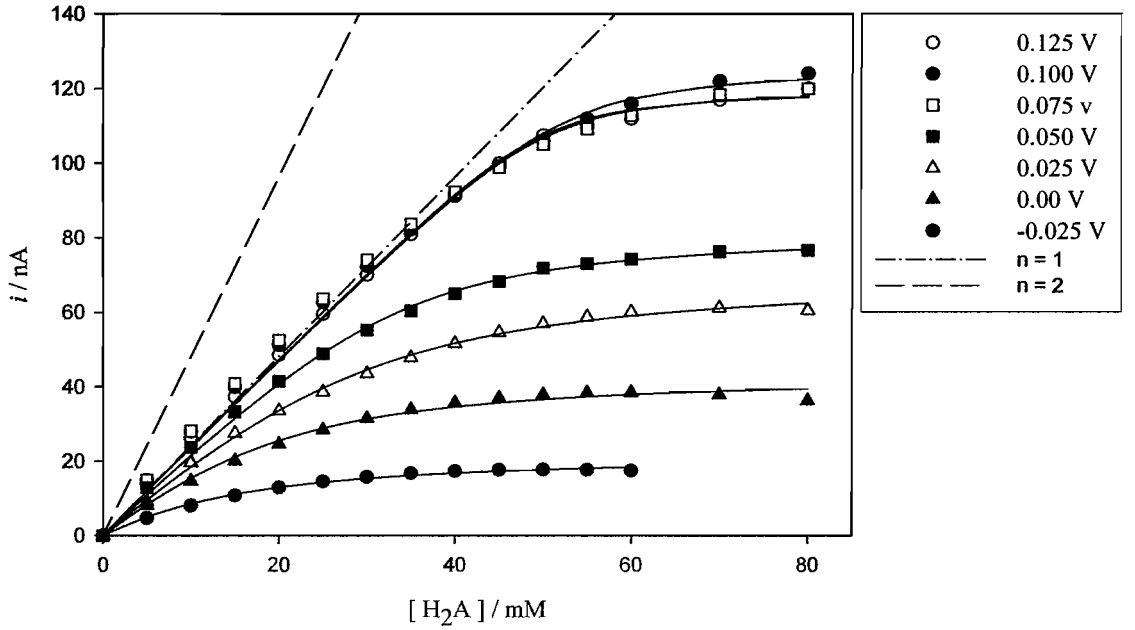

Fig 5.8 *Plots of the current as a function of ascorbate concentration for a Pt disc microelectrode A = 4.91 x 10^{-6} cm^2, coated with PANi-PSS (Q = 3.5 ± 0.3 mC cm^{-2}) at different potentials. The solid lines represent the best fit to equation. 5.9, considering n = 1, D = 4.8 x 10^{-6} cm^2 s^{-1} and a = 13.0 μm. The dashed line is the theoretical response for a pure mass transport control, given by equation.5.12 for n = 2 and the dashed dotted line is the equivalent for n = 1. Solution 0.1 M citrate / phosphate buffer, pH 7, at 25 °C, degassed with Ar for 15 min.*

As we did in figure 5.7, the experimental results were also fitted to the theoretical model proposed. The solid black lines in figure 5.8 represent the best fits to equation 5.9 while the points show the experimental data. The good fitting of the theoretical and experimental data is notable which might be a further indication of the validity for the proposed model.

Figure 5.8 also plots the theoretical response for a pure mass transport control process with n = 1 or 2, shown by the dashed dotted and dashed lines respectively. Table 5.3 shows the values obtained out of the fitting for each potential considering n = 1.

E vs. SCE	K_{ME} / mol cm^{-3} PANi-PSS, n = 1	k_{ME} / cm s^{-1} PANi-PSS, n = 1
0.125	(5.05 ± 0.07) X 10^{-5}	(4.63 ± 0.01) X 10^{-3}
0.100	(5.32 ± 0.10) X 10^{-5}	(4.63 ± 0.02) X 10^{-3}
0.075	(5.04 ± 0.10) X 10^{-5}	(4.64 ± 0.02) X 10^{-3}
0.05	(3.71 ± 0.07) X 10^{-5}	(4.31 ± 0.03) X 10^{-3}
0.025	(3.56 ± 0.10) X 10^{-5}	(3.83 ± 0.05) X 10^{-3}
0.000	(2.48 ± 0.10) X 10^{-5}	(3.43 ± 0.10) X 10^{-3}
-0.025	(1.94 ± 0.12) X 10^{-5}	(2.21 ± 0.08) X 10^{-3}

Table 5.3. *Best fit parameters obtained from figure 5.8 at different potentials, from the analysis of the limiting current for ascorbate oxidation at PANi-PSS modified electrode using equation 5.9. In each case the number of points considered during the fitting was* $\lambda = 15$.

As we are dealing with this curious effect of the number of electrons involved during ascorbate oxidation at PANi-PSS. Our experimental values were also fitted using the same non linear least mean square fit program but considering n = 2, at all the different potentials. The result of the fitting is presented in figure 5.9 where the points represent the same experimental response from figure 5.8 but this time the solid lines represent the best fit of the Lyons equation, 5.9, considering $n = 2$.

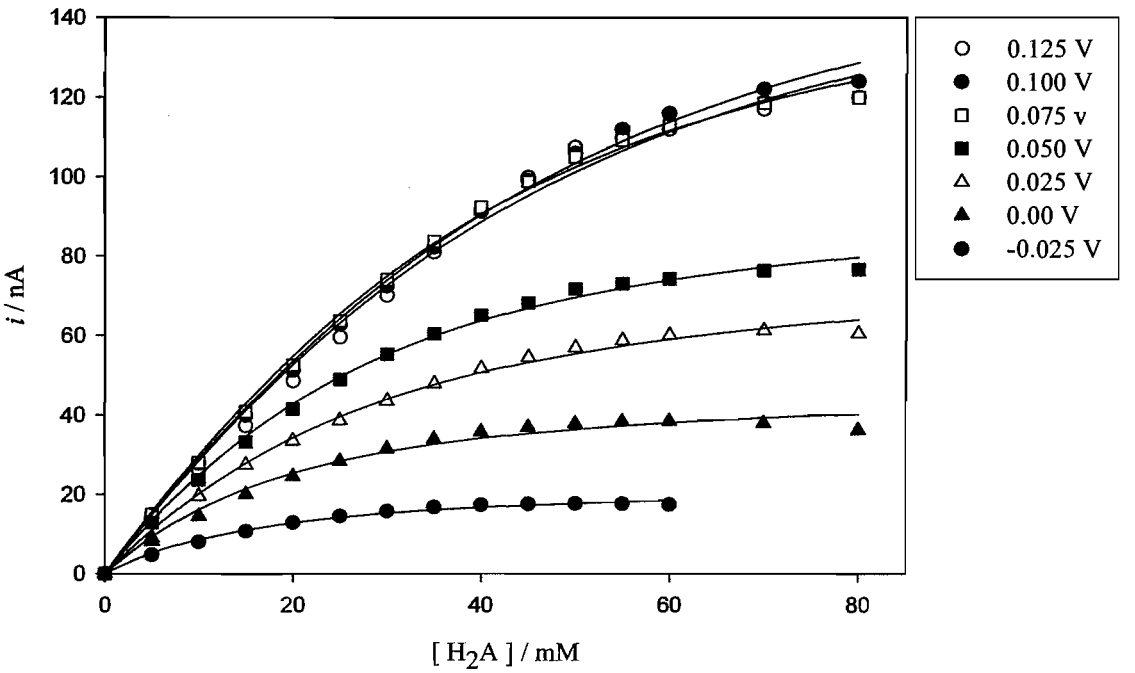

Fig 5.9 *Plots of the current as a function of ascorbate concentration for a Pt disc microelectrode A = 4.91 x 10^{-6} cm^2, potentiodynamically coated with PANi-PSS (Q = 3.2 mC cm^{-2}) at different potentials. The solid lines represent the best fit to equation. 5.9, considering n = 2, D = 4.8 x 10^{-6} cm^2 s^{-1} and a = 13.0 μm. Solution 0.1 M citrate / phosphate buffer, pH 7, at 25 °C, degassed with Ar for 15 min.*

As seen from figure 5.9, the fitting of the Lyons equation, 5.9, to the experimental response, considering $n = 2$ is also really good. This graph may lead to misleading conclusions if not analyzed properly. For guidance during our final discussion at the end of this Chapter, the best fit parameters obtained during the fitting from figure 5.9 are presented in table 5.4.

E vs. SCE	K_{ME} / mol cm^{-3} PANi-PSS, n = 2	k_{ME} / cm s^{-1} PANi-PSS, n = 2
0.125	(5.71 ± 0.5) X 10^{-5}	(2.98 ± 0.10) X 10^{-3}
0.100	(5.80 ± 0.30) X 10^{-5}	(3.01 ± 0.06) X 10^{-3}
0.075	(5.09 ± 0.20) X 10^{-5}	(3.13 ± 0.02) X 10^{-3}
0.05	(3.44 ± 0.10) X 10^{-5}	(2.76 ± 0.06) X 10^{-3}
0.025	(3.42 ± 0.19) X 10^{-5}	(2.30 ± 0.07) X 10^{-3}
0.000	(2.26 ± 0.20) X 10^{-5}	(2.04 ± 0.10) X 10^{-3}
-0.025	(1.86 ± 0.20) X 10^{-5}	(1.21 ± 0.07) X 10^{-3}

Table 5.4. *Best fit parameters obtained from figure 5.9 at different potentials, from the analysis of the limiting current for ascorbate oxidation at PANi-PSS modified electrode using equation 5.9. In each case the number of points considered during the fitting was* $\lambda = 15$.

Finally, due to the similarities between the calibration curves obtained for PANi-PVS obtained with our current PANi-PSS microelectrodes. The points shown in graph 5.10 show the experimental response we have currently obtained for PANi-PSS microelectrodes at three different potentials. However, the solid lines in figure 5.10 show the current calculated from equation 5.9 using the best fit parameters obtained by Bartlett and Wallace[135] with PANi-PVS composite and considering an electrode radius of a = 13.0 μm. This graph shows how the values of K_{ME} and k_{ME} differ between the RDE and the microelectrode.

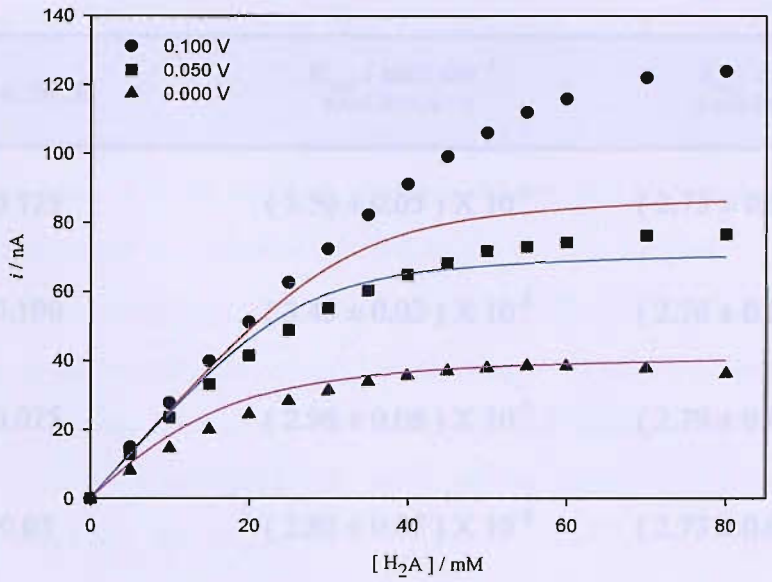

Fig 5.10 *Plots of the current as a function of ascorbate concentration for a Pt disc microelectrode A = 4.91 x 10^{-6} cm^2, potentiodynamically coated with PANi-PSS (Q = 3.2 mC cm^{-2}) at different potentials. Red, blue and pink solid lines represent the fit of equation 5.9 to the experimental data shown by the points at different potential. Using the best fit parameters obtained by Bartlett and Wallace[135] with PANi-PVS, n = 2. Assuming a diffusion coefficient of D = 5.0 x10^{-6} cm^2 s^{-1} and electrode radius, a = 13.0 μm. Solution 0.1 M citrate / phosphate buffer, pH 7, at 25 °C, degassed with Ar. for 15 min.*

Table 5.5 gives the best fit values by Bartlett and Wallace published in ref [135], for further comparison.

E vs. SCE	K_{ME} / mol cm^{-3} PANi-PVS, n = 2	$k_{ME}^{'}$ / cm s^{-1} PANi-PVS, n = 2
0.125	(3.50 ± 0.05) X 10^{-5}	(2.73 ± 0.02) X 10^{-3}
0.100	(3.43 ± 0.02) X 10^{-5}	(2.76 ± 0.01) X 10^{-3}
0.075	(2.96 ± 0.06) X 10^{-5}	(2.79 ± 0.02) X 10^{-3}
0.05	(2.82 ± 0.05) X 10^{-5}	(2.73 ± 0.02) X 10^{-3}
0.025	(1.77 ± 0.04) X 10^{-5}	(2.53 ± 0.03) X 10^{-3}
0.000	(1.99 ± 0.05) X 10^{-5}	(2.28 ± 0.03) X 10^{-3}
-0.025	(2.05 ± 0.07) X 10^{-5}	(1.98 ± 0.04) X 10^{-3}

Table 5.5. *Best fit parameters obtained from reference* [135]. *These values belong to the analysis of the limiting currents at different potentials for ascorbate oxidation at PANi-PVS modified electrode using equation 5.9 with n = 2.*

Summarizing, we have seen that the potential applied has a marked effect on the electrochemical reaction. The ascorbate concentration at which the current starts to deviate from linearity depends on the potential applied. From figure 5.10, it can be seen that approximately above 20 mM ascorbate, at E = 0.10 V *vs.* SCE, the current is no longer mass transport limited. The increase of the ascorbate concentration in the solution will start to saturate the polymer active sites. Therefore, the current will no longer be limited by $k_D^{'}$ and so will be limited by either the rate of electron transfer, $k_E^{'}$, or the rate of the electrocatalytic reaction, k_{cat}.

When a good fit of the experimental data with equation 5.9 is obtained, the non linear least mean squares program gives the best fit parameters for K_{ME} and k'_{ME}. The values obtained for different cases are presented in Tables 5.3, 5.4 and 5.5. Out of the fitting of the experimental data we can see that, knowing the values for electrode potential and ascorbate concentration the proposed model might be able to give us the numbers at which the electrochemical reaction will be limited by either k'_D, k'_E or k_{cat}. However, when comparing the best fit data obtained considering $n = 1$ or $n = 2$, presented in figures 5.8 and 5.9 we can not draw any final conclusions and further analysis is needed. The next section is aimed at clarifying the validity of our proposed by the analysis of the values obtained for K_{ME} and k'_{ME}.

5.10 Analysis of proposed model

5.10.1 Effect of k'_{ME}

In order to investigate the effect of electrode potential and the validity of the proposed model, we will analyze in detail the values obtained in Table 5.3, 5.4 and 5.5. We will start first with k'_{ME}, the effective electrochemical rate constant for the thin polymer film at low ascorbate concentrations.

By inspecting equation (5.6), $k'_{ME} = \left(\frac{K_M}{k_{cat}\Gamma_{site}} + \frac{1}{k'_D} \right)^{-1}$, we can determine which step is rate limiting at a given potential. It could be the mass transport rate constant, k'_D, or the surface reaction kinetics given by $\frac{k_{cat}\Gamma_{sites}}{K_M}$. Therefore, by plotting the experimental values obtained for k'_{ME} as a function of the electrode potential we should be able to assess which step is slower.

Figure 5.11 compares the values from Tables 5.3 and 5.5, as a function of the electrode potential for our current PANi-PSS, $n = 1$, microelectrodes versus the values obtained by Bartlett and Wallace[135] with PANi-PVS, $n = 2$, at the RDE.

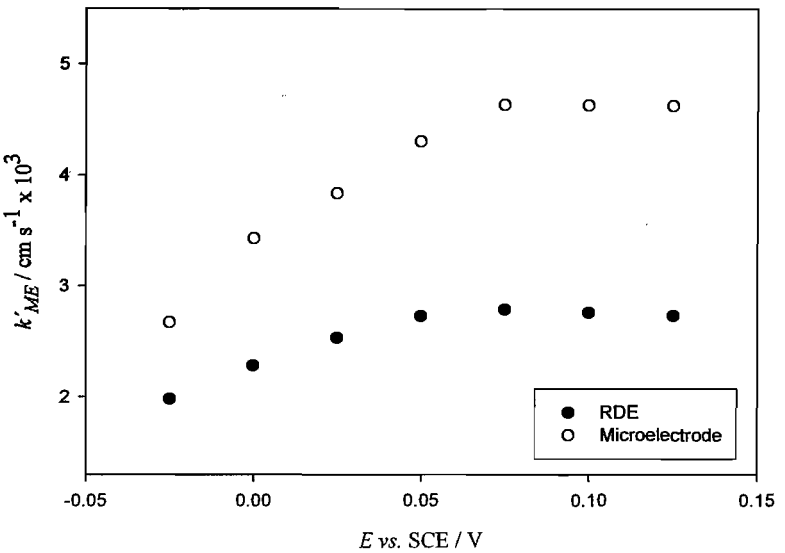

Figure 5.11 *Plot of k'_{ME} as a function of potential.* o *symbols represent our current values obtained for our PANi-PSS microelectrode studies, considering the mass transport rate constant approximated as* $k'_D = \frac{4D}{\pi a}$. • *symbols represent data from the previous RDE studies*[135]. *The data are taken from table 5.3,* o *PANi-PSS, n = 1, and table 5.5,* • *PANi-PVS, n = 2.*

This representation clearly shows which step is limiting as we can see two clear regions for both cases. From figure 5.11 we can see that below 0.075 V *vs.* SCE, k'_{ME} is dependent of the electrode potential. However, above this potential, k'_{ME} is independent of the potential. If we assume that the Michaelis-Menten constant, K_M and the mass transport rate constant of the substrate, k'_D, are both independent of potential, from equation (5.6), any potential dependence seen in k'_{ME} will be due to a variation in the concentration of active sites, Γ_{sites}. Hence, as seen from figure 5.11, the potential dependence seen for potentials below 0.075 V *vs.* SCE has to be due to an increase in the value of $k_{cat}\Gamma_{sites}$.

Rewriting equation 5.6 as, $k'_{ME} = \frac{k_{cat}\Gamma_{sites}k'_D}{K_M k'_D + k_{cat}\Gamma_{sites}}$ and following figure 5.11 we can see that for potentials below 0.075 V, $k_{cat}\Gamma_{sites} << K_M k'_D$, and $k'_{ME} = \frac{k_{cat}\Gamma_{sites}}{K_M}$.

This agrees with our experimental values, as $k_{cat}\Gamma_{sites}$ increases with the electrode potential and so does k'_{ME} with a slope that has to be proportional to the inverse of the Michaelis-Menten constant. On the other hand, when the potential is higher than 0.075 V, the opposite occurs and now $k'_{ME} = k'_D$.

Therefore, if the model proposed is consistent with the data, the experimental values obtained for k'_{ME} at potentials higher than 0.075 V, should match with the theoretical mass transport rate constant, k'_D. For the RDE at a rotation rate of 9 Hz, $k'_D = 1.56 D^{2/3} \nu^{-1/6} W^{1/2}$ = 2.93 10^{-3} cm s^{-1} and for a microelectrode, $k'_D = \frac{4D}{\pi a}$ = 4.70 x 10^{-3} cm s^{-1}. The diffusion layer thickness approximated as $\delta = \frac{k'_D}{D}$ is approximately 17 and 13 μm for the RDE at 9Hz and the microelectrode respectively. It is extremely pleasant to see that at high potentials, our experimental values for k'_{ME} are close to the calculated k'_D values. This is now a more clear indication of the validity of the proposed model.

Furthermore, we want to emphasize that a careful analysis of the experimental data is needed in order to interpret the results correctly. For instance, an excessive trust in the fitting of the experimental data using a non linear least mean squares program can lead to misleading results. i.e. if we consider n = 2 for a PANi-PSS microelectrode, we can see from figure 5.9 that a good fitting of the experimental data to the Lyons equation is obtained. The fitting program gives the values for k'_{ME} and K_{ME}, and presented in table 5.4. As we can see, k'_{ME} has a given value of 3.01 x 10^{-3} cm s^{-1}, E = 0.10 V. This value clearly differs from the calculated value k'_D = 4.70 x 10^{-3} cm s^{-1} and therefore will lead your results to an incorrect analysis. The same analysis applies to PANi-PVS composites.

5.10.2 Effect of K_{ME}

Following with the study of the proposed model, the effect of potential on K_{ME} was also studied and it is presented in figure 5.12. In the case of the RDE, we find that a potentials below 0.05 V, K_{ME} is potential independent, and above this value becomes potential dependent. Similar behaviour in response is seen for the microelectrode, but somewhat shifted. However, we can see that if the potential is held at 0.00 V and in between 0.075 and 0.125 V, K_{ME} is potential independent. As we mentioned before, any change seen with potential may be related to a change in $k_{cat}\Gamma sites$.

Hence, if we assume that for these potentials the rate of electron transfer is faster than the rate of the chemical reaction we can rewrite K_{ME} as, $K_{ME} = K_M + \frac{k_{cat}\Gamma_{sites}}{k_{ME}^{'}}$. Therefore, for the potential independent region, $K_{ME} = K_M$, and for the potential dependent region, $K_{ME} = \frac{k_{cat}\Gamma_{sites}}{k_{ME}^{'}}$. If we consider the case where $k_{cat} << k_E^{'}$, equation 5.5 can be expressed as $K_{ME} = K_M + \frac{k_{cat}\Gamma_{site}}{k_D^{'}}$.

Finally, as K_{ME} is related to $k_E^{'}$, we can obtain, $K_{ME} = \frac{k_{cat}\Gamma_{sites}}{k_{ME}^{'}}$.

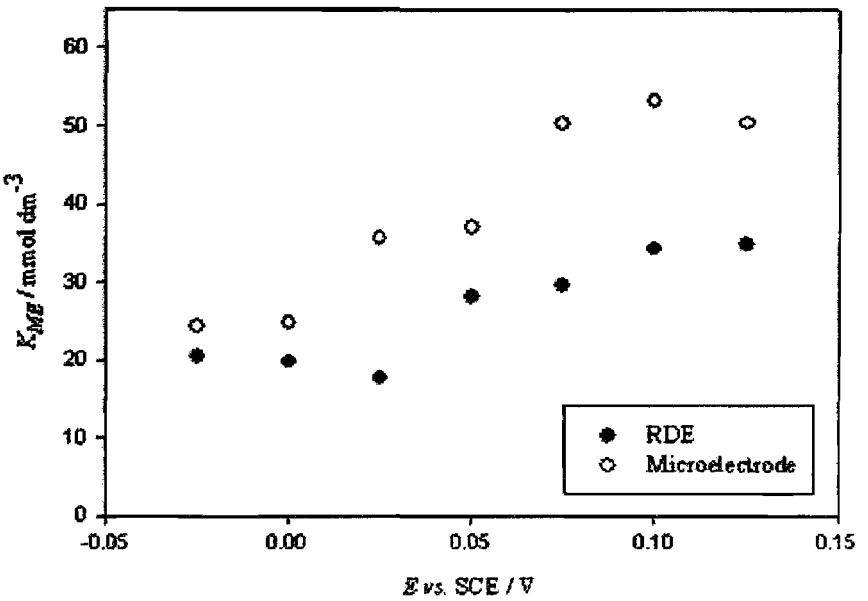

Figure 5.12 *Plot of K_{ME} as a function of potential. The data are taken from table 5.3* • *and* ○ *symbols represent data from our previous RDE studies*[89, 135] *and our current microelectrode respectively.*

According to this calculation we can now obtain the next equations, $K_M = K_{ME}(1-\frac{k_{ME}^{'}}{k_D^{'}})$ and $k_{cat}\Gamma_{sites} = K_{ME}k_{ME}^{'}$.

Using these equations, we can build Tables 5.6 and 5.7. Which give the values for the Michaelis-Menten constant K_M and the concentration of active sites $k_{cat}\Gamma_{sites}$ for each potential for our previous RDE and the current microelectrode studies.

E vs. SCE	K_M / mol dm^{-3} x 10^{-6} PANi-PVS, n = 2	$k_{cat}\Gamma_{site}$ / mol cm^{-2} s^{-1} x 10^{-8} PANi-PVS. n = 2
0.125	2.39 ± 0.47	9.56 ± 0.14
0.100	1.99 ± 0.19	9.47 ± 0.06
0.05	1.92 ± 0.42	7.70 ± 0.05
0.000	4.41 ± 0.46	4.54 ± 0.12

Table 5.6. *Values obtained for K_M and $k_{cat}\Gamma_{site}$ using the best fit parameters given in tables 5.5 and assuming that the electrochemical reaction is fast enough to be neglected, $k_{cat} << k_E^{'}$. These values came from the work carried out by Bartlett and Wallace[135] at PANi-PVS modified RDE, $n = 2$.*

E vs. SCE	K_M / mol dm^{-3} x 10^{-6} PANi-PSS, n = 1	$k_{cat}\Gamma_{site}$ / mol cm^{-2} s^{-1} x 10^{-8} PANi-PSS, n = 1
0.125	0.75 ± 0.36	23.38 ± 0.08
0.100	0.79 ± 0.03	24.63 ± 0.12
0.050	3.08 ± 0.08	15.99 ± 0.10
0.000	6.7 ± 0.39	8.51 ± 0.2

Table 5.7. *Values obtained for K_M and $k_{cat}\Gamma_{site}$ using the best fit parameters given in tables 5.3 and assuming that the electrochemical reaction is fast enough to be neglected, $k_{cat} << k_E^{'}$. These values came from table 5.3, PANi-PSS, n=1, figure 5.8.*

The logarithm of the values obtained for K_M are represented for each electrode potential in figures 5.13.

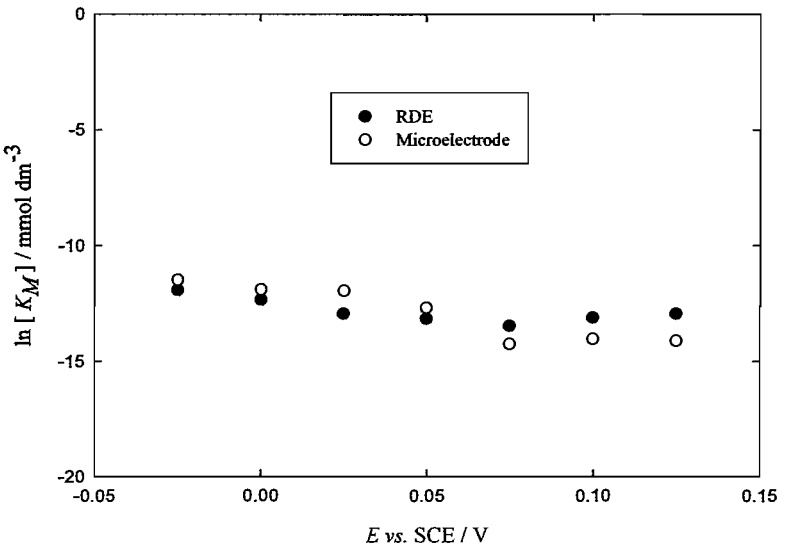

Figure 5.13. *Plot of the experimental values of the* Michaelis-Menten *constant, K_M versus potential. Values obtained from Tables 5.6 and 5.7.*

The data shows that K_M is little dependent on the electrode potential and the values obtained for the PANi/PSS microelectrode and the PANi/PVS RDE are similar. As we were expecting, the counter ion within the PANi film does not affect the binding constant between ascorbate and the polymer active sites. The active sites have to be the same independently of the counter ion. A higher value in the Michaelis-Menten constant means a strong attachment of the substrate to the polymer active sites and vice versa[207].

5.11 Case diagrams

The kinetic analysis just presented may be conveniently summarized in terms of a kinetic case diagram. In this type of representation, the dimensionless parameters, which govern the limiting behaviour of the kinetic rate equations, are plotted in either a two or a three dimensional format. The case diagram will summarize the entire kinetic model and therefore, it can be used as a map to locate the required needs for a specified system. Different publications available in the literature, contain detailed information about how to build a case diagram[89, 90, 92, 135, 205, 207, 211-214].

A case diagram can be two, three or more dimensional, depending on the experimental variables taken into account. For simplicity we have considered a two dimensional plot. It is probably the most difficult part while building a case diagram to choose the correct variables on the diagram axes. The purpose of the case diagram is to simplify the entire analysis from a complicated kinetic model, therefore choosing the wrong axis will complicate its use. In our case, it is helpful to have the ascorbate concentration on one axis and the concentration of active sites on another. In that way, the case diagram shows the effect of increasing of ascorbate concentration and the effect of the potential applied. This is mainly the base of our experiments. Before building the whole diagram, it is probably constructive to know how the experimental data will look with the variables chosen. Using the best fit parameters from tables 5.1 to 5.7 and after some simple calculations, we can plot all the experimental results as shown in figure 5.14. The experimental data for the three cases we have considered during this chapter are summarized in this plot at all the electrode potentials analyzed. The filled circles •, represent the best fit values obtained by Bartlett and Wallace[89, 135] for a PANi-PVS modified RDE. These values lie on vertical lines, which are identified from right to left for each potential analyzed, -0.025, 0.000, 0.025, 0.050, 0.075, 0.100 and 0.125V *vs.* SCE respectively. These values spread along the axis and are limited by the dash-dot-dot blue line as aid to the reader.

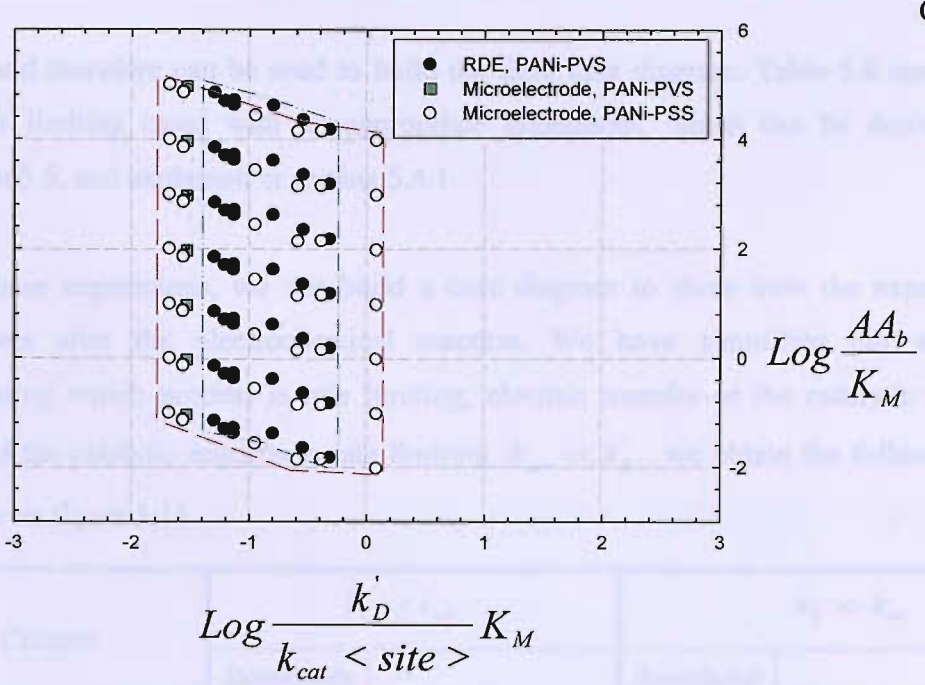

Figure 5.14 *Plot of experimental data obtained during the analysis of the proposed kinetic model, λ = 7.*

Following exactly the same analysis, the open circles in figure 5.14 represent the best fit parameters obtained for our current PANI-PSS modified microelectrodes. As for the RDE, these values lie on vertical lines, which are identified from right to left for each potential analyzed, -0.025, 0.000, 0.025, 0.050, 0.075, 0.100 and 0.125V *vs.* SCE respectively. The points are now confined within by the dashed red line. Finally, the best fit parameters obtained for our PANi-PVS modified microelectrodes are plotted as green squares on figure 5.20. In this case these points lie also on a vertical line which represent the best fit parameters for a single electrode potential, $E = 0.100$ V *vs.* SCE.

As seen from figure 5.14, the experimental data is limited on the abscissa ordinate by the range of ascorbate concentrations that we can experimentally measure. The lower value on these rectangle will show the sensor-probe detection limit and for the higher limit the maximum concentration of ascorbate which can be measured. The ordinate coordinate is however, limited by different factors: the potential applied will affect the concentration of active sites, Γ_{sites}. It will be also highly dependent on the mass transport rate constant $k_D^{'}$. The current analysis of figure 5.14 shows that the axis chosen help to simplify the kinetic

model and therefore can be used to build the final case diagram. Table 5.8 summarizes the four limiting cases with its appropriate boundaries, which can be derived from equation 5.5, and explained in section 5.4.1.

From these expressions, we can build a case diagram to show how the experimental conditions alter the electrochemical reaction. We have simplified our study by determining which process is rate limiting, electron transfer or the catalytic reaction. Hence if the catalytic reaction is rate limiting, $k_{cat} << k_E^{'}$, we obtain the following case diagram on figure 5.15.

Current	$k_E^{'} << k_{cat}$		$k_E^{'} >> k_{cat}$	
	Boundaries		Boundaries	
$i_I = nFAk_D^{'}[AA_{bulk}]$	**1/2**	$k_D^{'} = \frac{k_E^{'}\,\Gamma_{sites}}{K_M}$	**1/2**	$k_D^{'} = \frac{k_{cat}\,\Gamma_{sites}}{K_M}$
$i_{II} = \frac{nFAk_{cat}\Gamma_{site}[AA_{bulk}]}{K_M}$	**2/3**	$\frac{[AA_{bulk}]}{K_M} = \frac{k_E^{'}}{k_{cat}}$	**2/3**	$[AA_{bulk}] = K_M$
$i_{III} = nFAk_E^{'}\Gamma_{sites}$				
$i_{IV} = nFAk_{cat}\Gamma_{sites}$	**1/3**	$\frac{1}{[AA_{bulk}]} = \frac{k_D^{'}}{k_E^{'}\,\Gamma_{sites}}$	**1/3**	$[AA_{bulk}] = \frac{k_{cat}\,\Gamma_{sites}}{K_M}$

Table 5.8 *Limiting cases derived from equation 5.5 and relation within cases.*

It is clear because of the experimental conditions case 4 cannot be reached because to do so the rate of the electrochemical reaction $k_E^{'}$ has to be much slower than k_{cat}. At the potential used E = 0.100 V *vs.* SCE the polymer is conducting enough to maintain the relation $k_E^{'} >> k_{cat}$.

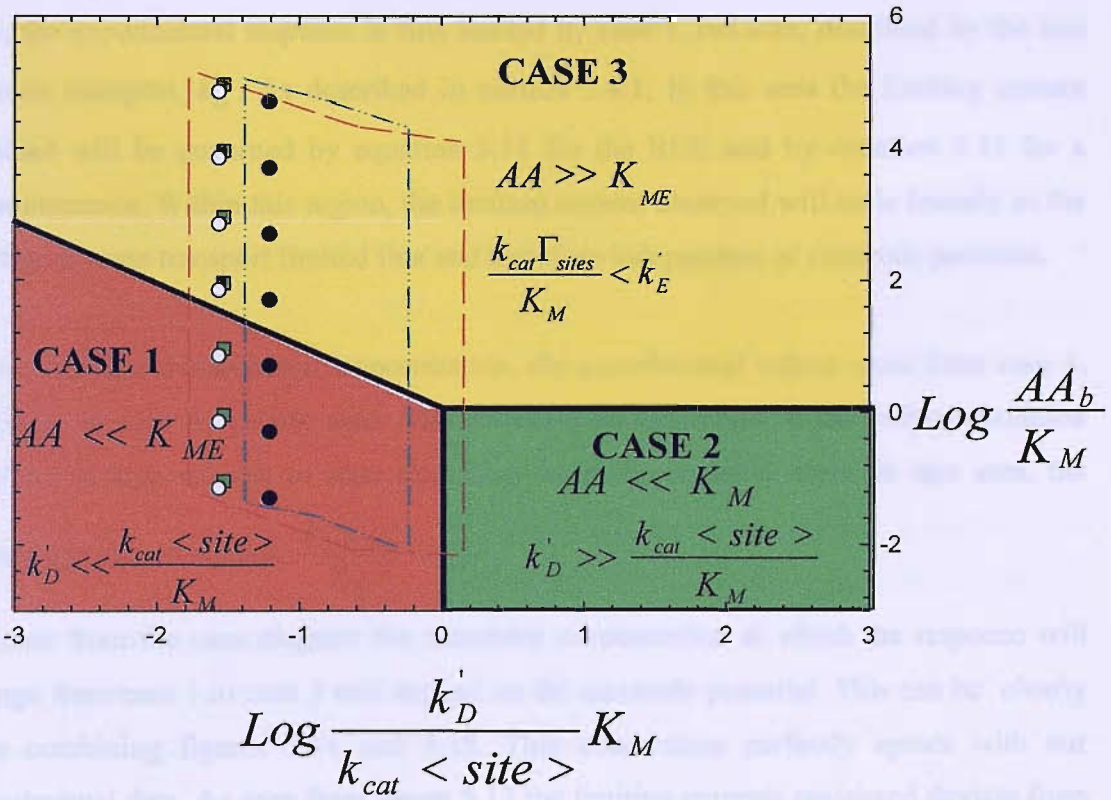

Figure 5.15 *Case diagram for ascorbate oxidation valid to study the kinetic analysis on a PANi-PVS or a PANi-PSS modified electrode, when the catalytic reaction is rate limiting,* $k_{cat} << k_E'$. *Filled circles, ●, represent the best fit parameters for a PANi-PVS modified RDE at 0.10 V. Open circles, ○, represent the best fit parameters for a PANi-PSS modified microelectrode at 0.10 V. Green squares, represent the best fit parameters for a PANi-PVS microelectrode at 0.10 V. The red dashed line and the blue dash-dot-dot line represent where all the experimental data lies for PANi-PVS and PANi-PSS composites, as shown in figure 5.14.*

Figure 5.15 also plots the best fit parameters obtained for our previous PANi-PVS modified RDE, and our current PANi-PVS and PANi-PSS microelectrodes. For a clearer analysis, we have plotted the best fit parameters at the same electrode potential for all of them. Using the same procedure as in figure 5.14.

Considering this, we can start analyzing our kinetic model. As we can see from figure 5.21, the experimental response is first limited by case 1, red area, described by the rate of mass transport, $k_D^{'}$. As described in section 5.4.1, in this area the limiting current obtained will be governed by equation 5.11 for the RDE and by equation 5.12 for a microelectrode. Within this region, the limiting current observed will scale linearly as the reaction is mass transport limited flux and therefore independent of electrode potential.

As we increase the ascorbate concentration, the experimental values cross from case 1, red area, to case 3, yellow area. The substrate concentration at the polymer/solution interface is high enough to start saturating the polymer active sites. In this area, the current expression applies, $\frac{k_{cat}\Gamma_{sites}}{K_M} < k_E^{'}$.

As seen from the case diagram the ascorbate concentration at which the response will change from case 1 to case 3 will depend on the electrode potential. This can be clearly seen combining figures 5.14 and 5.15. This observation perfectly agrees with our experimental data. As seen from figure 5.13 the limiting currents registered deviate from linearity at different ascorbate concentration for each potential applied. Hence the deviation from linearity for the PANi composites under study means that the reaction switches from being mass transport controlled to being controlled by the concentration of polymer actives sites, Γ_{sites}. Highly dependent on the potential applied.

Moreover, if we compare the experimental response plotted in figure 5.15. We can see that for PANi-PVS and PANi-PSS modified microelectrodes the response changes from case 1 to case 3 at the same ascorbate concentration. This observation also agrees with our experimental results shown in figure 5.7.

When comparing our PANi-PVS microelectrodes with previous PANi-PVS modified electrodes, we see that at the same potential the results are clearly shifted. These means, that a PANi-PVS microelectrode will hold its limiting current as mass transport limited at slightly higher ascorbate concentrations compared to a PANi-PVS RDE. In other words, the ascorbate concentrations at which we will start to saturate the polymer active sites

will be higher for a PANi-PVS microelectrode. This observation seems to agree when we compared our results in figure 5.7 with our previous data. However, PANi-PVS microelectrodes are located further negative in the abscissa axis.

Hence, for a given potential, the PANi composite able to obtain higher ratio $k_{cat}\Gamma_{sites} >> k_D' K_M$, will have a response limited by the rate of mass transport for higher ascorbate concentrations. Accepting we cannot get higher limiting currents than the mass transport limited, the area where we want our modified electrode to work is the more negative side in case 1.

Summarizing, a case diagram is a useful tool for the chemist as it allows simplifying the analysis of complicated models. These case diagrams allow making theoretical calculations of the range of concentrations we can realistically reach and the range of currents expected with the potential applied. Understanding these diagrams allows the experimenter to a faster progress in his experiments.

5.12 Conclusions

The theoretical model proposed by Lyons and Bartlett has been successfully applied to microelectrodes obtaining interesting data of the electrode kinetics. We have shown that the theory applied to macroelectrodes can be successfully applied to microelectrodes in the conditions where planar diffusion dominates towards radial diffusion. This will only happen when the thickness of the polymer film is much lower than the microelectrode radius. As expected, ascorbate oxidation at PANi films occurs at the polymer/solution interface, and therefore independent of the polymer thickness. This is a clear advantage towards sensor design.

Ascorbate oxidation on PANi/PVS and PANi/PSS composites is under mass transport control for low ascorbate concentrations and becomes kinetically limited at high concentrations. The electrochemical reaction is highly dependent on the potential applied and this is due to the concentration of actives sites. The counter ion present within the

PANi film affects the gross morphology of the polymer and somehow, seems to affect the reaction mechanism.

Surprisingly PANi/PSS composites presented half the limiting currents compared to PANi/PVS composites. Indicating that in some way, PANi/PSS follow a one electron process instead of the expected two electron process. In the case of PANi/PSS the reaction has to differ to the one previously proposed for PANi/PVS[134, 135]. Where the reaction is thought to happen through a hydride transfer, without the formation of a radical anion intermediate.

We believe that the diimine groups, the PANi active sites, are the same for both composites independently of the counter ion. If this is correct and assuming the reaction occurs via Michaelis-Menten type mechanism, the value for K_M has to be the same for both composites. This was confirmed through the analysis of the proposed model in figure 5.15. Therefore, ascorbate diffuses through the Nernst diffusion layer and binds to the polymer active sites. What happens afterwards seems to be dependent on the counter ion present within the PANi film. PVS and PSS counter ions present different chemical structures but it is unlikely that they play any roll during the reaction. It may happen that the reaction occurs the generation of an ascorbate radical anion intermediate that in the case of PANi/PSS diffuses to the bulk solution without being further oxidized to DHA. We can not just to speculate with the electrochemical data. Further analysis has to be done prior to certify the correct mechanism. Unfortunately, this was out of the aim of this thesis but it is encouraging of further research. A rotating ring disc experiment or fast scan rate using microelectrodes may help to detect reaction ascorbate intermediates. In addition, measuring the presence of the ascorbate radical anion intermediate by Electron Spin Resonance/Electron Paramagnetic Resonance (EPR/ESR) will also help to answer this difficult question.

Chapter 6

Applications to real systems

6.1 Objective

Our aim in this chapter is to apply our PANi/PSS and PANi/PVS microelectrodes in real systems. Examples described in this chapter include the application of PANi/PSS microelectrodes for AA measurement in human plasma samples (100 μL) and the application of PANi/PVS microelectrodes for the monitoring of AA in plant leaves. The results provided in this section are designed to show that our modified microelectrodes are suitable for use in *in vivo* applications.

6.2 Introduction

In vivo electrochemistry is a useful analytical technique, which allows scientists to characterize living organisms. However, these measurements are complicated due to the complexity of the composition of physiological fluids. *In vivo* measurements are often carried out in small volumes or in reduced spaces. Therefore, due to their small dimensions and electrochemical properties, needle type microelectrodes are suitable for use as analytical tools for *in vivo* measurements. With the advances in technology, scientists are now able to implant these small electrodes inside the human brain[28], in the vicinities of single cells[228] or even inside the pores of plant leaves[229]. This offers a significant achievement and it is now possible to study systems *in vivo* without modification. Ewing and Wightman were pioneers in using carbon fibre microelectrode to monitor the levels of different neurotransmitters, such as dopamine, in brain tissue[230]. Continuing their work, scientists have modified the surface of these needle type microelectrodes in order to achieve better selectivity and sensitivity. For instance, microelectrodes modified with conducting polymers offer the advantage of molecular recognition. This is a real advantage during *in vivo* measurements as biological fluids present a wide range of molecules prone to oxidation. Therefore modified needle type microelectrodes are used today for monitoring different substrates in real time, in medicine and physiology.

In the earlier chapters of this thesis we have shown that modified PANi, films can be successfully electrodeposited on small platinum microelectrodes. PANi films have been shown to be selective for oxidation of ascorbate in the presence of common interferences present in living organisms. Therefore, we decided to test our homemade microelectrodes and commercial needle type microelectrodes on real samples.

This chapter describes our efforts to measure AA in low volumes of human plasma and inside the pores of a plant leaf. It is believed that this is the first time these two measurements have been attempted.

6.3 Ascorbate measurements in human plasma

For reasons of health and safety, it is not easy to handle whole blood samples inside our laboratory at Southampton University. Hence, electrochemical *in vitro* measurements in human plasma were carried out in collaboration with Dr. Janis Shute, at the Pharmacology Department of the University of Portsmouth. Samples were collected, early in the morning, from healthy volunteer patients, who did not follow any special diet or treatment during the course of our measurements. Therefore, the levels of AA we have obtained during this specific work are just representative for the particular interest of this thesis and presented here as proof of concept.

6.3.1 Preparation prior to the electrochemical experiments

Blood samples of approximately 5 mL, were collected straight from patients in heparin or ethylenediaminetetraacetic acid, EDTA, test tubes. Heparin and EDTA are common anticoagulants used in blood analysis. An anticoagulant is a substance that prevents blood from clotting. Afterwards, samples were centrifuged at 2000 rpm for 10 min at room temperature in order to separate the blood proteins from the plasma. Blood plasma is the liquid component of blood in which the blood cells are suspended and is the largest single component of blood comprising about 55% of total blood volume. It is mainly composed of water, blood proteins, inorganic electrolytes and human serum albumin. It serves as a transport medium for glucose, lipids, amino acids, hormones, metabolic end products,

carbon dioxide and oxygen[231, 232]. As seen from figure 6.1, plasma is a transparent liquid with a faint straw colour.

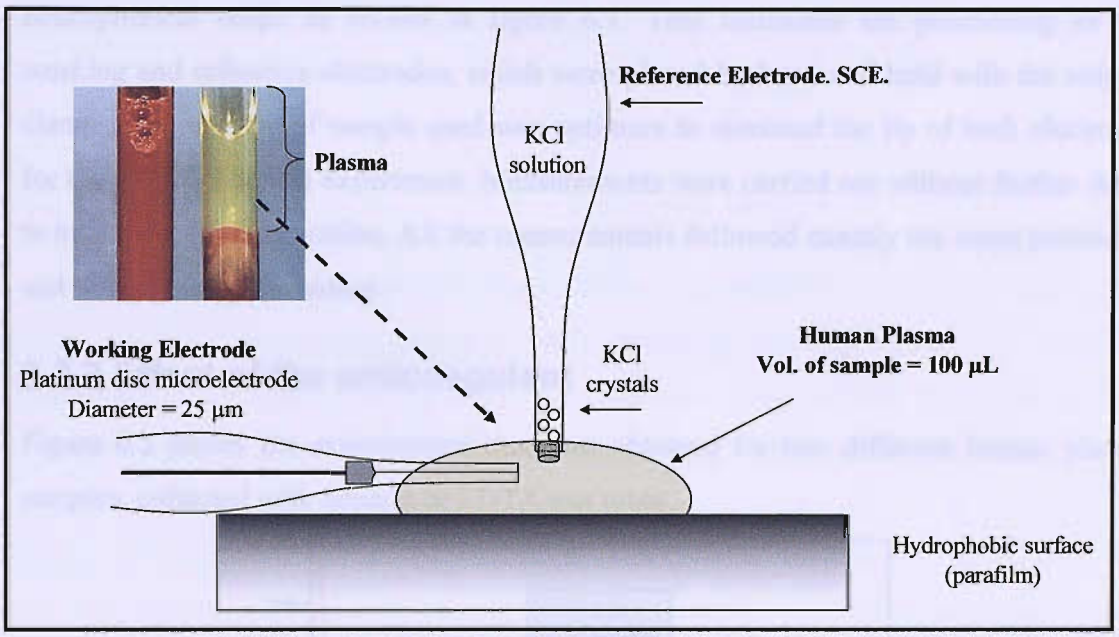

Figure 6.1 *Experimental set up for ascorbate measurements in blood plasma, 100μL. The working electrode was a Pt disc microelectrode, a = 12.5 μm, modified with a thin film of PANi/PSS, deposition charge density Q = 3.65 mC cm^2. The electrochemical oxidation of AA in human plasma was carried out at constant potential, E = 0.10 V vs. SCE. Experiments were done at room temperature with the use of a faraday cage. Inset in figure shows the Heparin test tubes containing a collected blood sample before and after separation. The yellowish liquid is the plasma divided from the blood proteins after being centrifuged at 2000 rpm during 10 min at room temperature.*

Approximately 0.5 mL of plasma from each patient was pipetted out from the test tube by Dr. Janis Shute, and collected in a 2 mL eppendorf tube. To prevent oxidation of ascorbate in the sample 5% w/v metaphosphoric acid was added to the plasma. The resulting samples were introduced immediately inside an ice bath, to prevent fast oxidation. Samples were stored frozen in case further analyses were needed. After preparing plasma samples, electrochemical measurements were carried out.

From the eppendorf tube, 100 µL of plasma was pipetted and deposited on top of a parafilm surface. This hydrophobic surface causes the plasma sample to adopt a hemispherical shape as shown in figure 6.1. This facilitates the positioning of the working and reference electrodes, which were placed by hand and held with the help of clamps. The volume of sample used was optimum to surround the tip of both electrodes for the electrochemical experiment. Measurements were carried out without further delay to avoid sample evaporation. All the measurements followed exactly the same procedure and were done by the author.

6.3.2 Effect of the anticoagulant

Figure 6.2 shows the experimental response obtained for two different human plasma samples, collected with heparin or EDTA test tubes.

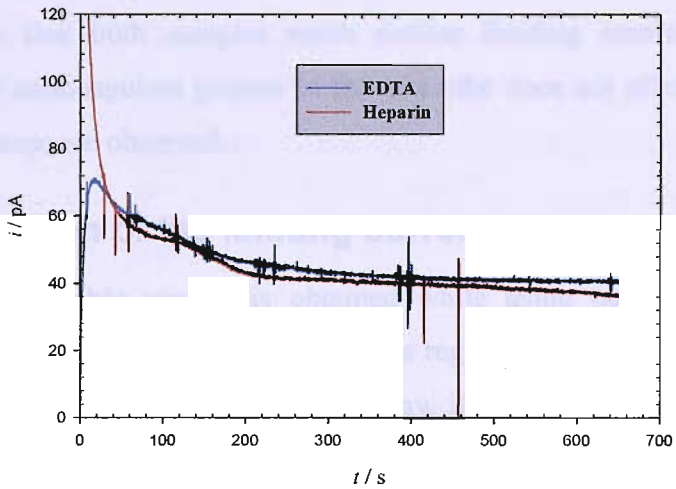

Figure 6.2 *Electrochemical measurements on human plasma using a PANi-PSS modified platinum disc microelectrode, deposition charge density Q = 3.65 mC cm^2, a = 12.5 µm. The working and reference electrodes were positioned as shown in figure 6.1. Afterwards the potential was held at -0.20 V for 3 min and stepped from -0.20 to +0.10 V vs. SCE. The PANi-PSS films were cycled, between -0.20 and +0.50 V vs. SCE at 50 mV s^{-1}, in a solution containing 22% PSS and 1M HCl, between experiments. Experiments were carried out at room temperature with the use of a faraday cage. The data is presented as it was collected without any modification.*

The experimental response obtained presents considerable electrical noise as compared to our previous experiments. As we are working with currents in the range of picoamps, electrical isolation from the mains and electrical equipment around is needed. The current measurements were carried out at the Pharmacology department of the University of Portsmouth where isolation from electrical noise was difficult.

As seen from figure 6.2, the current decays with time until it reach a constant value after approximately 6.5 minutes. Similar response was presented in Chapter 4, during our experiments in the presence of AA in buffer solutions, although the current achieved steady state much faster. The time to reach steady state is related with the rearrangement of the PANi chains when the potential is switched from -0.20 to +0.10 V *vs.* SCE [233].

Figure 6.2 show that both samples reach similar limiting currents. Therefore, we conclude that the anticoagulant present in the test tube does not affect significantly the electrochemical response observed.

6.3.3 Identification of the limiting current to AA

Seeing that a measurable current is obtained while using our PANi-PSS modified microelectrodes, we went on to see if the currents registered were due to the oxidation of AA present in human plasma. In the simplest way, if a fresh plasma sample is analyzed using exactly the same procedure as shown in figure 6.2, but adding known amounts of AA, the limiting current should increase in proportion to the amount of AA and reach a stable value. However, if the response does not increase, decreases or does not reach a plateau over the same time period it will indicate that the limiting currents obtained are due to the oxidation of some other substances.

Figure 6.3 shows the experimental response obtained while spiking a fresh sample with known amounts of AA.

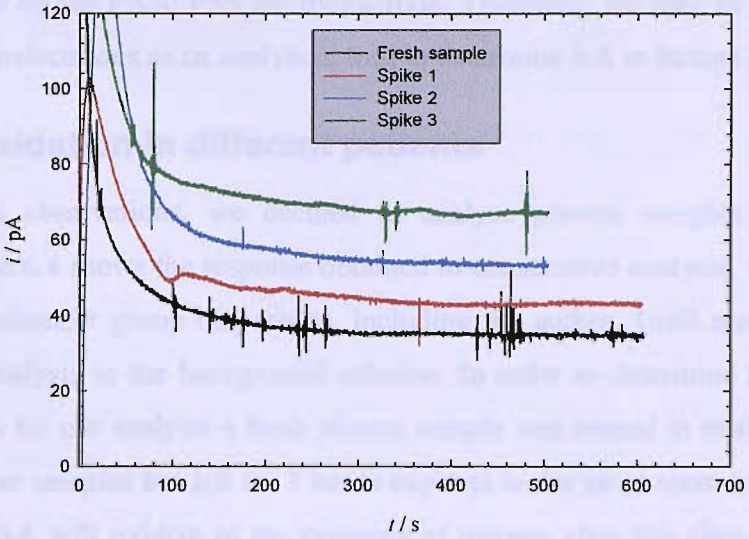

Figure 6.3 *Electrochemical measurements in human plasma with a PANi-PSS modified Pt disc microelectrode. The solid black line, presents the experimental response obtained from a fresh plasma sample. The red, blue and green lines represent the response after successive additions of 100 μM AA to the blank solution. The PANi-PSS films were cycled, between -0.2 and +0.5 V vs. SCE at 50 mV s^{-1}, in a solution containing 22% PSS and 1M HCl, between experiments. The experimental conditions are the same as described in figure 6.1 and 6.2.*

The first observation to notice from figure 6.3 is that the response obtained is similar to the one presented in figure 6.2. The response decays with time and reaches a stable value after 5 minutes. The black line, represents the response from a fresh plasma sample. It can be seen that it reaches a limiting current of approximately 38 pA, which is close to the limiting currents observed in figure 6.2. This observation may indicate that the levels of AA between these two patients were similar.

The red, blue and green lines represent the experimental response obtained after successive additions of 100 μM AA to the blank solution. It can be clearly seen that the addition of AA to the fresh plasma solution clearly affects the response obtained. The current decays with time and stabilizes at approximately similar times. The current increases linearly with the addition of AA. Based on this observation, we believe that the limiting currents registered are due at least to the oxidation of AA and probably

something else by the PANi-PSS microelectrode. Therefore, we may be able to use our modified microelectrodes as an analytical tool to determine AA in human plasma.

6.3.4 AA oxidation in different patients

Following our observations, we decided to analyse plasma samples from different patients. Figure 6.4 shows the response obtained to consecutive analysis, within the same day, from a volunteer group of patients, including the author. Until now, we have not referred our analysis to the background solution. In order to determine the background current present for our analysis a fresh plasma sample was treated in exactly in the same way as the other samples but left for 3 hours exposed to the air at room temperature. It is believed that AA will oxidize in the presence of oxygen after this time. Therefore, the response obtained from this sample can be used as a blank in our measurements. This is shown as the solid black line in figure 6.4. It is clear that a lower limiting current is obtained which is half of the value of the previous limiting currents observed in figures 6.2 and 6.3.

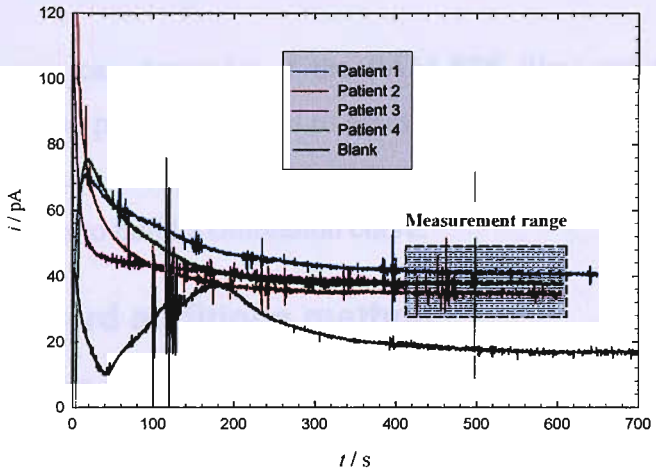

Figure 6.4 *Electrochemical measurements in human plasma with a PANi-PSS modified Pt disc microelectrode. The experimental conditions are the same as described in figure 6.3. The solid black line, is for a plasma sample exposed to air for a few hours and this is called a blank solution. The red, green, pink and blue lines represent the experimental response obtained from fresh samples of human plasma from different patients. The shaded blue rectangle shows the range where and averaged value of the limiting current was taken.*

However, this value is somehow quite large to be just due to the background electrolyte. We believe that something else might be oxidized at the same time as AA. Considering the complexity of analytes forming the human plasma, answering this question is not trivial and will be time consuming. A good method to answer this question will be repeating the same experiment shown in figure 6.3, but spiking the solution with different analytes, following the same procedure as presented in chapter 4, section 4.4.4. The substance showing an increase in the limiting current will be the interferent to consider. However, as we had a limited time to do these experiments and considering the plasma samples have to be analysed as soon as possible, to prevent AA oxidation, we were unable to do this screening for interferences during the present work.

As seen from figure 6.4 the limiting currents obtained for different patients reach comparable values. Indicating similar concentration of AA. This response observed is a further indication that our PANi-PSS microelectrodes might be used to measure AA in low volumes of human plasma.

However before we can determine if the PANi-PSS films are a reliable method to measure AA in human plasma, we need to asses the real concentration of AA within this sample. Using a simple and well-known analytical method called the standard additions method, we were able to build a calibration curve.

6.3.5 The standard additions method

The standard additions method is commonly used to determine the concentration of an analyte that is in a complex matrix such as biological fluids. The reason for using the standard additions method is that the matrix may contain other components that interfere with the analyte signal causing inaccuracy in the determined concentration.

The procedure for standard additions is simple. The sample, in our case, the plasma, is divided into several even aliquots in separate volumetric flasks of the same volume. The first flask is then diluted to volume with the selected diluent. In our case, the selected diluent was 0.1 M phosphate / 0.2M citrate buffer pH = 7. A standard containing the

analyte, AA, is then added in increasing volumes to the subsequent flasks and each flask is then diluted to volume with the selected diluent, the buffer solution. The change in instrument response between the sample and the spiked samples is assumed to be due only to change in the analyte concentration. The AA concentration for the unknown solution is obtained by extrapolation, as shown in figure 6.5. The values obtained for the different patients are summarized in table 6.1.

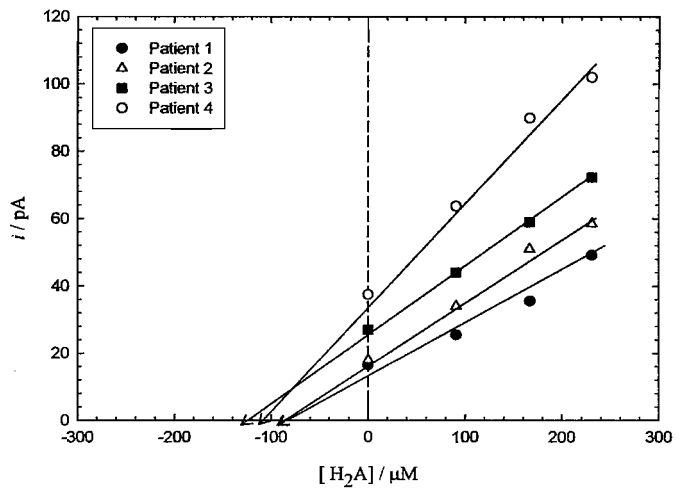

Figure 6.5 *Standard addition method used to calculate the AA concentration in human plasma with PANi-PSS microelectrodes. The experimental values were obtained using the same procedure as explained in figures 6.3 and 6.4. The background current was subtracted from the experimental signal. The solid lines are an extrapolation of the regression lines to the x-axis, to obtain the concentration of the sample analyzed. The values obtained for the different patients are summarized in table 6.1.*

	i_{exp} / pA	[H_2A] / μM
Patient 1	34.50	85
Patient 2	36.00	85
Patient 3	45.00	133
Patient 4	55.50	110

Table 6.1. *Experimental limiting currents obtained from different patients using the procedures explained in figure 6.4. The AA concentrations were calculated using the standard addition method shown in figure 6.5. The background current, 18 pA, obtained from the blank was subtracted from the experimental signal,* i_{exp}.

As mentioned, the concentration of AA in plasma, can differ from one patient to another, but values obtained from literature[232, 234, 235] range from (20 – 150) μM. This large variation depends on many parameters such as the diet, weight, health, etc. It is pleasing to see that the values we have obtained lie in the range of reasonable concentrations expected in human plasma. The electrochemical method proposed is a positive step forward in the methodology present in literature as the time of analysis, cost and sample pretreatment is considerable reduced. However before a final conclusion, our results were compared to a different analytical technique in order to asses the validity and reliability of the proposed method.

6.3.6 Determination of AA by HPLC

After the results observed during the previous section, in order to complete the analytical characterization for the electrochemical measurements we decided to compare our results by high-performance liquid chromatography, HPLC.

HPLC is frecuently used in biochemistry and analytical chemistry to separate components of a mixture based on a variety of chemical interactions between the substance being analyzed and the chromatography column. For health and safety reasons these experiments were carried out in artificial serum as a substitute for human plasma. Artificial serum albumin offers the great advantage of being free of pathogens and

therefore it was suitable to be used in our laboratory. Bovine serum albumin, BSA, is readily available in different compositions as a liquid or as a lyophilized powder. BSA is a single polypeptide chain consisting of about 583 amino acid residues and no carbohydrates[236].

The experiments shown in this section were carried in collaboration with Dr. Roach in chemical biology at the University of Southampton, a PhD student, Martin, F. and Dr. Kilmartin, visiting lecturer from the University of Auckland, New Zealand.

Following the expertise from our collaborators, it was determined to use high performance reversed phase liquid chromatography. This is the technique of choice for the analysis of small molecular weight compounds in the pharmaceutical industry, chemical industry and biochemical research. In reverse phase chromatography, the column packing is non polar and the solvent is polar with respect to the sample. Retention inside the chromatography column is the result of the interaction of the nonpolar components of the solutes and the nonpolar stationary phase. A buffer of increasing hydrophobicity is used to dissociate the bound molecule. At a point at which the hydrophobic interaction between the exposed patches and the immobilized matrix is less favourable than the interaction between the bound molecule and the solvent the molecule releases from the matrix and elutes. The retention time of a solute, t_R, is taken as the elapsed time between the time of injection of a solute and the time of elution of the peak maximum of that solute. It is a unique characteristic of the solute and can be used for identification purposes. Typical stationary phases are nonpolar hydrocarbons, waxy liquids or bonded hydrocarbons such as C_{18}, C_8, C_4, etc. and the solvents are polar aqueous-organic mixtures such as methanol-water or acetonitrile-water.

Standard solutions of BSA, diluted in 0.1 M citrate / 0.2M phosphate buffer, pH = 7, were prepared and used as the blank solution. In order to be able to identify AA in BSA, the blank solution has to give an HPLC chromatogram, which does not interfere with AA. Hence, to achieve the required conditions, we followed similar settings present in the literature[237]. A reverse phase C18 column, (C18, 4.6X250 mm, 5 μm, 300 Å), with a

gradient program for the solvent was used as the HPLC column. Buffer A: water, 0.1% trifluoroacetic acid, TFA, and buffer B: acetonitrile, 0.1% TFA. The acid, TFA, is used to improve the chromatographic peak shape and to provide a source of protons in reverse phase. Figure 6.6 shows the experimental chromatograms obtained for BSA, black line, and BSA spiked with 100 μM AA, red line, under the conditions chosen.

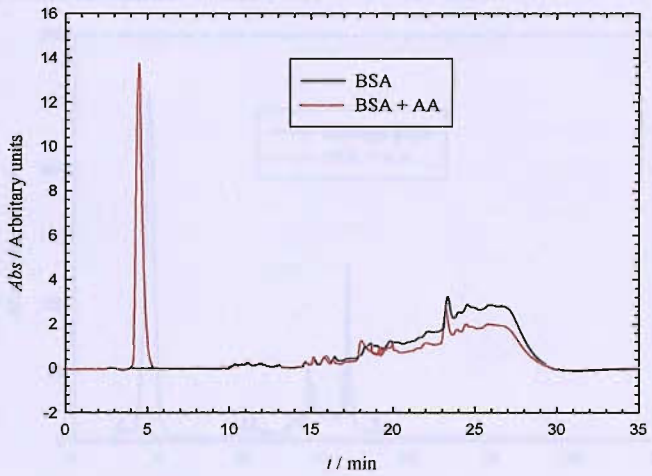

Figure 6.6. *Experimental HPLC chromatograms obtained for bovine serum albumin, BSA, in the absence, black line, and in the presence of 100 μM ascorbic acid, BSA+AA, red line. Samples were diluted with 0.1M citrate / 0.2M phosphate buffer solution, final pH = 7. The peak appearing at* $t_{R(AA)} = 4.59$ *min is due to the presence of AA in BSA. Peaks appearing at* $t_R > 13$*min. are due to other chemical compounds present in the solution matrix, BSA, and of no interest for our analysis. A blank solution containing deionized water was injected before, after and between runs, using exactly the same gradient program. The total time for each analysis was 40 min.*

It was pleasing to see that the different components in BSA do not elute from the column until approximately 10 minutes. Unretained compounds eluted at $t_{Ro} = 2.05$ min. This is extremely good as the analytes we are aiming to analyze present low retention times. It was also positive to observe the extra peak appearing at short retention times, when the sample BSA+AA, solid red line, was analyzed. As the samples only differ by the addition of AA, this extra peak has to be due to the presence of AA. Alternatively, this observation was double checked by running a diluted sample of pure orange juice.

Orange juice is an excellence source for AA. The sample was obtained from an orange fruit, where the juice was extracted, filtered and diluted with buffer solution. The analysis was performed under the same conditions as previous. Figure 6.7, compares the response obtained, using exactly the same experimental conditions, for orange juice, black line, and our previous sample, BSA+AA, red line. The differences in peak area are due to differences in the concentration of AA.

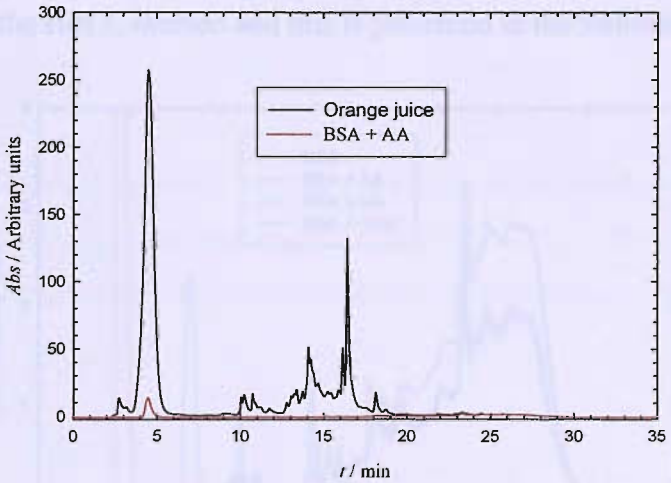

Figure 6.7. *Experimental HPLC chromatograms obtained for a sample of a diluted orange juice, black line, and bovine serum albumin in the presence of 100 μM ascorbic acid, BSA+AA, red line. Samples were diluted with 0.1M citrate / 0.2M phosphate buffer solution, final pH = 7. Exactly same conditions as in figure 6.6 were used for this analysis.*

It is clearly seen that the peak for AA, elutes from the column at the same time for both samples. Indicating that the retention time, t_R, of AA in the presence of BSA, is $t_{R(AA)}$ = 4.59 min. Continuing with our analysis, we carried out similar measurements for common interferences that may be present in human plasma. Therefore, samples containing 100 μM uric acid in BSA, and 100 μM glutathione in BSA, were analysed using exactly the same procedure as for AA. Figure 6.8 shows the experimental results for all the solutions under study. The purpose of this experiment is to clarify that under the experimental conditions chosen, a real sample of human plasma can be injected into the HPLC system, and AA can be measured, using the characteristic retention time. As seen from figure 6.8, narrow and well defined peaks for AA, uric acid and glutathione

clearly elute from the column at different retention times. The peaks appearing at $t_{R(AA)}$ = 4.59 min, $t_{R(UA)}$ = 8.31 min, $t_{R(AA)}$ = 11.12 min are due to the presence of AA, uric acid and glutathione in BSA, respectively. Unretained compounds eluted at t_{Ro} = 2.05 min, and the corrected retention times can be calculated from here, t_R - t_{Ro}. Summarizing, the experimental conditions chosen are suitable for the detection of AA in the presence of common interferences. Our electrochemical results were compared and validated versus the HPLC method and this is presented in the following section.

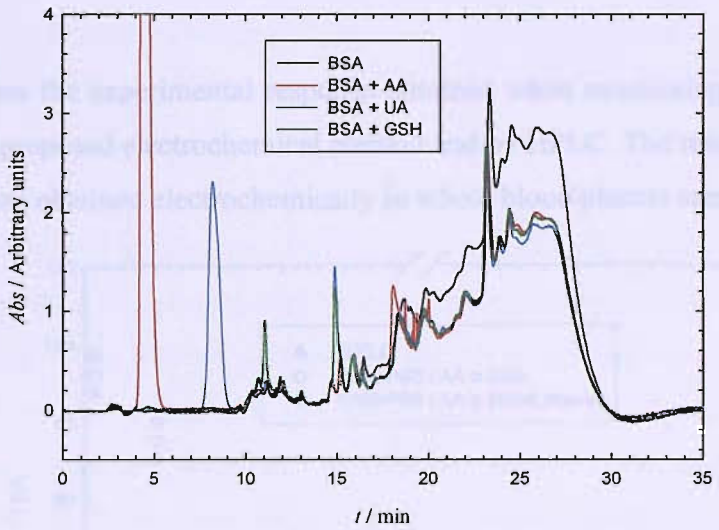

Figure 6.8 *Experimental HPLC chromatograms obtained for bovine serum albumin, BSA, in the absence, black line, and in the presence of 100 μM ascorbic acid, BSA+AA, red line, 100 μM uric acid, BSA+UA ,blue line and 100 μM glutathione, BSA+ GSH, green line. The peaks appearing at $t_{R(AA)}$ = 4.59 min, $t_{R(UA)}$ = 8.31 min, $t_{R(AA)}$ = 11.12 min is due to the presence of AA, uric acid and glutathione in BSA, respectively. Exactly same conditions as in figure 6.7 were used for this analysis.*

6.3.7 Monitoring AA degradation

It is well known that AA oxidises in the presence of oxygen. In order to test our electrochemical method against the HPLC system we decided to monitor the degradation of AA with time for a single sample. For reasons of health and safety, the validation of our electrochemical method against the HPLC was carried out in artificial human plasma. A solution of AA in BSA was prepared and used on the same day for both analyses.

HPLC analyses were carried out in diluted samples of artificial human plasma, bovine serum albumin, BSA, spiked with known amounts of AA, UA and GSH. The experimental procedure has been explained in detail through section 6.3. The sample was kept in an open ice bath during measurements to avoid fast degradation. Electrochemical measurements in BSA with known amount of AA were carried out in exactly the same way as in human plasma and presented in section 6.2. Samples were also kept in an open ice bath.

Figure 6.9 shows the experimental response obtained when monitoring AA degradation in BSA by our proposed electrochemical method and by HPLC. The results are compared with the response obtained electrochemically in whole blood plasma samples.

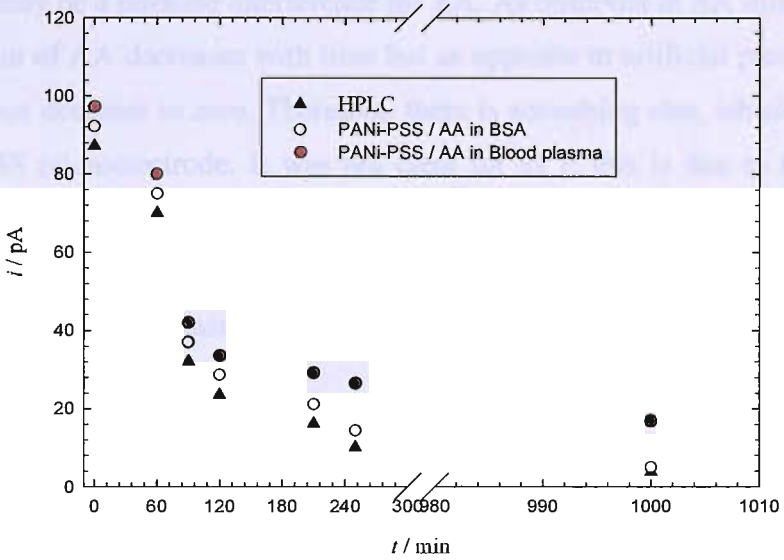

Figure 6.9 *Monitoring the degradation of AA in BSA with time. The triangles represent the experimental values obtained via HPLC. The open circles show the response obtained with the PANi-PSS microelectrode. The red circles represent the response obtained with a PANi-PSS microelectrode. The experimental procedures are explained in detail through sections 6.2 and 6.3.*

As it was expected, the concentration of AA decreases with time due to AA oxidation in the presence of oxygen and ascorbate oxidase. The initial concentration, t = 0 min, is

similar for both methods but lower that the theoretical value, 100 μM AA. Although we were careful with the time of analysis, AA oxidizes quite rapidly. Therefore, the time of analysis is crucial in order to obtain a real value. It is pleasant to see that the response obtained via HPLC and with our PANi-PSS microelectrode give similar values. Indicating that PANi-PSS microelectrodes may be suitable for monitoring AA in blood plasma.

Figure 6.9 compares the responses obtained electrochemically in artificial plasma BSA with the response obtained in whole blood plasma, red circles. It can be seen that the AA concentration is slightly higher than expected. This could be related to our previous observation in section 6.3.4 figure 6.4 where a rather large background current was observed. This may be due to the oxidation of some other analytes present in the human plasma, which may be a possible interference for AA. As observed in AA diluted in BSA, the concentration of AA decreases with time but as opposite to artificial plasma now the response does not decrease to zero. Therefore, there is something else, which is oxidized at the PANi-PSS microelectrode. It was not clear for us if this is due to the complex matrix of the human plasma or due to a possible interference. The experiments presented here validate the proof of concept that PANi-PSS microelectrodes might be suitable for AA determination in human plasma.

6.4 In vivo electrochemistry on Barley leaves

6.4.1 Introduction

As in humans, it is important to determine the ascorbate concentration in plants because of its direct influence in the pathogen defence system[238]. It is believed that the concentration of AA can be determined from the apoplastic solution that surrounds the substomatal cavities. As shown in figure 6.10, these substomatal cavities are free air spaces located below the plant pores. Therefore, it might be possible to implant a microelectrode through the leaf pores, which can reach the apoplastic solution, and measure the concentration of AA electrochemically. Ascorbate measurements in plant leaves were attempted in collaboration with Dr. Stefan Hanstein at the Botanic Institute, University of Giessen, Germany. Our approach to this scientific challenge, known as the nano-infusion method, is explained in this section.

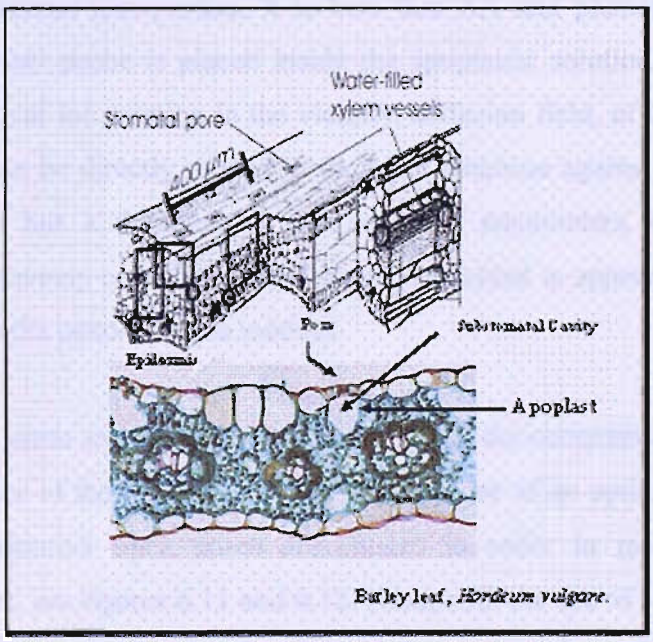

Figure 6.10 *Cross section of a Barley leaf. The substomatal cavities are free air spaces located just below the plant pores. These cavities are surrounded by the apoplastic solution, where ascorbic acid can be possibly found.*

6.4.2 Our approach

As seen in figure 6.10, substomatal cavities are irregular free air spaces, located just below each pore, and are extended linearly through the whole leaf. The cavities are internally connected by conducting vessels and have a separation of approximately 150 μm from centre to centre of each cavity[229]. They are directly accessible through the leaf pores. On average, there is a density of 50 pores per mm^2. The dimensions of the pores are approximately 7 μm width by 30 μm length in the maximum open state. The aperture of the leaf pores depends on various factors such as the concentration of water and the concentration of CO_2 near the plant leaf. In the presence of light, a low CO_2 concentration, below 360 μmol mol^{-1} air, causes the opening of the plant pores[239].

The apoplastic fluid, with an average thickness between 0.3 and 1.0 μm, is in direct contact with the plasma membrane of the plant cells. It constitutes a compartment that reflects transport and redox processes at the plant plasma membrane, which contain diverse ion and electron transporters. It is here that AA and phenolic compounds are found. If the electrode-probe is placed inside the apoplastic solution, it will be able to obtain electrochemical information in the vicinity, diffusion field, of the cell wall space. This information can be directly related to the plant response against pathogens. As the apoplastic solution has a thickness in the range of nanometers, attempting such a measurement is extremely complicated and we have decided to approach the problem by a method known as the nano-infusion method.

In this method, the pores are fully opened by controlling the composition of the supply of air above the surface of the plant leaf. Then, with the use of an optical microscope (fig. 6.11C) three consecutive open pores are chosen in order to reach three different substomatal cavities, see figures 6.11 and 6.12. Next, with the use of a micropositioner, a micropipette is placed inside a substomatal cavity and a physiological solution is directly injected. Following exactly the same procedure, the combined reference/counter and working electrodes are implanted in the neighbouring cavities. This complicated operation can take hours and requires the expertise of an experienced physiologist.

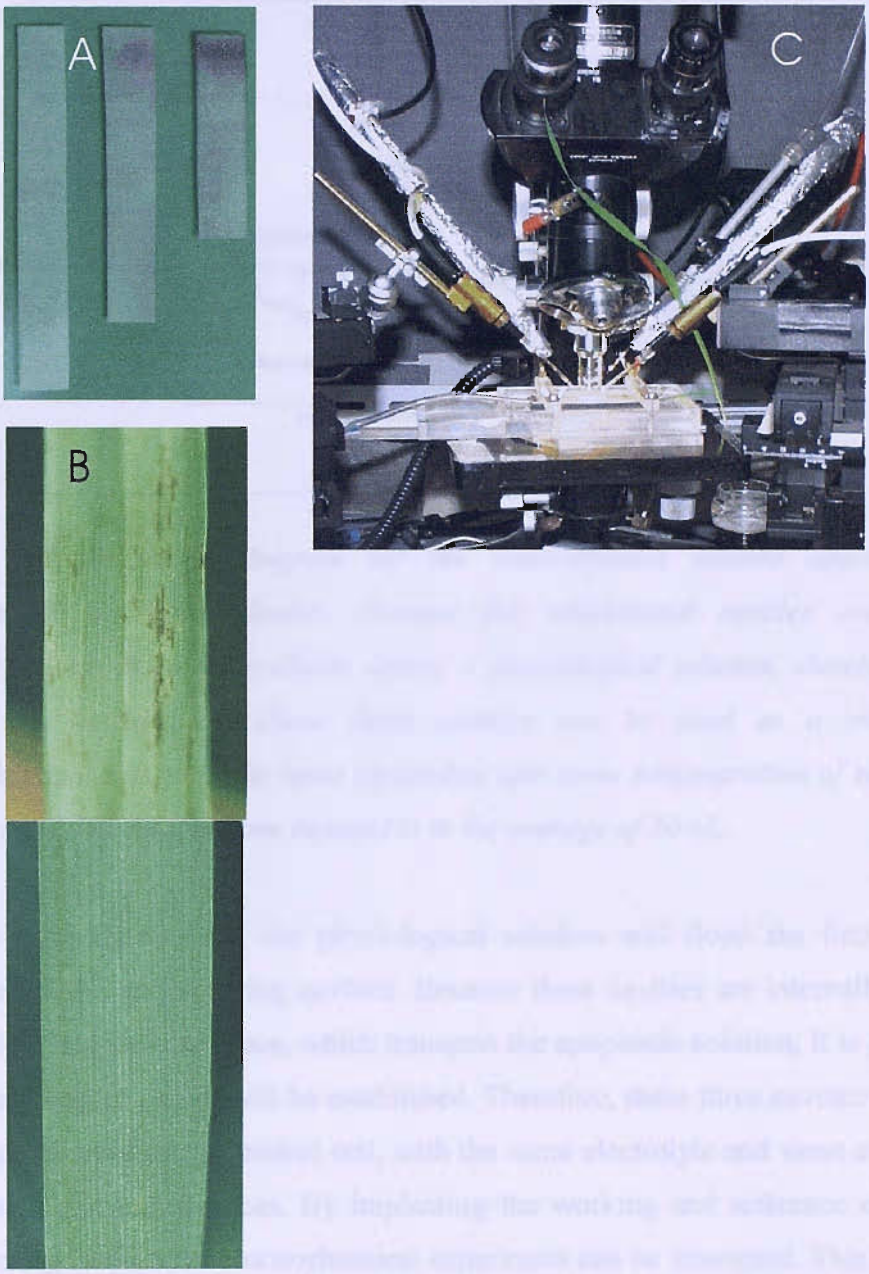

Figure 6.11 *Applications of PANi/PVS microsensors under in-vivo-conditions: A) in buffer during enzymatic lignin formation with peroxidase; shown is proof of colloidal lignin (brown) extracted from 2 assays, left: control without enzyme. B) In stomata pores (spots) of barley leaves, top: mlo mutant with necrosis from spontaneous oxidative bursts, bottom: wild type. C) In barley leaf (horizontal cuvette) of intact seedling. Pictures provided by Dr. Stefan Hanstein.*

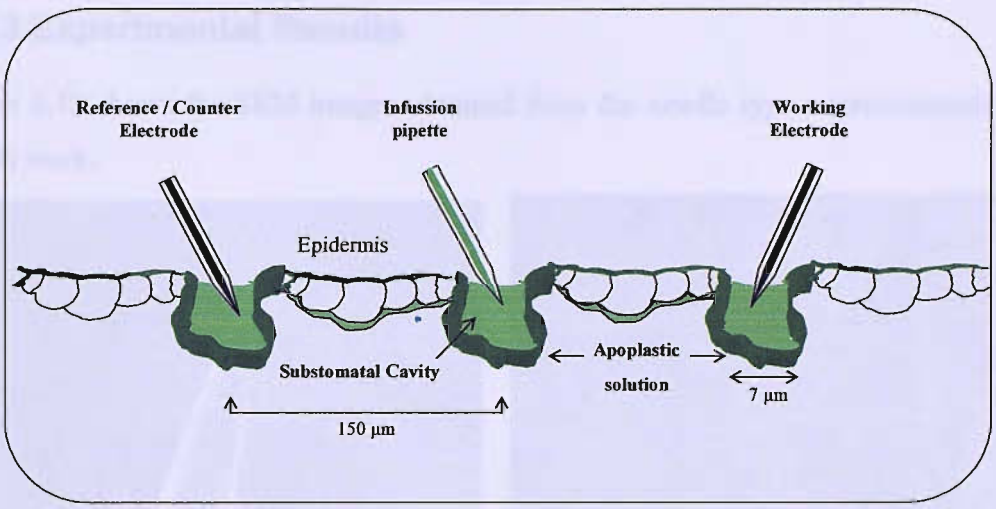

Figure 6.12 *Schematic diagram for the nano-infusion method applied for AA determination on Barley leaves. Because the substomatal cavities are connected internally by air-filled intercellular space, a physiological solution, sketched in green colour, can be injected. These three cavities can be used as a single micro-electrochemical cell, with the same electrolyte and same concentration of substrate and interferences. The total volume injected is in the average of 30 nL.*

As seen from figure 6.12, the physiological solution will flood the first cavity and subsequently the neighbouring cavities. Because these cavities are internally connected by air-filled intercellular space, which transport the apoplastic solution, it is possible that an electrochemical circuit will be established. Therefore, these three cavities can be used as a single micro-electrochemical cell, with the same electrolyte and same concentration of substrate and interferences. By implanting the working and reference electrodes in neighbouring cavities, an electrochemical experiment can be attempted. This method will provide information about ascorbate levels inside substomatal cavities.

6.4.3 Experimental Results

Figure 6.13 shows the SEM images obtained from the needle type microelectrodes used in this work.

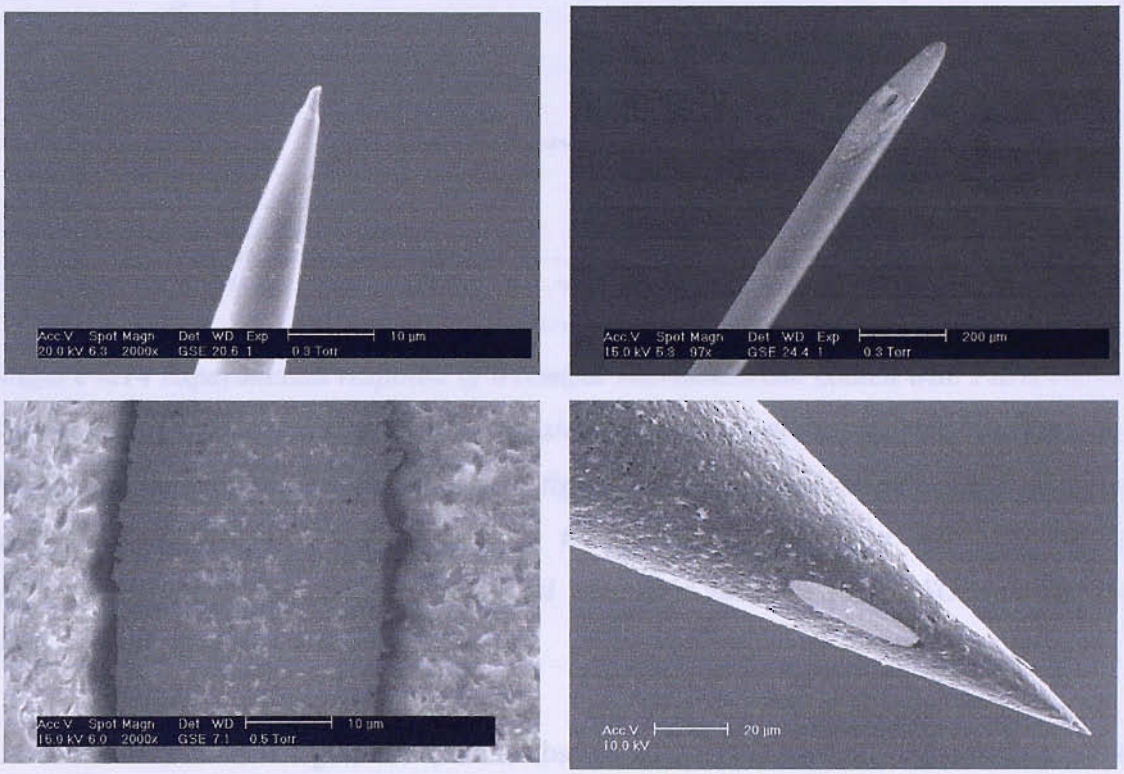

Fig. 6.13 *Electrodes for in-vivo applications supplied by Thomas Recording GmbH, Giessen, Germany. Top left: Conical electrode applied for monitoring vitamin C behind stomatal pore in barley leaf; platinum tip protruding through quartz glass insulation. Top right: Atraumatic electrode for vitamin C analysis in the brain; Pt electrode is an elliptical disk. Bottom left: Elliptical disk surface after depositing growth nuclei of PANi/PVS. Bottom right: Electrode with four Pt channels (tetrode); three lateral elliptical Pt disks plus Pt cone at the very tip. Pictures taken in collaboration with Dr. Stefan Hanstein*[240].

In collaboration with Dr. Stefan Hanstein, needle type microelectrodes were coated with PANi/PVS composite following procedures described in chapter 3. Afterwards the substomatal cavities of a plant leaf were flooded with physiological solution as described in figure 6.12. The experimental response obtained is shown in figure 6.14.

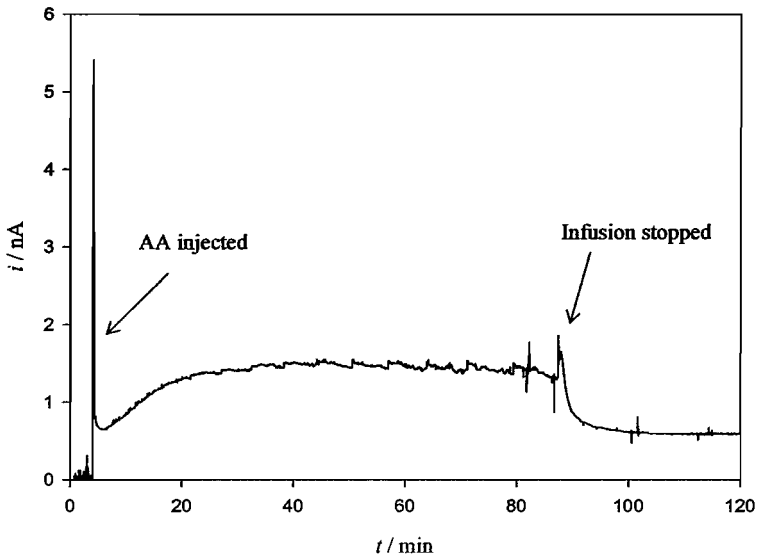

Figure 6.14 *Experimental response of a conical microelectrode coated with PANi/PVS in aged Barley leaf one day after cut. The substomatal cavities of the plant leaf were flooded with physiological solution as shown in figure 6.14. At t = 1.83 min 300 µM AA in physiological solution was injected to the plant. The infusion was stopped at t = 89.67 min. The electrode potential was held at +0.1 V vs. SCE during the experiment.*

As it can be seen from figure 6.14, in the absence of AA, the currents registered are close to zero. At t = 1.83 min a solution of 300 µM AA in physiological solution was injected to the plant and it can clearly be seen that the current increases and reach a stable value during the course of the experiment. As soon as the AA infusion was stopped, the current slowly decreased to the initial value. This experiment indicated that PANi/PVS microelectrodes might be suitable for monitoring AA on substomatal cavities of plant leafs. Currently, Dr. Stefan Hanstein continues this work and has successfully extended the applications by measuring AA in rat brain. The results from his work has been recently accepted for publication and appear in the journal Sensor and Actuators B[240].

6.5 Conclusions

PANi/PPS were successfully applied for the detection of ascorbate in low volumes of human plasma. The concentration of AA measured in plasma calculated by the standard additions method was in the range of the expected values. Although the results presented here are just a preliminary attempt. Our work in collaboration with Dr. Stefan Hanstein has also shown that AA can be monitored in plan leaves.

This is a real novel result and to the best of the author knowledge, no such attempts have been reported in the literature. Therefore, our proof of concept can open interesting applications in medicine and in physiology. Part of this work has been recently accepted for publication[240].

Chapter 7

Conclusions and further work

The work presented in this thesis has demonstrated that good and reproducible PANi coatings on small Pt microelectrodes with different geometries can be achieved. The resulting films have been proven to be excellent electrocatalytic surfaces for AA oxidation and promising materials to be used in real systems.

The electrodeposition of PANi films on small Pt microelectrodes is highly dependent on the experimental conditions. Reproducible PANi coatings can only be achieved when the electrode R_f is carefully controlled. This is a technical parameter to control if a company such as Thomas Recording GmbH decides to produce coatings on needle type microelectrodes for commercial purposes. The polymerization growth rate was seen to be dependent on the electrolyte and counter ion used. The addition of a large counter anion such as PVS or PSS decreased the growth rate by a factor of two. Growth rate followed the order PANi/H_2SO_4 > PANi/HCl > PANi/ H_2SO_4/PVS > PANi/ H_2SO_4/PSS > PANi/HCl/PVS > PANi/HCl/PSS.

Preliminary results indicate that PANi morphology can be controlled in a better manner during potential cycling than via constant potential. SEM images showed evidence that controlling polymer spill over becomes more difficult as the microelectrode radius decreases. This is due to the high values of the mass transport rate constant achieved for small microelectrodes. Nevertheless flat PANi films with thickness much lower than the microelectrode radius can be achieved via cyclic voltammetry. Electrodeposition at constant potential resulted in anomalous mushroom shaped films with a high degree of polymer spillover. Following research in the literature, and out of many coatings produced within the work presented here, it is believed that potential cycling helps the PANi chains to accommodate and reorganize during oxidation/reduction cycles. The control of the anodic potential limit used during polymerization to avoid quinoimines units within the film also helps to obtain highly conductive PANi films. Although further

work is needed to improve polymerization under constant potential it is though to be more difficult to control compared to CV, despite faster growth rates. Different growth methods can be found in the literature. Rajendran and Tsakova used the pulse potentiostatic method[170] with good results and it is worth investigating in the future work.

PANi-PVS, PANi-PSS and alkylated films retained polymer conductivity when electrodeposited on small microelectrodes. Surprising results were found when films were characterized at neutral pH. The counter ion molecular weight was seen to be important to reach a more stable response. Initially it was though that attaining H^+ equilibrium within the PANi film was not dependent on the counter ion used as long at it provided the extra negative charge. Furthermore, when these films were used as electrocatalytic surfaces for AA the limiting currents registered were double for PANi-PVS than for PANi-PSS. This curious result was unexpected and led us to an interesting study of the kinetics of the reaction. Assuming that AA oxidation occurs at the polymer solution interface the mechanism at which ascorbate oxidizes at neutral pH is open to discussion.

The fact that PANi-PSS present half the limiting currents compared to PANi-PVS suggest that ascorbate oxidizes via a different mechanism. This is difficult to believe, as the counter ion should not play a role at the molecular level. This finding was not just the result of coincidence as it was observed by different collaborators during the course of this research and similar results were found in the literature. Therefore, the results here are reproducible and representative. The kinetic model proposed agrees with the assumption that ascorbate react at PANi composite via Michaelis-Menten mechanism. This result agreed with previous RDE studies in this laboratory. The awkward observation of $n = 1$ for PANi-PSS has to be related to the generation of an ascorbate anion radical which is able to diffuse away to the solution before it is further oxidized to DHA releasing the second electron. Rotating ring disc, fast scan cyclic voltammetry at a microelectrode and/or Electron Spin Resonance/Electron Paramagnetic Resonance (EPR/ESR) will help to identify the presence of the ascorbate radical anion intermediate and answer this difficult question.

Composite PANi and alkylated films were found to have excellent electroanalytical properties for AA oxidation. A detection limit of 1 μM was obtained in buffer solution. Different detection limit can be found during in physiological solutions due to the background current. Modified PANi films were found to remain stable for weeks if the PANi film is cycled in an acidic solution containing the desired counter ion. However, it is still not clear if the problem with stability is due to polymer deprotonation or to loss of the counter anion. FT-IR analysis of the solution could help to answer this question as the SO_3 groups can be measured in the solution if leached from the film.

Although results were not included in this thesis, work has been done to improve PANi stability. Following the assumption that quinoimine units are reactive towards a nucleophilic it is though that PANi cross-linking can help to attain a more stable polymer. Figure 7.1 shows the chemical structure behind the idea.

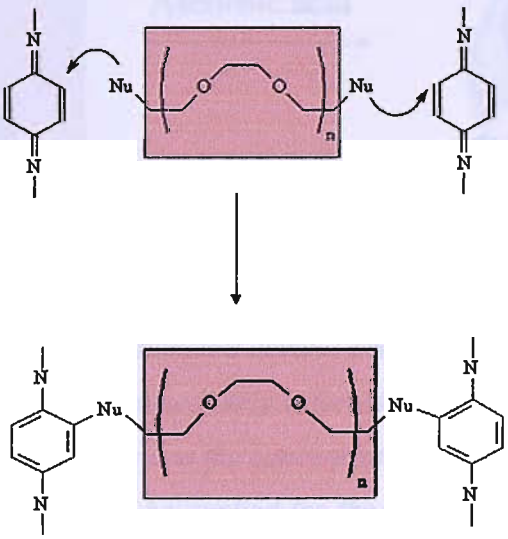

Figure 7.1 *Cross-linking of PANi with a dinucleophile.*

It will be interesting to use a polyethylene chain with two nucleophiles attached at each end. It is believed that nucleophiles will react with quinoimines rings of the emeraldine state under the correct conditions. Using a cross-linker chain containing intercalated oxygen atoms which will provide a more flexible "bridge" compared with a fully alkyl chain. In addition, polyethylene chains, it is expected to produce a less soluble polymer,

like epoxy resins. Therefore, the resulting polymer will have the PANi chains cross-linked and will result in an increase of polymer stability. Sulphonation of the resulting chains will be needed to retain conductivity at neutral pH. It is the hope of this idea to produce a highly stable water resistant polymer.

The preliminary experiments in real systems have demonstrated that thin films of PANi-PSS or PANi/PVS can be potentially electrodeposited on a screen-printed electrode, and using similar technology as for the measurement glucose in human blood, AA can be precisely monitored with time. This would be a significant advantage compared to the current methods present in the market. Figure 7.2 shows an illustrative image of the future measurements for AA in human blood.

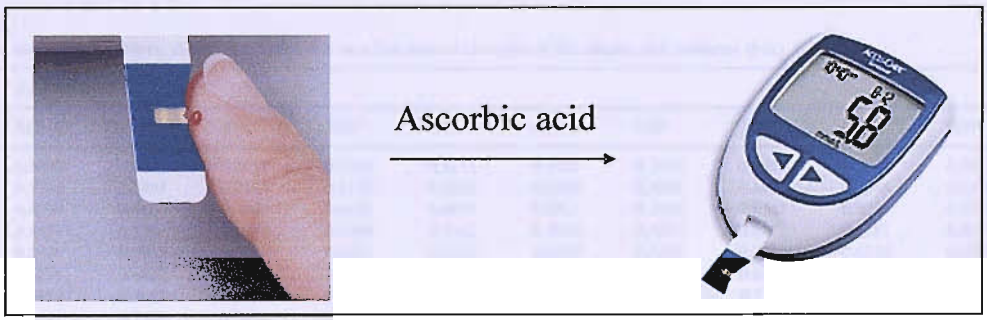

Figure 7.2 *Current technology for the electrochemical measurement of glucose using a screen-printed electrode and an automated device. The blood sample is placed on top of the screen-printed electrode, and immediately inserted inside the electronic device. Then the electrochemical reaction occurs and the concentration of glucose in blood appears on the screen. Similar technology can be applied for the monitoring of AA in human blood by the electrodeposition of thin films of PANi-PSS on a screen-printed electrode and using our methodology presented through this thesis.*

Out of this work, a patent has been applied at the European patent office.
WO2006063576. See Appendix A.4 for a brief description

Chapter 8

Appendix

A.1

Calculation of the limiting current with an elliptical microelectrode

Table provided by Bruckenstein and Janiszewska[150] used to calculate the term $G(m)^{-1}$ in equation 3.1. The ellipse major axis is denoted as (a) and the minor axis as (b).

Table 3
Ratio of current at an elliptic disk to a circular disk as a function of the ratio of the elliptic disk semiaxes (b/a)

b/a	$(G(1-b^2a^{-2})^{1/2})^{-1}$									
	0.00	0.01	0.02	0.03	0.04	0.05	0.06	0.07	0.08	0.09
0.00	0.0000	0.2478	0.2783	0.2998	0.3172	0.3321	0.3454	0.3575	0.3687	0.3791
0.10	0.3890	0.3984	0.4073	0.4159	0.4242	0.4322	0.4399	0.4475	0.4548	0.4620
0.20	0.4690	0.4759	0.4826	0.4892	0.4957	0.5021	0.5084	0.5147	0.5208	0.5269
0.30	0.5329	0.5388	0.5446	0.5504	0.5562	0.5619	0.5676	0.5732	0.5787	0.5843
0.40	0.5898	0.5953	0.6007	0.6061	0.6115	0.6169	0.6222	0.6275	0.6328	0.6381
0.50	0.6434	0.6487	0.6539	0.6592	0.6644	0.6697	0.6749	0.6802	0.6854	0.6907
0.60	0.6959	0.7012	0.7064	0.7117	0.7170	0.7223	0.7276	0.7330	0.7383	0.7437
0.70	0.7492	0.7546	0.7601	0.7656	0.7712	0.7768	0.7825	0.7882	0.7940	0.7998
0.80	0.8057	0.8117	0.8178	0.8240	0.8303	0.8367	0.8432	0.8499	0.8568	0.8638
0.90	0.8711	0.8786	0.8865	0.8947	0.9034	0.9127	0.9227	0.9339	0.9468	0.9630

Circular disk radius is equal to the major axis of the elliptic disk. The ellipse is inscribed in the circle.

Example;

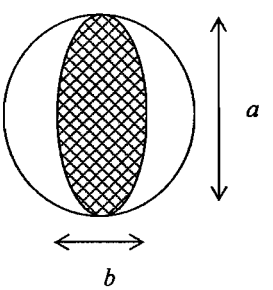

$$i_{elliptical} = 4nFDCaG(m)^{-1} \quad \textbf{(3.1)}$$

$C = 10\ mM = 10^{-5}\ mol\ cm^{-3}$

$n=1$

$D=6.5 X 10^{-6}\ cm^2 s^{-1}$

$a=13\ X\ 10^{-4}\ cm$

$b=10\ X\ 10^{-4}\ cm$

$i_{elliptical}=4\ x\ (1)\ x\ (96480)\ x\ (6.5\ X\ 10^{-6})\ x\ (13\ X\ 10^{-4})\ x\ G(m)^{-1} = 3.26\ X\ 10^{-4}\ x\ G(m)^{-1}$

$$b/a = 10/13 = 0.769$$

from table for m=0.77, $G(m)^{-1}=0.7882$

Hence

$i_{elliptical}= 3.26\ X\ 10^{-8}\ x\ G(m)^{-1}= 3.26\ X\ 10^{-8}\ x\ 0.7882 = 25.7\ nA$

A.2

PANi nucleation mechanism at Pt microelectrodes

In the case of the 2D islands, the current transients for instantaneous and progressive nucleation in a non-dimensional form are given by equations (1) and (2) respectively[140]. On the other hand, theoretical plots for instantaneous and progressive 3D nucleation processes are given by non-dimensional equations (3) and (4) respectively[241]. The parameters (t, t_m) and (I , I_m) in equations (1) and (2) are the coordinates of the current-time maximum. However, equations (3) and (4) are written in terms of the current density, i , and the maximum of the current density, i_m . Figure 8.1 shows the non-dimensional plot of the experimental deposition shown in Chapter 3, figure 3.6.

$$\frac{I}{I_m} = \left(\frac{t}{t_m}\right)^2 \exp\left(-\frac{2}{3}\frac{(t^3 - {t_m}^3)}{{t_m}^3}\right) \qquad (8.1)$$

$$\frac{I}{I_m} = \frac{t}{t_m}\exp\left(-\frac{1}{2}\frac{(t^2 - {t_m}^2)}{{t_m}^2}\right) \qquad (8.2)$$

$$\left(\frac{i}{i_m}\right)^2 = 1.2254\left(\frac{t}{t_m}\right)^{-1}\left\{1 - e^{\left[-2.3367\left(\frac{t}{t_m}\right)^2\right]}\right\}^2 \qquad (8.3)$$

$$\left(\frac{i}{i_m}\right)^2 = 1.9542\left(\frac{t}{t_m}\right)^{-1}\left\{1 - e^{\left(-1.2564\left(\frac{t}{t_m}\right)\right)}\right\}^2 \qquad (8.4)$$

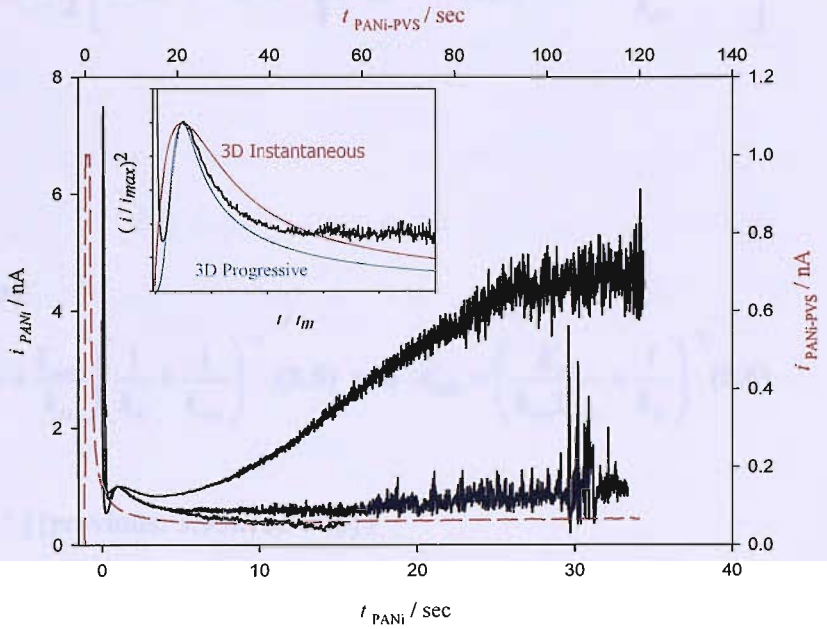

Figure 8.1 *Non-dimensional plot of current maximum obtained at the initial stage of amperometric deposition, compared with theoretical curves for 2D and 3D nucleation given in equations (1) to (4). Experimental details are described in Chapter 3, figure 3.6.*

A.3

Non linear regression obtained with Sigmaplot 8.0

Equation

$$i = nFA\frac{k_D'}{2}\left[(K_{ME} + AA_{bulk}) \pm \sqrt{(K_{ME} + AA_{bulk})^2 - \frac{4k_{ME}' K_{ME} AA_{bulk}}{k_D'}}\right] \quad \textbf{(5.8)}$$

[Variables]

j = col(3)

c = col(2)

[Parameters]

$$K_{ME} = \left(\frac{K_M}{k_{cat}} + \frac{\Gamma_{site}}{k_D'}\right)\left(\frac{1}{k_E'} + \frac{1}{k_{cat}}\right)^{-1} \textbf{(5.5)} \text{ and } k_{ME}' = \left(\frac{K_M}{k_{cat}\Gamma_{site}} + \frac{1}{k_D'}\right)^{-1} \textbf{(5.6)}$$

K_{ME} = 1e-5 ' {{previous: 3.95673e-005}}

k_{ME}' = 1e-3 ' {{previous: 0.00395365}}

[Equation]

kd=(4*4.8e-6)/(3.1416*13e-4)

f=(1*96480*3.1416*13*13*1e-8)*(kd/2)*((KM+c)-sqrt((KM+c)^2-(4*KM*k*c/kd)))

fit f to j

[Constraints]

[Options]

tolerance=0.000100

stepsize=10

iterations=100

The regression produces a perfect fit

R = 0.99856810 Rsqr = 0.99713826 Adj Rsqr = 0.99691812

Standard Error of Estimate = 0.0000

	Coefficient
KM	0.0001
k	0.0030

Analysis of Variance:

	DF	SS	MS	F	P
Regression	1	0.0000	0.0000	(+inf)	(NAN)
Residual	13	0.0000	0.0000		
Total	14	0.0000	0.0000		

PRESS = 0.0000

Durbin-Watson Statistic = 0.5479

Normality Test: K-S Statistic = 0.1667 Significance Level = 0.7600

Constant Variance Test: Failed (P = 0.0413)

Power of performed test with alpha = 0.0500: 1.0000

A.4

Coating made from an electroactive polymer

Patent number: WO2006063576

Publication date: 2006-06-22

Inventor(s): HANSTEIN STEFAN MARTIN (DE); BARTLETT PHILIP N (GB); MARTINEZ BONASTRE ALEXANDRO (ES)

Applicant: JUSTUS LIEBIG UNI GIESSEN (DE); HANSTEIN STEFAN MARTIN (DE); BARTLETT PHILIP N (GB); MARTINEZ BONASTRE ALEXANDRO (ES)

Application number: WO2005DE02264 20051214

Priority number(s): DE200410060680 20041215

Abstract

The invention relates to a coating of at least one electroactive polymer, made from poly(aniline), alkylated poly(aniline), a mixture of poly(aniline) and poly(vinylsulphonic) acids or similar, for the coating of micro- and nano-electrodes. According to the invention, the stability and water-resistance of known coatings may be improved, whereby the at least one electroactive polymer is cross-linked with selected compounds comprising a group from aromatic alcohols, phenols and ethers, aromatic aldehydes, saturated and unsaturated araliphatic alcohols, aldehydes and ethers, aromatic carboxylic acids and carboxylate esters, saturated and unsaturated araliphatic carboxylic acids and carboxylate esters, aromatic amino acids and combinations thereof. The invention further relates to an electroactive laminate comprising said coating, in particular in the form of a micro- or nano-electrode, a method for production of such laminates and a method for the quantitative determination of an analyte, in particular, of ascorbate, in a sample.

References

(1) Montenegro, M. I.; Queirós, M. A.; Daschbach, J. *Microelectrodes: Theory and Applications*, 1st ed.; Kluwer Academic Publishers: Alvo (Portugal), **1990**.

(2) Oldham, K. B. *J. Electroanal. Chem.* **1992**, 53-76.

(3) Bond, A.; Oldham, K.; Zoski, C. G.; Luscombe, D. *J. Electroanal. Chem.* **1988**, 1-14.

(4) Ewing, A. G.; Wightman, R. M.; Dayton, M. A. *Brain Res.* **1982**, *249*, 361-370.

(5) Denuault, G.; Fleischmann, M.; Pletcher, D.; Tutty, O. R. *J. Electroanal. Chem.* **1990**, *280*, 243-254.

(6) Wightman, R. M.; Wipf, D. O. *Electroanal. Chem.* **1989**, *15*, 267-353.

(7) Wightman, R. M. *Anal. Chem.* **1981**, *53*, 1125-&.

(8) Deakin, M. R.; Wipf, D.; Wightman, R. M. *J. Electrochem. Soc.* **1986**, *133*, C135-C135.

(9) Wightman, R. M. *Science* **2006**, *311*, 1570-1574.

(10) Zoski, C. G. *Electroanalysis* **2002**, *14*, 1041-1051.

(11) Oldham, K. B. *J. Electroanal. Chem.* **1990**, 1-14.

(12) Phillips, P. E. M.; Wightman, R. M. *TrAC* **2003**, *22*, 509-514.

(13) Stulik, K.; Amatore, C.; Holub, K.; Marecek, V.; Kutner, W. *Pure Appl. Chem.* **2000**, *72*, 1483-1492.

(14) Nugues, S.; Denuault, G. *J. Electroanal. Chem.* **1996**, *408*, 125-140.

(15) Yang, Y. F.; Denuault, G. *J. Electroanal. Chem.* **1996**, *418*, 99-107.

(16) Yang, Y. F.; Denuault, G. *J. Chem. Soc. Faraday Trans.* **1996**, *92*, 3791-3798.

(17) Southampton Electrochemistry Group *Instrumental Methods in Electrochemistry*, 1st ed.; Ellis Horwood: Chichester, **1990**.

(18) Bard, A. J.; Faulkner, L. R. *Electrochemical Methods*, 2nd ed.: New York, **1980**.

(19) Oldham, K. B. *J. Electroanal. Chem.* **1987**, *237*, 303-307.

(20) Andrieux, C. P.; Audebert, P.; Hapiot, P.; Nechtschein, M.; Odin, C. *J. Electroanal. Chem.* **1991**, *305*, 153-162.

(21) Bruckenstein, S.; Wehmeyer, K. *J. Electroanal. Chem.* **1985**, *196*, 417-421.

(22) Oldham, K. B. *J. Electroanal. Chem.* **1981**, *122*, 1-17.

(23) Ewing, A. G.; Wightman, R. M. *Abstr. Am. Chem. Soc.* **1982**, *183*, 63.

(24) Kawagoe, K. T.; Wightman, R. M. *Talanta* **1994**, *41*, 865-874.

(25) Kuhr, W. G.; Wightman, R. M. *Brain Res.* **1986**, *381*, 168-171.

(26) Logman, M. J.; Budygin, E. A.; Gainetdinov, R. R.; Wightman, R. M. *J. Neurosci. Meth.* **2000**, *95*, 95-102.

(27) Wightman, R. M.; Leszczyszyn, D. J.; Jankowski, J. A. *Abstr. Am. Chem. Soc.* **1990**, *200*, 27-ANYL.

(28) Wightman, R. M.; Miele, M. *J. Neurosci. Meth.* **1996**, *70*, 15-19.

(29) Wightman, R. M.; Phillips, P. *TrAC* **2003**, *22*, 509.

(30) Wightman, R. M.; Venton, B. J.; Heien, L.; Troyer, K. P. *Anal. tech.* **2002.**

(31) Miele, M.; Fillenz, M. *J. Neurosci. Methods* **1996**, *70*, 15-19.

(32) Cahill, P. S.; Walker, Q. D.; Finnegan, J. M.; Mickelson, G. E.; Travis, E. R.; Wightman, R. M. *Anal. Chem.* **1996**, *68*, 3180-3186.

(33) Anson, F. C. *J. Electroanal. Chem.* **1973**, *47*, 279-285.

(34) Wang, J. *Electroanalysis* **1991**, *3*, 255-259.

(35) Murray, R. W. *Electroanal. Chem.* **1984**, *13*, 191-368.

(36) Muller, U.; Schmiemann, U.; Dulberg, A.; Baltruschat, H. *Surf. Sci.* **1995**, *335*, 333-342.

(37) Sidqi, M.; Ligner, G.; Jagiello, J.; Balard, H.; Papirer, E. *Chromatographia* **1989**, *28*, 588-592.

(38) Pilloud, D. L.; Chen, X. X.; Dutton, P. L.; Moser, C. C. *J. Phys. Chem. B* **2000**, *104*, 2868-2877.

(39) Epstein, A. J.; Ginder, J. M.; Zuo, F.; Bigelow, R. W.; Woo, H. S.; Tanner, D. B.; Richter, A. F.; Huang, W. S.; Macdiarmid, A. G. *Synth. Met.* **1987**, *18*, 303-309.

(40) Kanazawa, K. K.; Diaz, A. F.; Gill, W. D.; Grant, P. M.; Street, G. B.; Gardini, G. P. *Synth. Met.* **1980**, *1*, 329-336.

(41) Su, W. P.; Schrieffer, J. R.; Heeger, A. J. *Phys. Rev. Lett.* **1979**, *42*, 1698-1701.

(42) Chiang, C. K.; Fincher, C. R.; Park, Y. W.; Heeger, A. J.; Shirakawa, H.; Louis, E. J.; Gau, S. C.; Macdiarmid, A. G. *Phys. Rev. Lett.* **1977**, *39*, 1098-1101.

(43) Shirakawa, H. *Synth. Met.* **2001**, *125*, 3-10.

(44) Blythe, T.; Bloor, D. *Electrical Properties of Polymers*, 2nd ed.; Cambridge University Press: Cambridge, **2005**.

(45) Heeger, A. J. *Angew. Chem.-Int. Edit.* **2001**, *40*, 2591-2611.

(46) MacDiarmid, A. G. *Angew. Chem.-Int. Edit.* **2001**, *40*, 2581-2590.

(47) Shirakawa, H. *Rev. Mod. Phys.* **2001**, *73*, 713-718.

(48) Brandrup, J.; Immergut, E. H.; Grulke, E. A.; Abe, A.; Bloch, D. R. *Polymer Handbook*, 4th ed.; John Wiley & Sons, **2005**.

(49) Kang, E. T.; Neoh, K. G.; Tan, K. L. *Prog. Polym. Sci.* **1998**, *23*, 277-324.

(50) Comisso, N.; Cattarin, S.; Zotti, G. *J. Electroanal. Chem.* **1987**, *235*, 259-273.

(51) Lyons, M. E. G. In *Advances in Chemical Physics*, **1996**; Vol. XCIV, p 297-624.

(52) Kanazawa, K. K.; Diaz, A. F.; Gardini, G. P.; Street, G. B. *J. Electrochem. Soc.* **1979**, *126*, C130-C130.

(53) Sbaite, P.; Huerta-Vilca, D.; Barbero, C.; Miras, M. C.; Motheo, A. J. *Eur. Polym. J.* **2004**, *40*, 1445-1450.

(54) Morales, G. M.; Llusa, M.; Miras, M. C.; Barbero, C. *Polymer* **1997**, *38*, 5247-5250.

(55) Tsakova, V.; Milchev, A. *Electrochim. Acta* **1991**, *36*, 1579-1583.

(56) Tsakova, V.; Milchev, A.; Schultze, J. W. *J. Electroanal. Chem.* **1993**, *346*, 85-97.

(57) Zhang, A. Q.; Cui, C. Q.; Lee, J. Y. *Synth. Met.* **1995**, *72*, 217-223.

(58) Gu, M.; Liao, C. *Thin solid Films* **2002**, *408*, 37-42.

(59) Luthra, V.; Singh, R.; Gupta, S. K.; Mansingh, A. *Curr. Appl. Phys.* **2003**, *3*, 219-222.

(60) Miras, M. C.; Barbero, C.; Haas, O. *Synth. Met.* **1991**, *43*, 3081-3084.

(61) Sun, J. J.; Zhou, D. M.; Fang, H. Q.; Chen, H. Y. *Talanta* **1998**, *45*, 851-856.

(62) Kalakodimi, R. P.; Nookala, M. *Anal. Chem.* **2002**, *74*, 5531-5537.

(63) Casella, I. G.; Guascito, M. R. *Electroanalysis* **1997**, *9*, 1381-1386.

(64) Arsov, L. D. *J. Solid State Electrochem.* **1998**, *2*, 266-272.

(65) Desilviestro, J.; Scheifele, W. *J. Mater. Chem.* **1993**, *3*, 263-272.

(66) Jones, V. W.; Kalaji, M.; Walker, G.; Barbero, C.; Kotz, R. *J. Chem. Soc.-Faraday Trans.* **1994**, *90*, 2061-2064.

(67) Levon, K.; Park, K. C.; Cai, C. *Synth. Met.* **1997**, *84*, 335-338.

(68) Michaelson, J. C.; McEvoy, A. J.; Kuramoto, N. *React. Polym.* **1992**, *17*, 197-2006.

(69) Andrade, G. D.; Aguirre, M. J.; Biaggio, S. R. *Electrochim. Acta* **1998**, *44*, 633-642.

(70) Cui, C. Q.; Su, X. H.; Lee, J. Y. *Polym. Degrad. Stabil.* **1993**, *41*, 69-76.

(71) Mazeikiene, R.; Malinauskas, A. *Eur. Polym. J.* **2002**, *38*, 1947-1952.

(72) Greef, R.; Kalaji, M.; Peter, L. M. *Faraday Discuss.* **1989**, *88*, 277-+.

(73) Allen J. Bard, I. R. *Electroanalytical Chemistry*, Hardcover ed.; Dekker Incorporated, Marcel, **1996**.

(74) Macdiarmid, A. G.; Chiang, J. C.; Richter, A. F.; Epstein, A. J. *Synth. Met.* **1987**, *18*, 285-290.

(75) Bartlett, P. N.; Wang, J. H. *J. Chem. Soc.-Faraday Trans.* **1996**, *92*, 4137-4143.

(76) Chartier, P.; Mattes, B.; Reiss, H. *J. Phys. Chem.* **1992**, *96*, 3556-3560.

(77) Mafe, S.; Manzanares, J. A.; Reiss, H. *J. Chem. Phys.* **1993**, *98*, 2325-2331.

(78) Mafe, S.; Manzanares, J. A.; Reiss, H. *J. Chem. Phys.* **1993**, *98*, 2408-2410.

(79) Duic, L.; Mandic, Z. *J. Electroanal. Chem.* **1992**, *335*, 207-221.

(80) Kalaji, M.; Nyholm, L.; Peter, L. M. *J. Electroanal. Chem.* **1991**, *313*, 271-289.

(81) Barbero, C.; Morales, G. M.; Grumelli, D.; Planes, G.; Salavagione, H.; Marengo, C. R.; Miras, M. C. *Synth. Met.* **1999**, *101*, 694-695.

(82) Bartlett, P. N.; Birkin, P. R. *Synth. Met.* **1993**, *61*, 15-21.

(83) Gerard, M.; Chaubey, A.; Malhotra, B. D. *Biosens. Bioelectron.* **2002**, *17*, 345-359.

(84) Asturias, G. E.; Jang, G. W.; Macdiarmid, A. G.; Doblhofer, K.; Zhong, C. J. *Berichte Der Bunsen-Gesellschaft-Phys. Chem. Chem. Phys.* **1991**, *95*, 1381-1384.

(85) Macdiarmid, A. G.; Epstein, A. J. *Synth. Met.* **1995**, *69*, 85-92.

(86) Acevedo, D. F.; Salavagione, H. J.; Miras, M. C.; Barbero, C. A. *J. Braz. Chem. Soc.* **2005**, *16*, 259-269.

(87) Barbero, C.; Salavagione, H. J.; Acevedo, D. F.; Grumelli, D. E.; Garay, F.; Planes, G. A.; Morales, G. M.; Miras, M. C. *Electrochim. Acta* **2004**, *49*, 3671-3686.

(88) Grumelli, D. E.; Forzani, E. S.; Morales, G. M.; Miras, M. C.; Barbero, C. A.; Calvo, E. J. *Langmuir* **2004**, *20*, 2349-2355.

(89) Bartlett, P. N.; Wallace, E. N. K. *Phys. Chem. Chem. Phys.* **2001**, *3*, 1491-1496.

(90) Bartlett, P. N.; Simon, E. *Phys. Chem. Chem. Phys.* **2000**, *2*, 2599-2606.

(91) Bartlett, P. N.; Birkin, P. R.; Wallace, E. N. K. *J. Chem. Soc.-Faraday Trans.* **1997**, *93*, 1951-1960.

(92) Bartlett, P. N.; Wallace, E. N. K. *J. Electroanal. Chem.* **2000**, *486*, 23-31.

(93) Raffa, D.; Leung, K. T.; Battaglini, F. *Anal. Chem.*, 4983-4987.

(94) Sivakumar, R.; Saraswathi, R. *Synth. Met.* **2003**, *138*, 381-390.

(95) Ernst, H.; Knoll, M. *Anal. Chim. Acta* **2001**, *449*, 129-134.

(96) Granot, E.; Katz, E.; Basnar, B.; Willner, I. *Chem. Mater.* **2005**, *17*, 4600-4609.

(97) Brezina, M.; Loucka, T.; Koryta, J.; Marsikov.D; Pradac, J. *J. Electroanal. Chem.* **1972**, *40*, 13-&.

(98) Lyons, M. E. G.; Breen, W.; Cassidy, J. *J. Chem. Soc.-Faraday Trans.* **1991**, *87*, 115-123.

(99) Hu, I. F.; Kuwana, T. *Anal. Chem.* **1986**, *58*, 3235-3239.

(100) Rueda, M.; Aldaz, A.; Sanchez-Burgos, F. *Electrochim. Acta.* **1978**, *23*, 419-424.

(101) Aldaz, A.; Jimenez, R.; Piazza, C.; Vazquez, J. L. *An. Quim.* **1974**, *70*, 410-414.

(102) Ruiz, J. J.; Aldaz, A.; Dominguez, M. *Can. J. Chem.* **1977**, *55*, 2799-2806.

(103) Ruiz, J. J.; Aldaz, A.; Dominguez, M. *Can. J. Chem.* **1978**, *56*, 1533-1537.

(104) Gomez, M. M.; Manzano, A.; Aldaz, A.; Vara, J. M. *An Qim-Fis Tec* **1980**, *76*, 35-39.

(105) Ruiz, J. J.; Dominguez, M.; Aldaz, A. *An Qim-Fis Tec* **1980**, *76*, 197-200.

(106) Gomez, M. M.; Diez, E.; Alda, E.; Aldaz, A. *J. Electroanal. Chem.* **1984**, *165*, 207-219.

(107) Ruiz, J. J.; Rodriguez -Mellado, J. M.; Dominguez, M.; Aldaz, A. *J. Chem. Soc.-Faraday Trans. T1* **1989**, *85*, 1567-1574.

(108) Climent, M. A.; Rodes, A.; Valls, M. J.; Perez, J. M.; Feliu, J. M.; Aldaz, A. *J. Chem. Soc.-Faraday Trans.* **1994**, *90*, 609-615.

(109) Deutsch, J. C. *J. Chromatogr. A* **2000**, *881*, 299-307.

(110) Kokoh, K. B.; Hahn, F.; Metayer, A.; Lamy, C. *Electrochim. Acta* **2002**, *47*, 3965-3969.

(111) Karabinas, P.; Jannakoudakis, D. *J. Electroanal. Chem.* **1984**, *160*, 159-167.

(112) Aldaz, A.; Alquie, A. M. *J. Electroanal. Chem.* **1973**, *47*, 532-534.

(113) Gomez, M. M.; Diez, E.; Alda, E.; Aldaz, A. *J. Electroanal. Chem.* **1984**, *165*, 207-219.

(114) Falat, L.; Cheng, H. Y. *Anal. Chem.* **1982**, *54*, 2108-2111.

(115) Vankoppenhagen, J. E.; Majda, M. *J. Electroanal. Chem.* **1987**, *236*, 113-138.

(116) Vankoppenhagen, J. E.; Majda, M. *J. Electroanal. Chem.* **1985**, *189*, 379-388.

(117) Andrieux, C. P.; Saveant, J. M. *Molecular design of electrode surfaces*; Wiley-Interscience: New York, **1992**.

(118) Andrieux, C. P.; Saveant, J. M. *J. Electroanal. Chem.* **1980**, *111*, 377-381.

(119) Andrieux, C. P.; Dumasbouchiat, J. M.; Saveant, J. M. *J. Electroanal. Chem.* **1980**, *114*, 159-163.

(120) Andrieux, C. P.; Dumasbouchiat, J. M.; Saveant, J. M. *J. Electroanal. Chem.* **1982**, *131*, 1-35.

(121) Andrieux, C. P.; Saveant, J. M. *J. Electroanal. Chem.* **1982**, *142*, 1-30.

(122) Andrieux, C. P.; Saveant, J. M. *J. Electroanal. Chem.* **1982**, *134*, 163-166.

(123) Andrieux, C. P.; Dumasbouchiat, J. M.; Saveant, J. M. *J. Electroanal. Chem.* **1981**, *123*, 171-187.

(124) Diaz, A. F.; Kanazawa, K. K.; Gardini, G. P. *J. Chem. Soc., Chem. Commun.* **1979**, 635-636.

(125) Diaz, A. F.; Orozcorosales, F. A.; Kanazawa, K. K. *J. Electroanal. Chem.* **1979**, *103*, 233-242.

(126) Kanazawa, K. K.; Diaz, A. F.; Geiss, R. H.; Gill, W. D.; Kwak, J. F.; Logan, J. A.; Rabolt, J. F.; Street, G. B. *J. Chem. Soc., Chem. Commun.* **1979**, 854-855.

(127) Kanazawa, K. K.; Diaz, A. F.; Gardini, G. P.; Gill, W. D.; Kwak, J. F.; Street, G. B. *Bull. APS* **1979**, *24*, 326-326.

(128) Kanazawa, K. K.; Diaz, A. F.; Street, G. B. *Bull. APS* **1981**, *26*, 415-415.

(129) Diaz, A. F.; Castillo, J.; Kanazawa, K. K.; Logan, J. A.; Salmon, M.; Fajardo, O. *J. Electroanal. Chem.* **1982**, *133*, 233-239.

(130) Salmon, M.; Kanazawa, K. K.; Diaz, A. F.; Krounbi, M. *J. Polym. sci. pol. lett.* **1982**, *20*, 187-193.

(131) Saraceno, R. A.; Pack, J. G.; Ewing, A. G. *J. Electroanal. Chem.* **1986**, *197*, 265-278.

(132) Temkin, M. I. *Fiz. Khim* **1941**, *15*, 296.

(133) Conway, B. E.; Gileadi, E. In *Modern Aspects of Electrochemistry*; Vayenas, C., Ed.; Plenum Press: New York, **1969**; Vol. 3, p 147.

(134) Wallace, E. N. K. Poly(aniline) composites as bioelectrochemical sensors, *PhD thesis*, Southampton University, Bartlett, P. N. **1997**.

(135) Bartlett, P. N.; Wallace, E. N. K. *Phys. Chem. Chem. Phys.* **2001**, *3*, 1491-1496.

(136) Lyons, M. E. G.; Lyons, C. H.; Michas, A.; Bartlett, P. N. *J. Electroanal. Chem.* **1993**, *351*, 245.

(137) Kitani, A.; Miller, L. L. *J. Am. Chem. Soc.* **1981**, *103*, 3595-3597.

(138) Nuñez de Castro, I. *Enzimología*, 1 ed.; Ediciones Piramide: Madrid, **2001**.

(139) Bartlett, P. N. In *Biosensors: A Practical Approach,* 1st ed.; Cass, A. E. G., Ed.; Oxford University Press: Oxford, **1990**, p 47.

(140) Southampton Electrochemistry Group *Instrumental methods in Electrochemistry*, 1st ed.; Ellis Horwood Limited: Chichister, **1985**.

(141) Beriet, C.; Pletcher, D. *J. Electroanal. Chem.* **1994**, *375*, 213-218.

(142) Hyde, M. E.; Compton, R. G. *J. Electroanal. Chem.* **2003**, *549*, 1-12.

(143) Abyaneh, M. Y.; Fleischmann, M. *Electrochim. Acta* **1982**, *27*, 1513-1518.

(144) Fletcher, S.; Smith, A. *Can. J. Chem.-Rev. Can. Chim.* **1978**, *56*, 606-612.

(145) Fleischmann, M.; Pons, S.; Sousa, J.; Ghoroghchian, J. *J. Electroanal. Chem.* **1994**, *366*, 171-190.

(146) Fletcher, S. *J. Electroanal. Chem.* **2002**, *530*, 119-122.

(147) Bindra, P.; Fleischmann, M.; Oldfield, J. W.; Singleto, D. *Far. Discuss.* **1973**, 180-198.

(148) Deutscher, R. L.; Fletcher, S. *J. Electroanal. Chem.* **1990**, *277*, 1-18.

(149) Denuault, G.; Milhano, C.; Pletcher, D. *Phys. Chem. Chem. Phys.* **2005**, *7*, 3545-3551.

(150) Bruckenstein, S.; Janiszewska, J. *J. Electroanal. Chem.* **2002**, *538*, 3-12.

(151) Baur, J. E.; Wightman, R. M. *J. Electroanal. Chem.* **1991**, *305*, 73-81.

(152) Denuault, G.; Mirkin, M. V.; Bard, A. J. *J. Electroanal. Chem.* **1991**, *308*, 27-38.

(153) Beriet, C.; Pletcher, D. *J. Electroanal. Chem.* **1993**, *361*, 93-101.

(154) Dudko, O. K.; Szabo, A.; Ketter, J.; Wightman, R. M. *J. Electroanal. Chem.* **2006**, *586*, 18-22.

(155) Pfeiffer, B.; Thyssen, A.; Schultze, J. W. *J. Electroanal. Chem.* **1989**, *260*, 393.

(156) Cai, L. T.; Yao, S. B.; Zhou, S. M. *Acta Chim. Sinica* **1995**, *53*, 1150-1156.

(157) Desilvestro, J.; Scheifele, W. *J. Mater. Chem.* **1993**, *3*, 263-272.

(158) Brummer, S. B. *J. Phys. Chem.* **1965**, *69*.

(159) Bade, K.; Tsakova, V.; Schultze, J. W. *Electrochim. Acta* **1992**, *37*, 2255-2261.

(160) Hyodo, K.; Oomae, M. *Electrochim. Acta* **1990**, *35*, 827-829.

(161) Hyodo, K.; Omae, M.; Kagami, Y. *Electrochim. Acta* **1991**, *36*, 357-360.

(162) Mandic, Z.; Duic, L.; Kovacicek, F. *Electrochim. Acta* **1997**, *42*, 1389-1402.

(163) Caban, K.; Kulesza, P. J.; Stojek, Z.; Donten, M.; Miecznikowski, K.; Chojak, M. *Electroanalysis* **2004**, *16*, 1377-1384.

(164) Miwa, Y.; Nishizawa, M.; Matsue, T.; Uchida, I. *Bull. Chem. Soc. Jpn.* **1994**, *67*, 2864-2866.

(165) Matsue, T.; Nishizawa, M.; Uchida, I. *Nippon Kagaku Kaishi* **1995**, *7*, 493-501.

(166) Bartlett, P. N.; Wang, J. H.; Wallace, E. N. K. *Chem. Commun.* **1996**, *3*, 359-360.

(167) Jones, B. J. S.; Kalaji, M. *Electrochim. Acta* **2005**, *50*, 4505-4512.

(168) Bae, W. J.; Jo, W. H.; Park, Y. H. *Synth. Met.* **2003**, *132*, 239-244.

(169) Barbero, C.; Miras, M. C.; Haas, O.; Kotz, R. *J. Electrochem. Soc.* **1997**, *144*, 4170-4174.

(170) Rajendran, V.; Gopalan, A.; Vasudevan, T.; Chen, W. C.; Wen, T. C. *Mater. Chem. Phys.* **2000**, *65*, 320-328.

(171) Angelopoulos, M.; Asturias, G. E.; Ermer, S. P.; Ray, A.; Scherr, E. M.; Macdiarmid, A. G.; Akhtar, M.; Kiss, Z.; Epstein, A. J. *Mol. Cryst. Liq. Cryst.* **1988**, *160*, 151-163.

(172) Asturias, G. E.; Macdiarmid, A. G.; McCall, R. P.; Epstein, A. J. *Synth. Met.* **1989**, *29*, E157-E162.

(173) Chevion, S.; Moran, D. S.; Heled, Y.; Shani, Y.; Regev, G.; Abbou, B.; Berenshtein, E.; Stadtman, E. R.; Epstein, Y. *P. Natl. Acad. Sci. USA.* **2003**, *100*, 5119-5123.

(174) Macdiarmid, A. G.; Asturias, G. E.; Kershner, D. L.; Manohar, S. K.; Ray, A.; Scherr, E. M.; Sun, Y.; Tang, X.; Epstein, A. J. *Abstr. Am. Chem. Soc.* **1989**, *197*, 20-POLY.

(175) McCall, R. P.; Ginder, J. M.; Roe, M. G.; Asturias, G. E.; Scherr, E. M.; Macdiarmid, A. G.; Epstein, A. J. *Phys. Rev. B* **1989**, *39*, 10174-10178.

(176) McCall, R. P.; Roe, M. G.; Ginder, J. M.; Kusumoto, T.; Epstein, A. J.; Asturias, G. E.; Scherr, E. M.; Macdiarmid, A. G. *Synth. Met.* **1989**, *29*, E433-E438.

(177) McCall, R. P.; Ginder, J. M.; Leng, J. M.; Ye, H. J.; Manohar, S. K.; Masters, J. G.; Asturias, G. E.; Macdiarmid, A. G.; Epstein, A. J. *Phys. Rev. B* **1990**, *41*, 5202-5213.

(178) McCall, R. P.; Ginder, J. M.; Leng, J. M.; Coplin, K. A.; Ye, H. J.; Epstein, A. J.; Asturias, G. E.; Manohar, S. K.; Masters, J. G.; Scherr, E. M.; Sun, Y.; Macdiarmid, A. G. *Synth. Met.* **1991**, *41*, 1329-1332.

(179) Ray, A.; Asturias, G. E.; Kershner, D. L.; Richter, A. F.; Macdiarmid, A. G.; Epstein, A. J. *Synth. Met.* **1989**, *29*, E141-E150.

(180) Zuo, F.; McCall, R. P.; Ginder, J. M.; Roe, M. G.; Leng, J. M.; Epstein, A. J.; Asturias, G. E.; Ermer, S. P.; Ray, A.; Macdiarmid, A. G. *Synth. Met.* **1989**, *29*, E445-E450.

(181) Pletcher, D.; A., D. T.; Genders, D. J. *A first course in ion permeable membranes*, 1st ed.; The Electrochemical Consulatncy: England, **1997**.

(182) Jureviciute, I.; Bruckenstein, S.; Hillman, A. R. *J. Electroanal. Chem.* **2000**, *488*, 73-81.

(183) Javadi, H. H. S.; Angelopoulos, M.; Macdiarmid, A. G.; Epstein, A. J. *Synth. Met.* **1988**, *26*, 1-8.

(184) Berrada, K.; Quillard, S.; Louarn, G.; Lefrant, S.; Epstein, A. J. *Nonlinear optics* **1995**, *10*, 253-262.

(185) Fukuda, T.; Takezoe, H.; Ishikawa, K.; Fukuda, A.; Woo, H. S.; Jeong, S. K.; Oh, E. J.; Suh, J. S. *Synth. Met.* **1995**, *69*, 175-176.

(186) Zhao, B. Z.; Neoh, K. G.; Kang, E. T.; Tan, K. L. *Chem. Mat.* **2000**, *12*, 1800-1806.

(187) Bernard, M. C.; Hugot-Le Goff, A. *Synth. Met.*, *85*, 1145-1146.

(188) Mazeikiene, R.; Niaura, G.; Malinauskas, A. *Electrochem. commun.* **2005**, *7*.

(189) Tsukruk, V.; Wilber, Y. L.; Chaoyang, J. *Phys.rev.Lett.* **2005**, *95*, 115503.

(190) Alia, J.; Edwards, H.; Kiernan, B. *Spectrochim Acta A Mol Biomol Spectrosc.* **2004**, *60*, 1533-1542.

(191) Kalaji, M.; Peter, L. M.; Abrantes, L. M.; Mesquita, J. C. *J. Electroanal. Chem.* **1989**, *274*, 289-295.

(192) Hwang, G. W.; Wu, K. Y.; Hua, M. Y.; Lee, H. T.; Chen, S. A. *Synth. Met.* **1998**, *92*, 39-46.

(193) Albery, W. J.; Hillman, A. R. *J. Electroanal. Chem.* **1984**, *170*, 27-49.

(194) Albery, W. J.; Bartlett, P. N. *J. Electroanal. Chem.* **1985**, *194*, 211-222.

(195) Albery, W. J.; Bartlett, P. N.; Wilde, C. P.; Darwent, J. R. *J. Am. Chem. Soc.* **1985**, *107*, 1854-1858.

(196) Albery, W. J.; Bartlett, P. N.; Lithgow, A. M.; Riefkohl, J. L.; Rodriguez, L. A.; Romero, L.; Souto, F. A. *J. Org. Chem.* **1985**, *50*, 596-603.

(197) Albery, W. J.; McMahon, A. J. *J. Electroanal. Chem.* **1985**, *182*, 1-6.

(198) Albery, W. J.; Bartlett, P. N.; McMahon, A. J. *J. Electroanal. Chem.* **1985**, *182*, 7-23.

(199) Albery, W. J.; Jones, C. C. *Faraday Discuss.* **1984**, *78*, 193-201.

(200) Andrieux, C. P.; Dumasbouchiat, J. M.; Saveant, J. M. *J. Electroanal. Chem.* **1980**, *113*, 1-18.

(201) Andrieux, C. P.; Blocman, C.; Dumasbouchiat, J. M.; Mhalla, F.; Saveant, J. M. *J. Electroanal. Chem.* **1980**, *113*, 19-40.

(202) Lyons, M. E. G.; McCormack, D. E.; Smyth, O.; Bartlett, P. N. *Faraday Discuss.* **1989**, 139-+.

(203) Lyons, M. E. G.; McCormack, D. E.; Bartlett, P. N. *J. Electroanal. Chem.* **1989**, *261*, 51-59.

(204) Lyons, M. E. G.; Bartlett, P. N. *J. Electroanal. Chem.* **1991**, *316*, 1-22.

(205) Lyons, M. E. G.; Lyons, C. H.; Michas, A.; Bartlett, P. N. *J. Electroanal. Chem.* **1993**, *351*, 245-258.

(206) Lyons, M. E. G. *Analyst* **1994**, *119*, 805-826.

(207) Lyons, M. E. G.; Greer, J. C.; Fitzgerald, C. A.; Bannon, T.; Barlett, P. N. *Analyst* **1996**, *121*, 715-731.

(208) Lyons, M. E. G.; Bannon, T.; Hinds, G.; Rebouillat, S. *Analyst* **1998**, *123*, 1947-1959.

(209) Lyons, M. E. G.; Murphy, J.; Bannon, T.; Rebouillat, S. *J. Solid State Electrochem.* **1999**, *3*, 154-162.

(210) Rebouillat, S.; Lyons, M. E. G.; Flynn, A. *Analyst* **1999**, *124*, 1635-1644.

(211) Lyons, M. E. G. *Sensors* **2002**, *2*, 473-506.

(212) Lyons, M. E. G. *Sensors* **2002**, *2*, 314-330.

(213) Lyons, M. E. G. *Sensors* **2003**, *3*, 19-42.

(214) Rebouillat, S.; Lyons, M. E. G.; Flynn, A. *Analyst* **2000**, *125*, 1611-1628.

(215) Lyons, M. E. G.; Bannon, T.; Rebouillat, S. *Analyst* **1998**, *123*, 1961-1966.

(216) Che, G. L.; Dong, S. J. *Electrochim. Acta* **1992**, *37*, 2695-2699.

(217) Che, G. L.; Dong, S. J. *Electrochim. Acta* **1992**, *37*, 2701-2705.

(218) Che, G. L.; Dong, S. J. *Electrochim. Acta* **1993**, *38*, 2315-2319.

(219) Che, G. L.; Dong, S. J. *Electrochim. Acta* **1993**, *38*, 1345-1349.

(220) Che, G. L.; Dong, S. J. *Electrochim. Acta* **1993**, *38*, 581-588.

(221) Dong, S. J.; Che, G. L. *J. Electroanal. Chem.* **1991**, *315*, 191-199.

(222) Dong, S. J.; Che, G. L. *J. Electroanal. Chem.* **1991**, *309*, 103-114.

(223) Dong, S. J.; Che, G. L. *Electrochim. Acta* **1992**, *37*, 2587-2589.

(224) Harrison, J. A.; Thirsk, H. R. In *Electroanalytical Chemistry*; Bard, A. J., Ed.; Marcel Dekker: New York, **1971**; Vol. 5, p 67.

(225) Albery, W. J.; Knowles, J. R. *Biochemistry* **1976**, *15*, 5631-5640.

(226) Ding, H.; Park, S. M. *J. Electrochem. Soc.* **2003**, *150*, E33-E38.

(227) Chen, S. L.; Kucernak, A. *J. Phys. Chem. B* **2004**, *108*, 3262-3276.

(228) Dharmadhikari, J. A.; D'Souza, J. S.; Gudipati, M.; Dharmadhikari, A. K.; Rao, B. J.; Mathur, D. *Sensor Actuat B-Chem* **2006**, *115*, 439-443.

(229) Hanstein, S.; de Beer, D.; Felle, H. H. *Sensor Actuat B-Chem* **2001**, *81*, 107-114.

(230) Dayton, M. A.; Ewing, A. G.; Wightman, R. M. *J. Electroanal. Chem.* **1983**, *146*, 189-200.

(231) Hiratsuka, A.; Muguruma, H.; Nagata, R.; Nakamura, R.; Sato, K.; Uchiyama, S.; Karube, I. *J. Membr. Sci.* **2000**, *175*, 25-34.

(232) Polidori, M. C.; Stahl, W.; Eichler, O.; Niestroj, I.; Sies, H. *Free Radic. Biol. Med.* **2001**, *30*, 456-462.

(233) Javadi, H. H. S.; Zuo, F.; Cromack, K. R.; Angelopoulos, M.; Macdiarmid, A. G.; Epstein, A. J. *Synth. Met.* **1989**, *29*, E409-E416.

(234) Chevion, S.; Berry, E. M.; Kitrossky, N.; Kohen, R. *Free Radic. Biol. Med.* **1997**, *22*, 411-421.

(235) Mecocci, P.; Polidori, M. C.; Troiano, L.; Cherubini, A.; Cecchetti, R.; Pini, G.; Straatman, M.; Monti, D.; Stahl, W.; Sies, H.; Franceschi, C.; Senin, U. *Free Radic. Biol. Med.* **2000**, *28*, 1243-1248.

(236) Tukamoto, T.; Ozeki, S.; Hattori, F.; Ishida, T. *Chem. Pharm. Bull.* **1974**, *22*, 385-389.

(237) Karlsen, A.; Blomhoff, R.; Gundersen, T. E. *J. Chromatogr. B* **2005**, *824*, 132-138.

(238) Smirnoff, N.; Conklin, P. L.; Loewus, F. A. *Annu. Rev. Plant Physiol. Plant Molec. Biol.* **2001**, *52*, 437-+.

(239) Roelfsema, M. R. G.; Hanstein, S.; Felle, H. H.; Hedrich, R. *Plant J.* **2002**, *32*, 65-75.

(240) Hanstein, S.; Martinez-Bonastre, A.; Nestler, U.; Bartlett, P. N. *Sensor Actuat B-Chem* **2007**, *Accepted*.

(241) Scharifker, B.; Hills, G. *Electrochim. Acta* **1983**, *28*, 879-889.